INSTITUTE OF PETROLEUM GEOLOGY AND GEOPHYSICS SB RAS

УДК 550.837.6
ГРНТИ 38.57.23
Инв. No.

APPROVED:
Contractor: Trofimuk's Institute of Petroleum Geology and Geophysics, Siberian Branch of Russian Academy of Sciences
On behalf of Organization head _____/_____/ **Seal**

RESEACRH AND DEVELOPMENT REPORT

About operations for allocation of target testing objects at the geophysical test site near the Klyuchi settlement

23.12.2010

Contractors: **E.V. Balkov, Ph.D.**
T.A. Stoikin
A.K. Manstein, Ph.D.
Yu.G. Karin

Novosibirsk
2010

INTRODUCTION

Today modern geophysics has an arsenal of tools and methods applicable also in adjacent fields, like ecology, archeology, engineering geology, hydrogeology, construction, municipal utility management, etc. In particularly, the last two decades are remarkable in development and application of techniques known as shallow multifrequency sounding (MFS) and electrical impedance tomography (EIT).

The stationary station of IPGG SB RAS (on the territory of settlement Klyuchi near Nopvosibirsk) was chosen as a site for developing a geophysical testing site. This test site is required for trial field operations (skill drilling and operations debugging) using MFS and EIT methods and for testing of actual sounding capacity of available MFS devices.

The theoretical and practical researches are mainly oriented to using specific devices that exploit MFS and EIT methods; these results have been covered by the Report for the first stage of this Project. Since we need to present a self-sufficient text of report, the key characteristics of these devices are summarized here as well.

A three-coil MFS device can operate at 14 (fixed) frequencies in the range from 2.5 to 250 kHz and has a fixed span between coils equal to 1.5 and 2.5 m.

The electrical survey station SKALA-48 accomplishes the electrical impedance tomography using the measurements of resistivity (impedance) and method of induced polarization. This station is compatible with multi-electrode braids with 48 outlets; this configuration helps in performing tomography presentation with automatic communications.

RUNNING OF COMPREHENSIVE FIELD TESTS, AVALUATION OF COMPREHENSIVE DATA TREATMENT METHOD FOR DATA FROM SHALLOW MULITIFREQUENCY SOUNDING AND ELECTRICAL IMPEDANCE TOMPOGRAPHY

1 Development of configurations for targets and landscaping of electrical survey test site

Preliminary, the entire territory of the stationary facility has been scanned by MFS devices to map the configuration of any possible pipelines or cables underground before the works have been started; this would elucidate the ranges suitable for deploying a set of conducting targets.

These primary data gave us a map with plotting of a logarithm of specific conductivity for the scanned territory (measurement taken at a single frequency of 5.102 kHz); the map resolution in both directions was 1 meter. Evaluating this map, the territory of test site was divided into two areas (see images below).

Evaluating this primary information, we picked up 10 squared areas (100 m2 each) for deploying of 33 targets which were the mock-ups for real objects. The picture below shows the process of deploying one of the many objects: this was a piece of metal pipe with O.D. 100 mm buried at the depth of 1 m (Figure 1).

Figure 1 – Operations at the site on deploying of geophysical targets

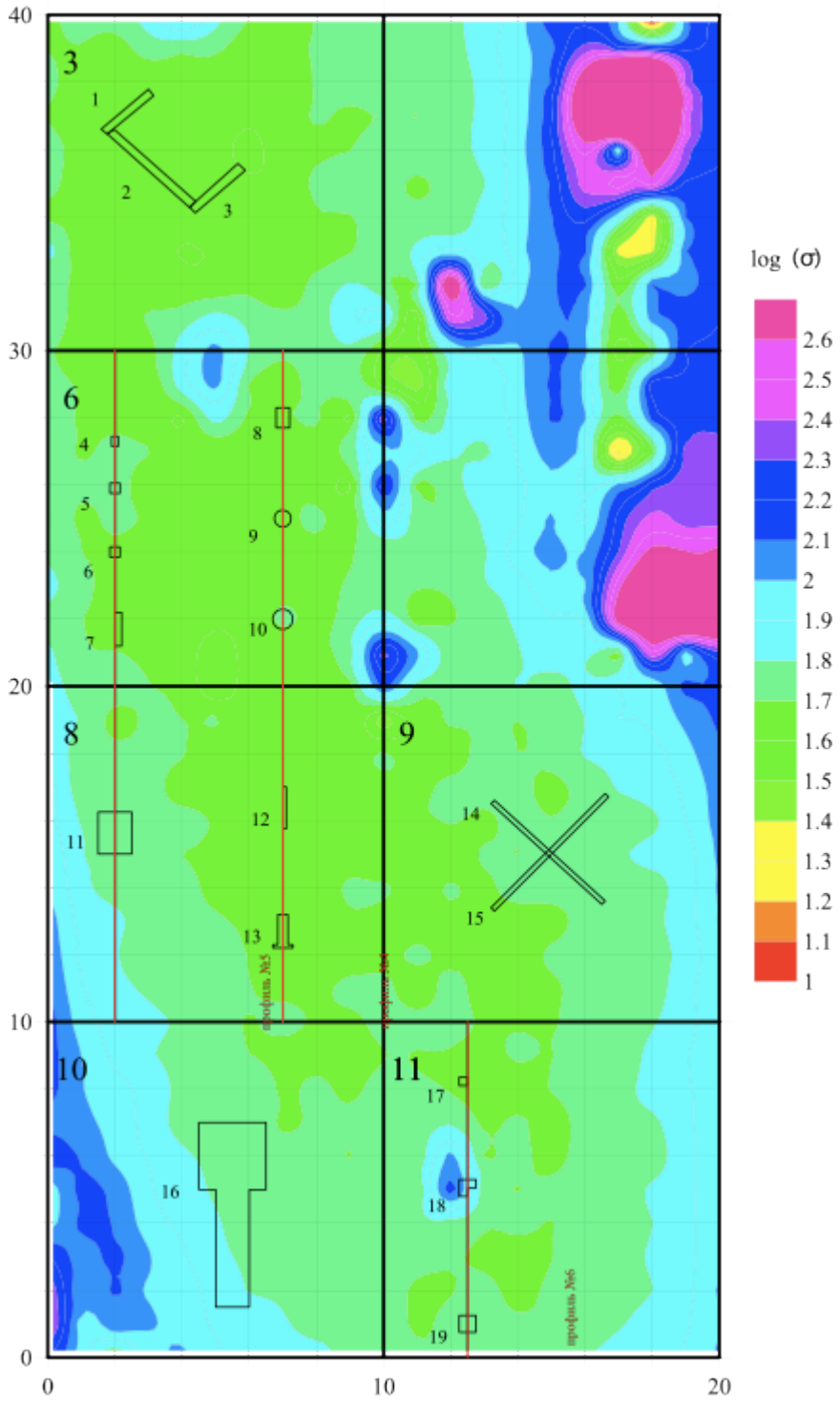

Figure 2 – A map with plotting of distribution of specific conductivity (logarithmic value) for the Area #1 of the Test Site.

Square #	*Target #*	*Target description*
03	**1**	Plastic pipe with length of 1.8 м, D 110 mm. Deploying depth is 0.5 м.
03	**2**	Plastic pipe with length of 3.7 m, D 60 mm. Deploying depth is 0.5 m.
03	**3**	Refilled trench without a target. Trench depth is 0.5m.
06	**4**	«Treasure-trove of 5 liters». Plastic bottle 1 item (5 l) with metal shave. Deployment depth is 0.5 m.
06	**5**	«Treasure-trove of 15 liters». Plastic bottle 3 items. (Total 15 l) with metal shave. Deployment depth is 0,8 м.
06	**6**	«Antipersonal landmine». Piece of metal pipe (D 100 mm). Target size is 30*30 cm. Deployment depth is 1.1 m.
06	**7**	«Antiaircraft projectile». Pieces of round metal bar with length of 1.1 and 0.7 m, D 7 cm. Pieces were laid side to side. Deployment depth is 1.5 m.
06	**8**	Aluminum sheet 60*40 cm. Deployment depth is 0.5 m.
06	**9**	Copper disk, D 0.5 m. Deployment depth is 0.5 m.
06	**10**	Iron disk, D 0.6 m. Deployment depth is 0.5 m.
08	**11**	Horizontal iron sheet 1*1,25 м. Deployment depth is 2 m.
08	**12**	Vertical iron sheet 1*1.25 m. Top edge is at the depth 1 m.
08	**13**	«Aviation bomb». Iron item made of steel pipe (0.85 m length м, D=0.3 m) and a welded basement 0.55-0.65 m. Basement H is 0.1 m. Deployment depth is 2 m.
09	**14**	Steel pipe with length of 4 m (from left-top to right-bottom angle), D 100 mm. Deployment depth is 1 m.
09	**15**	Steel pipe with length of 5 m (measured from left-bottom to right-top angle), D 100 mm. Deployment depth is 2 m.
10	**16**	Dug-out (room 2*2 m, corridor 1*3m), roof at the depth 1 м, depth of dig-out is 1.5 m.
11	**17**	Plastic can (1 item) (35*25*20 cm). Deployment depth is 0.5 m.
11	**18**	Plastic cans (3 items) (35*25*20 cm). Deployment depth is 1 m.
11	**19**	Plastic cans (4 items) (35*25*20 cm). Deployment depth is 1.5 m.
12	**20**	Brick wall. Wall thickness is 0.5 m, H =1 m. «П»-shaped masonry. The bar length is 3 m, left leg is 3.5 m, right leg is 2.3 m. The upper face buried at the depth of 0.5 m.
12	**21**	Alum. churn (left). D of bottom part is 0.35 m, H 0.5 m. Depth down to the lid 0.5 m.
12	**22**	Alum. churn (right). D of bottom part is 0.35 m, H 0.5 m. Depth down to the lid 2 m.
13	**23**	Iron barrel (left-top). D 0.56 m, H 0.9 m. Depth down to the upper face is 0.9 m.
13	**24**	Iron barrel (right-top). D 0.56 m, H 0.9 m. Depth down to the upper face is 2.5 m.
13	**25**	Iron barrel (left-bottom). D 0.56 m, H 0.9 m. Depth down to the upper face is 1.3 m.
13	**26**	Iron barrel (right-bottom). D 0.56 м, H 0.9 m. Depth down to the upper face is 1.8 m.
14	**27**	Horizontal copper sheet 1*0.6 m tilted to axis. Deployment depth is 0.8 m.
14	**28**	Vertical copper sheet 1*0.6 m. Depth down to the upper face is 0.45 m (put on the longer side of 1 m).
14	**29**	Horizontal copper sheet 0.5*0.6 m. Deployment depth is 0.2 m.
14	**30**	Vertical iron disk D 0.6 m. Depth down to the upper face is 0.5 m.
14	**31**	Horizontally laid iron disk D 0.6 m. Deployment depth is 1 m.
15	**32**	Steel pipe with length of 3 m, D 42 mm. Deployment depth is 0.65 m.
15	**33**	Iron bar with length 7.5 m. Cross-section is 20*30 mm. Deployment depth is 0.7 m.

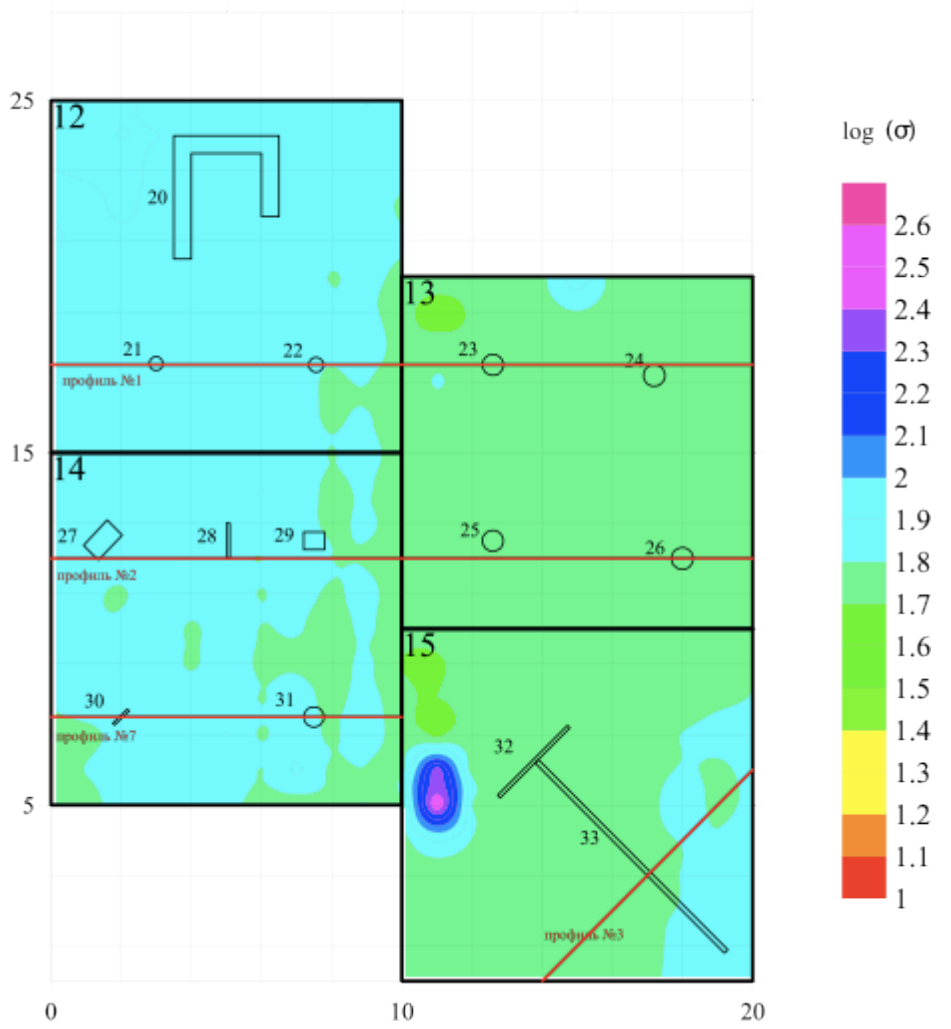

Figure 3 – A map with plotting of distribution of specific conductivity (logarithmic value) for the Area #2 of the Test Site.

The figures above (Figure 2 and Figure 3) show the diagram of deploying all targets underground. In these figures, large font numbers stand for the numbers of squared zones with a target(s) buried; the images show the positions of these targets, small fonts denote the ordinal number of a target. The detail description for all targets and their depths are summarized in the table below (see Table 1).

After some evaluation works, we chosen the basic lines (see Figure 2 and Figure 3, red lines), these lines were used later for actual measurements using different versions of MFS apparatuses.

The appendix presents a photo-report about on operations for test site landscaping, parameters and configuration of geophysical targets.Table 1 – Description of objects (targets) deployed at the test site

Here D – diameter, H – height.

2 Results of experimental activity on acquisition of geophysical data on the electric-conductivity tests site and data interpretation

Our experimental and methodological activity allowed us to classify results into three blocks. The block number one includes the line No. 1 and squares No. 12 and 13, the second block embraces line No. 2 and squares No. 13 and 14, the third block embraces lines No. 4 and 5 and square No. 6. So we divided later the outlay of experimental data according these territorial blocks. Besides, all results as viewed in different diagrams for all three blocks scanned by different versions of FMS devices No. 26, 27, 29 are collected in Appendix 2.

Other results were not allocated in block system and have only identification by the numbers of territory squares and lines.

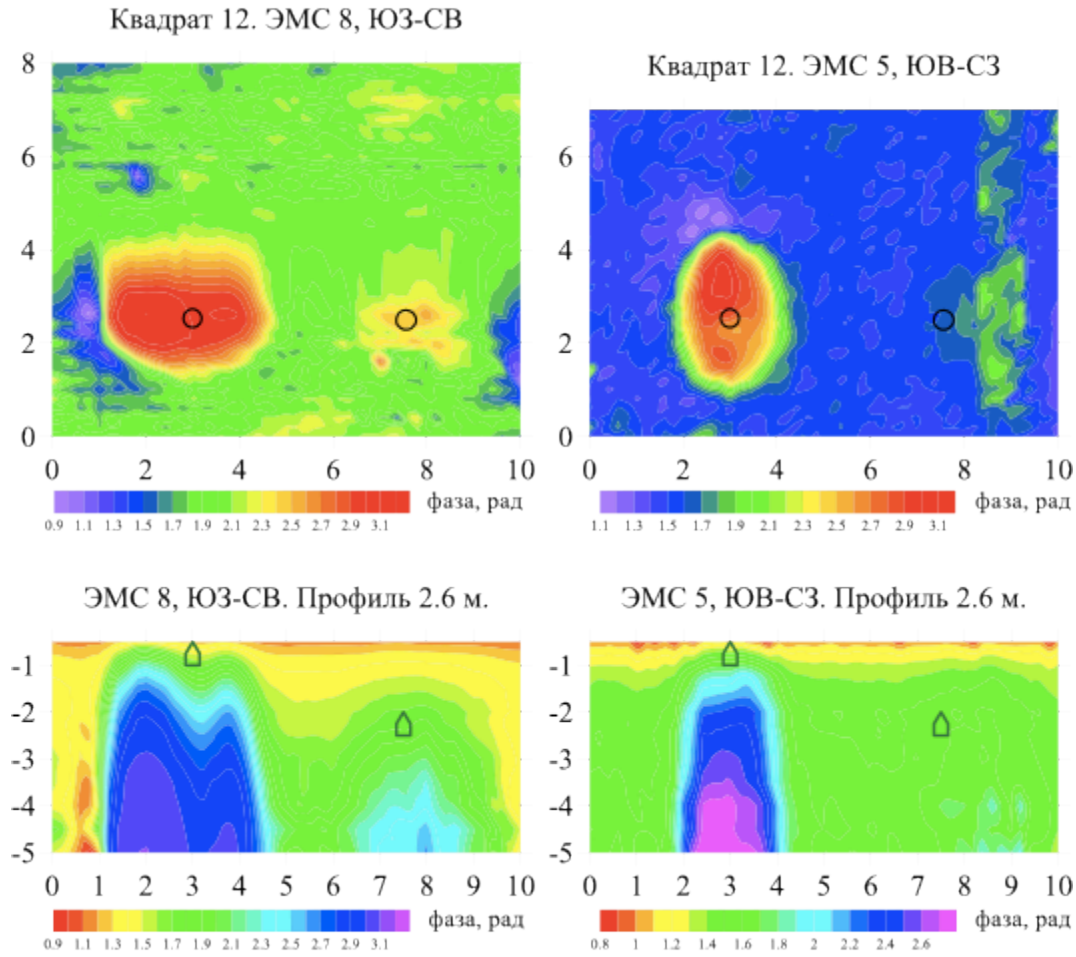

Figure 4 – Results of area screening for square No. 12. Operating frequency was 2.5 kHz.

2.1 Results on screening the objects from Block No.1 (Line No.1, Squares No. 12 and 13).

The following scanning results have been obtained for the area belonging to block No. 1:

- Survey of square No.12 using MFS version No.8 in direction SW-NE,

- Survey of square No.12 using MFS version No.5 in direction SE-NW,
- Sounding along line No.1 using MG|FS version No. 26, 27, 29.

Analysis of all maps and sections with different components and methods of signal transformation demonstrated that the phase of differential signal obtain by MFS equipment is the most effective parameter for depicting the reality.

In the previous pages (Figure 4) we presented the maps and sections for the same zone scanned in two orthogonal directions. We picked up a frequency that ensures the most distinctive results. We see an obvious “advantage” for the map plotted from data obtained by MFS device No.8 (SW-NE). Both targets can be tracked underground (these were aluminum churns). It is worthwhile to note that accurate distinguishing of a looped anomaly for the churn buried at higher depth was possible when we consider the signal phase at low frequencies. The section presentations have both anomalies nicely visible when operating the MFs scanner No. 8.

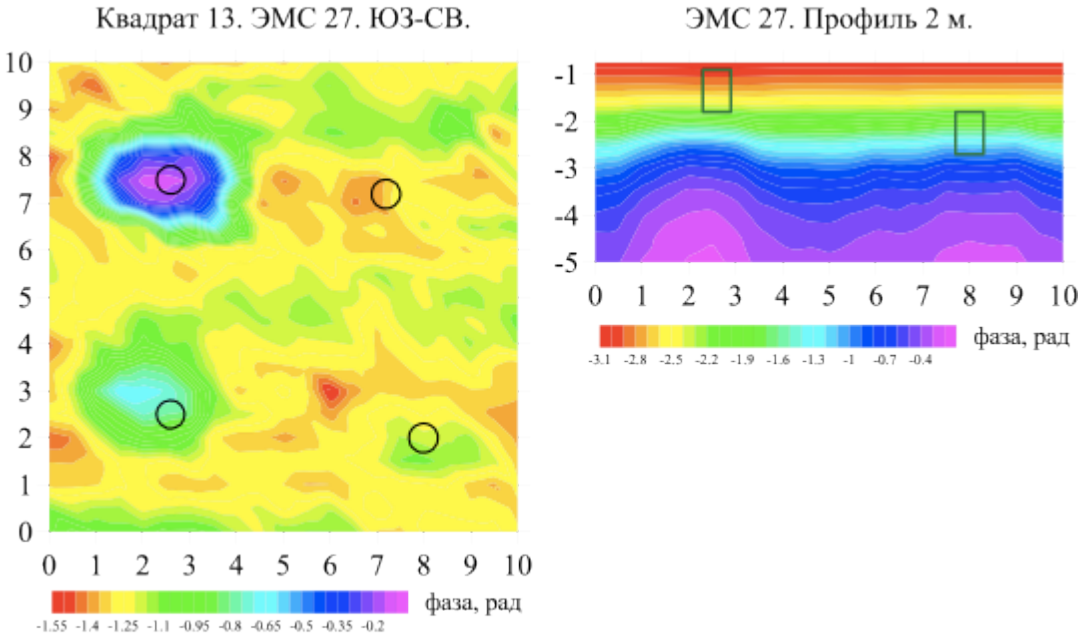

Figure 5 – Results of total scanning for square No. 13. Operating frequency was 2.5 kHz.

When we look at the map and a section for the square no. 13 (Figure 5), we can see distinctive three targets (they were iron barrels) – they we detected when measurements were conducted for the phase of differential signal. The barrel buried deeply (2.5 m from the surface to the upper face of barrel) failed to be found for any kind of measurements (see Appex 2).

As a demonstration of results obtained for the line No.1, we present primary data here (Figure 6) and section (Figure 7).

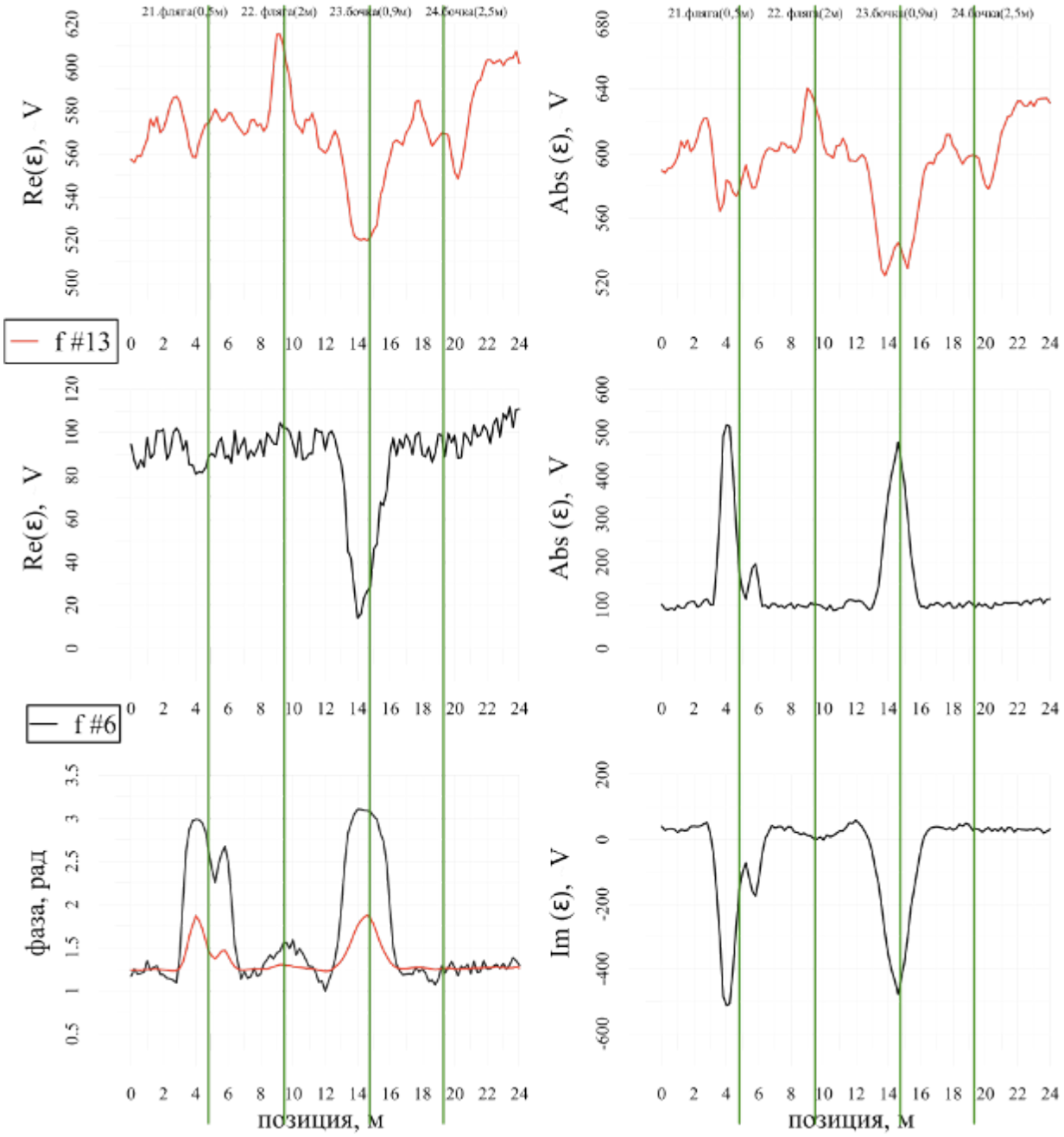

Figure 6 – Diagram for MFS signal No.29 along the line No.1

All the plottings (Figure 6) demonstrate perfectly the changes in signal from targets No. 21 and No.23 (a churn and a shallow-buried barrel). When the diagram depicts the phase o differential signal, the changes in the low-frequency signal (f#6=10 kHz) reveals the target No. 22 as well. The very same target is remarkable in that the signal modulus and the signal's real part become higher at a higher frequency (f#13=111.1 kHz). One can see in diagrams for the

signal's modulus and the real part a decrease in signal at the 20 m station. This kind of reduction takes place for both frequencies depicted (f#6=10 kHz, f#13=111.1 kHz), but this peak can be caused by target No.24, which was buried deeply at the same scanning line. But we cannot confirm this fact; however, other observations tell us that there was no such a change in signal in other line diagrams or at areal survey. The target No.21 in diagrams exposes itself by two peaks. This fact is related to asymmetry of MFS device configuration (two receiver coils allocated at different distances fro the generator coil) and also by the fact of a low depth for this target (0.5 m).

When we look at the multi-color sections along the line No.1 (Figure 7), we also (as on upper diagrams) can see targets No.21 and No.23, but the first target is revealed in the form of a double peak. The sections that show the signal phase of the imaginary part of signal are most informative among all reviewed types of sections. Except the images from targets No.21 and No. 23, one can see the image from target No.22, but less pronounced (due to a higher depth).

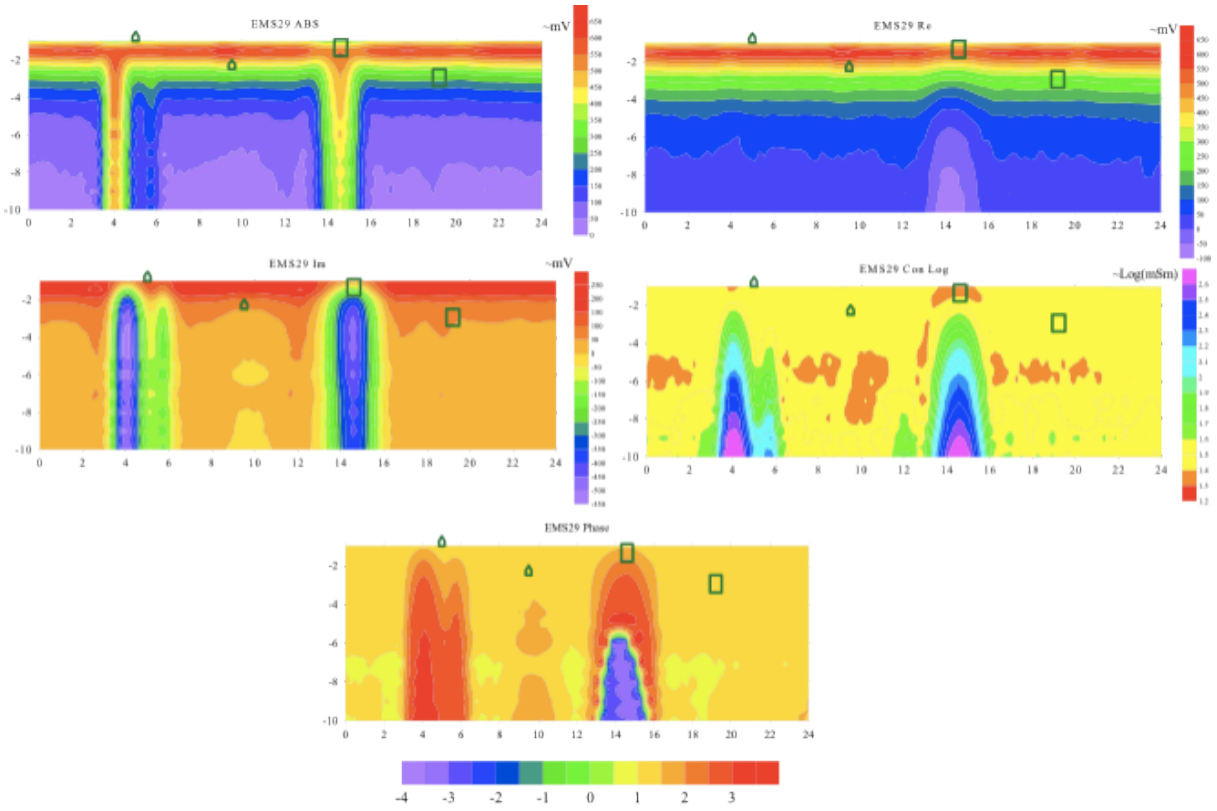

Figure 7 - Sections plotted from MFS data No.29 along the line No.1

2.2 Results of surveying the zones from Block No.2 (Line No.2, Squares No. 13 and 14).

Up to the present time, the following jobs were carried out at Block No.2:

- ◇ Survey of square No.13 using MFS device No.8 in direction SW-NE,
- ◇ Survey of square No.14 using MFS device No.8 in direction SW-NE,

- Sounding along the line No.2 using MFS device No. 26, 27, 29.

The maps for square No.14 (Figure 8) were plotted by different parameters. The map reveals all the targets available in this square, since the burial depth was low (up to 1 m). The images for all targets in the maps have accurate outlines. However, the map with plotting of differential signal phase are different from others (the maps of distribution of apparent resistivity and the maps of distribution of apparent conductivity logarithm): it shows a more uniform structure. Every target has different amount of mages on the map. The amount of images depends on direction of survey and placement of the target. Targets No.28 and No.30 were deployed vertically. But the target No.28 was oriented along the direction where the sounding device was carried, but target No.30 lays at an angle to this survey direction. Therefore target No.28 has four images in all maps, and target No.30 has three images. Targets No.27, No.29, and No.31 were placed horizontally, but target No.27 was placed at an angle to the survey direction (unlike two other targets). Therefore, target No.27 generates two images, but targets No.29 and No.31 generate three images. The asymmetry of positioning the images is related to asymmetry of scanning device (see explanation above). The results of areal survey for square No.13 (Figure 5) have been described in the informative block number one.

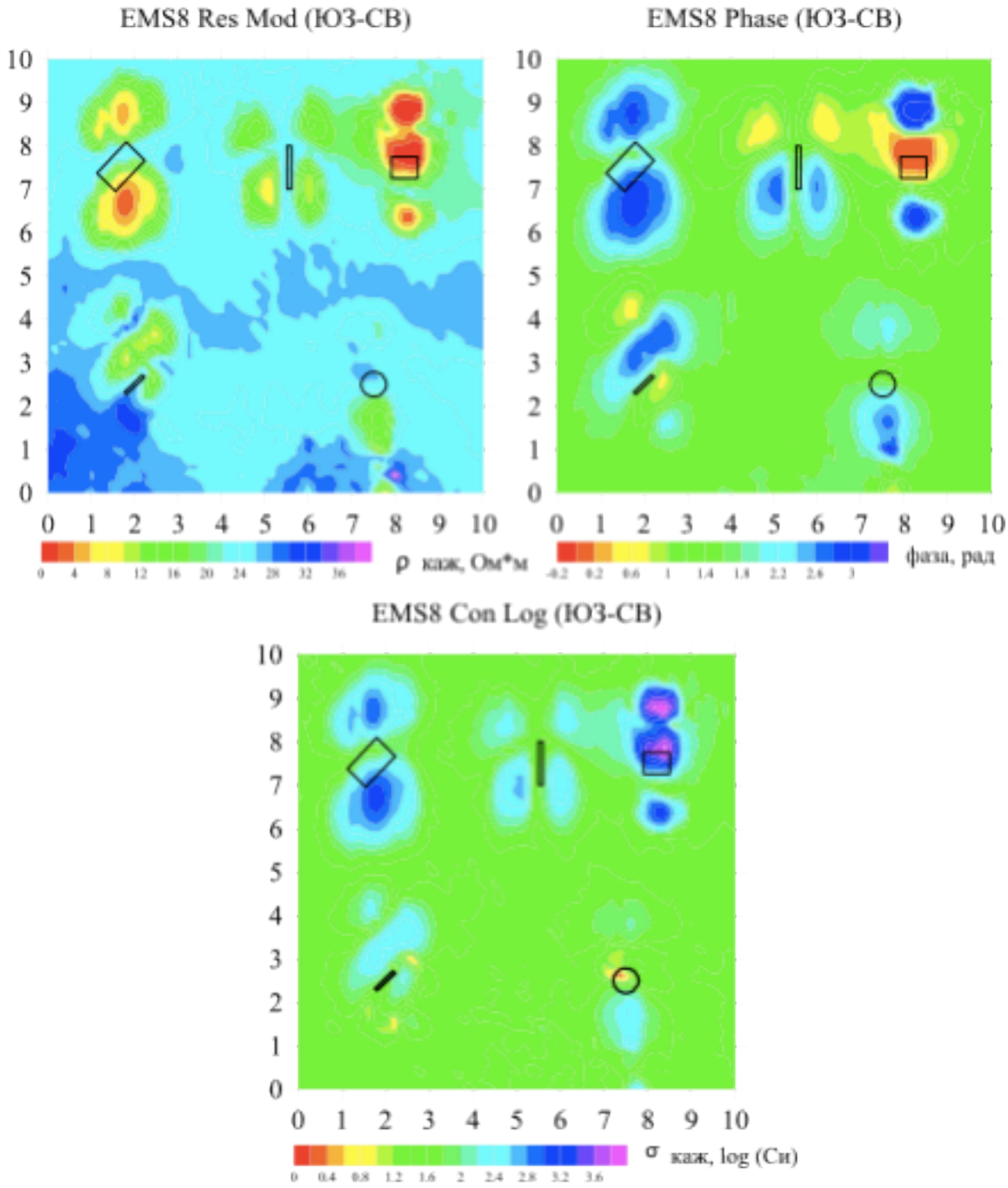

Figure 8 – Results of areal survey for square No. 14. Operating frequency was 3.9 kHz.

The results of surveying along the line No.2 are demonstrated in diagrams (Figure 9) and sections (Figure 10).

Line No.2 passes through targets deployed within square No.13 and No.14. The targets belonging to square No.13 have a lower depth, so they are more visible through variation of signal in those diagrams. The first three targets (No.27, No.28, No.29) are perfectly seen in all diagrams. Targets No.28 and No.29 (the smallest depth) exhibit a doubled peak in the diagram of signal modulus. This is obvious for surveying at a higher frequency. One can see that at one diagram different targets can be expressed through different variation of the signal. Targets No. 27 and No.28 on diagrams of the real and imaginary parts of signal (f#6=10 kHz) are revealed

through signal growth, but target No.29 is tracked down through signal decline. This is all about the distance between target on this line and the signal transition through zero. For deeply buried targets No. 25 and No. 26, the diagram of differential signal phase is most informative. This diagram illustrates how the signal varies during the passing of device ahead those targets. The real part signal diagrams (change in signal) gives information about targets No.25 and No.26. At a higher frequency (f#13=111.1 kHz) the anomaly of signal above these objects has a bigger amplitude in comparison with the low-frequency scanning (f#6=10 kHz).

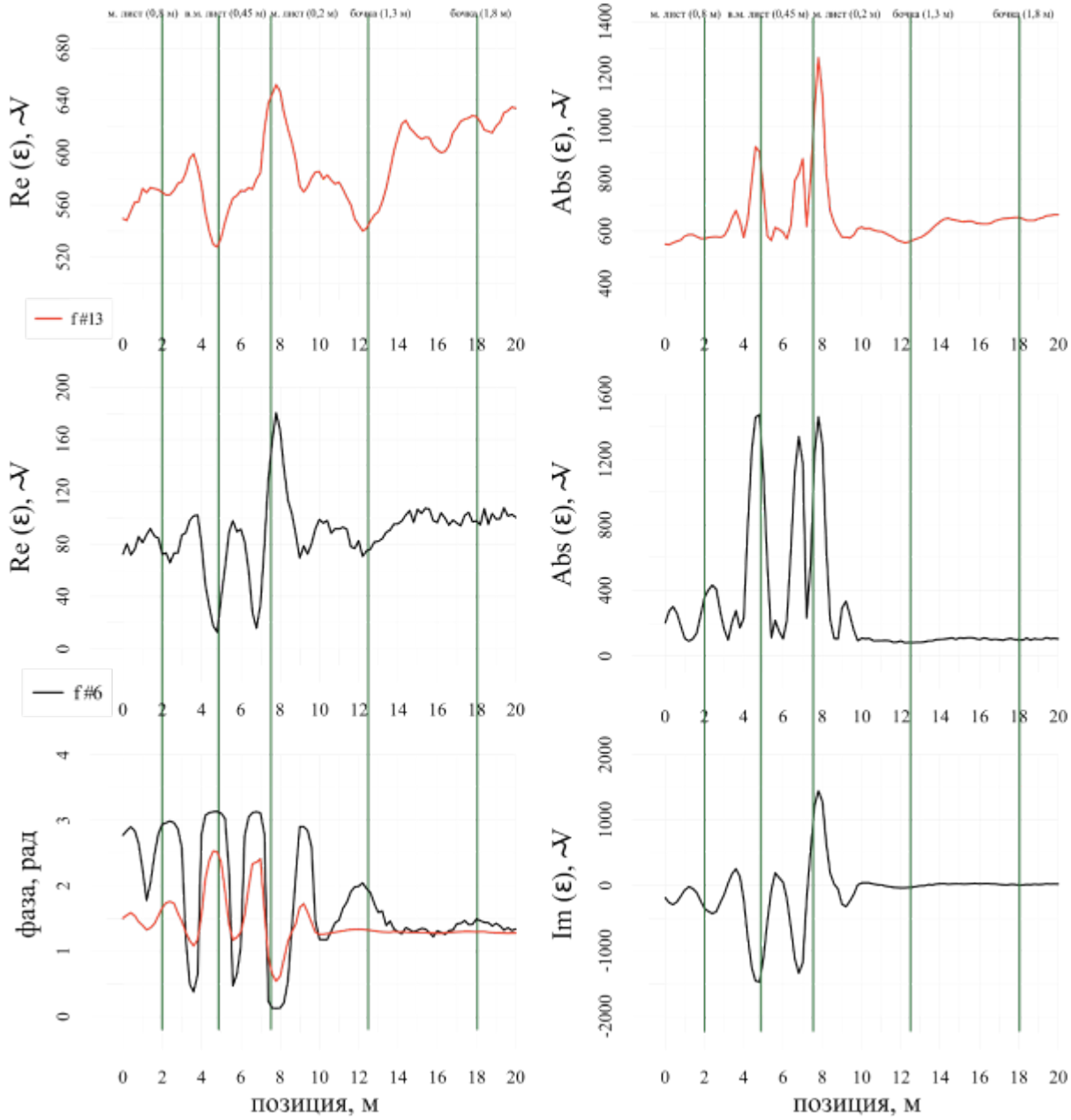

Figure 9 – Diagram for MFS signal No.29 along the line No.2.

The sections build from data along line No.2 (reconstruction from different parameters of targets No.27, No.28, No.29) one can see rather bright anomalies. But the section computed from the real part of signal can give us only targets No.28 and No.29 (smallest depth). The deeper targets No.25 and No.26 can be traced down in the sections computed from the imaginary part of

signal and from the phase of differential signal. Target No.26 is better seen in the section plotted from the differential signal phase. The section plotted as distribution of logarithm of conductivity, one can see an anomaly produced by target No.25.

We should emphasize that typically the diagrams of the real part of signal are more informative that the diagrams based on imaginary part of signal (when we want to detect the deeper targets). However, for the case of presentation of data in the form of sections, the deeper objects can be seen from treatment of imaginary signal (but the real part is less informative).

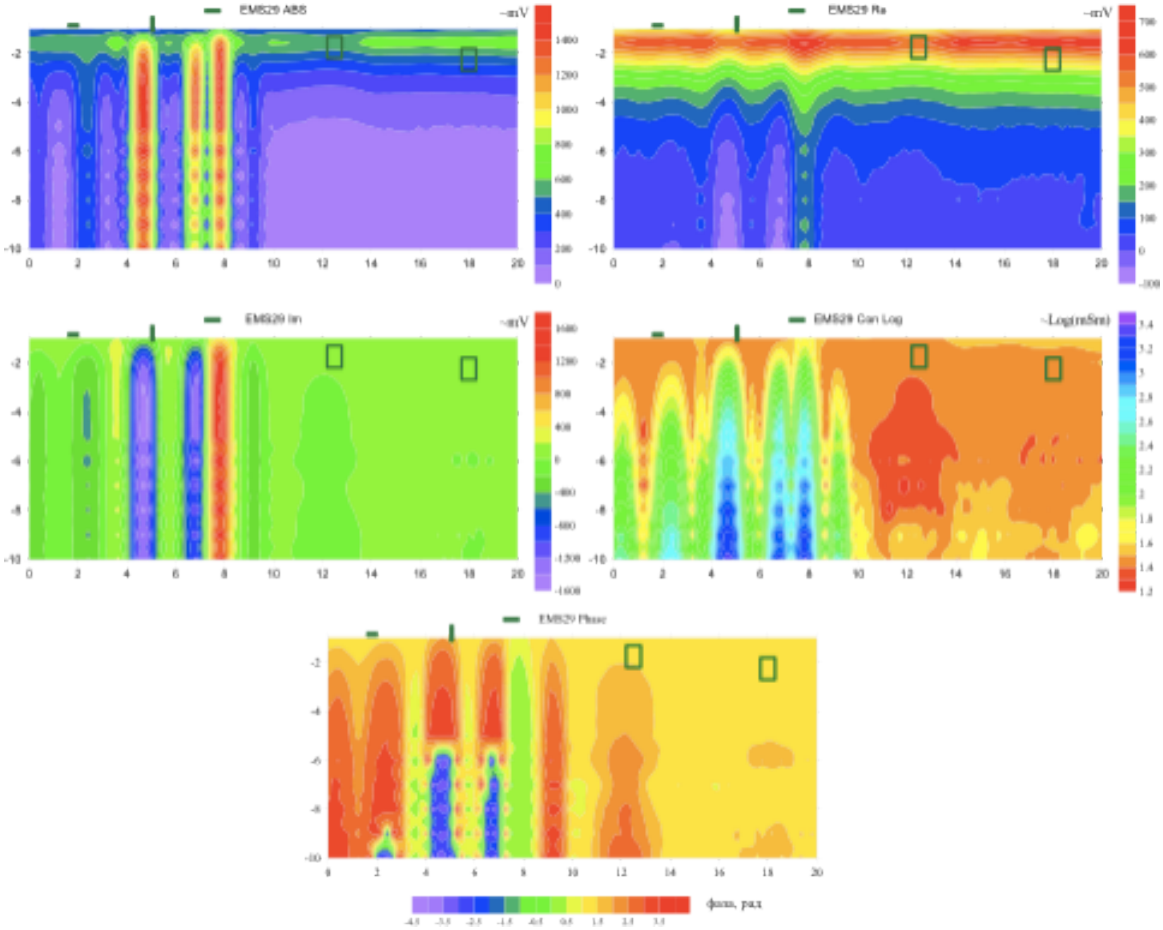

Figure 10 - Sections plotted from MFS data No.29 along the line No.2

2.3 Results of jobs for Block No.3 (Lines No. 4 and 5, Sqaure No. 6).

To the present moment, the following jobs were performed for the objects allocated within block No.3:

- ◇ Survey of square No.6 using MFS device No.5 in direction SW-NE,
- ◇ Survey of square No.6 using MFS device No.5 in direction SE-NW,
- ◇ Sounding along the line No.4 using MFS device No. 26, 27, 29,

◇ Sounding along the line No.5 using MFS device No.27

Areal survey for square No.6 (Figure 11) was carried out in two directions. This gives a clue to more accurate identification of coordinates of targets buried. These maps shows only targets No.8, No.9, No.10 (big-size targets). In the map of survey direction the SE-NW we see three images for every target (this is how all three coils of MFS device are passing ahead the target). Then the map was plotted for the SW-NE direction, the amount of images is less. Now the distance between objects is comparable with the length of the scanning device, so some images were overlapped.

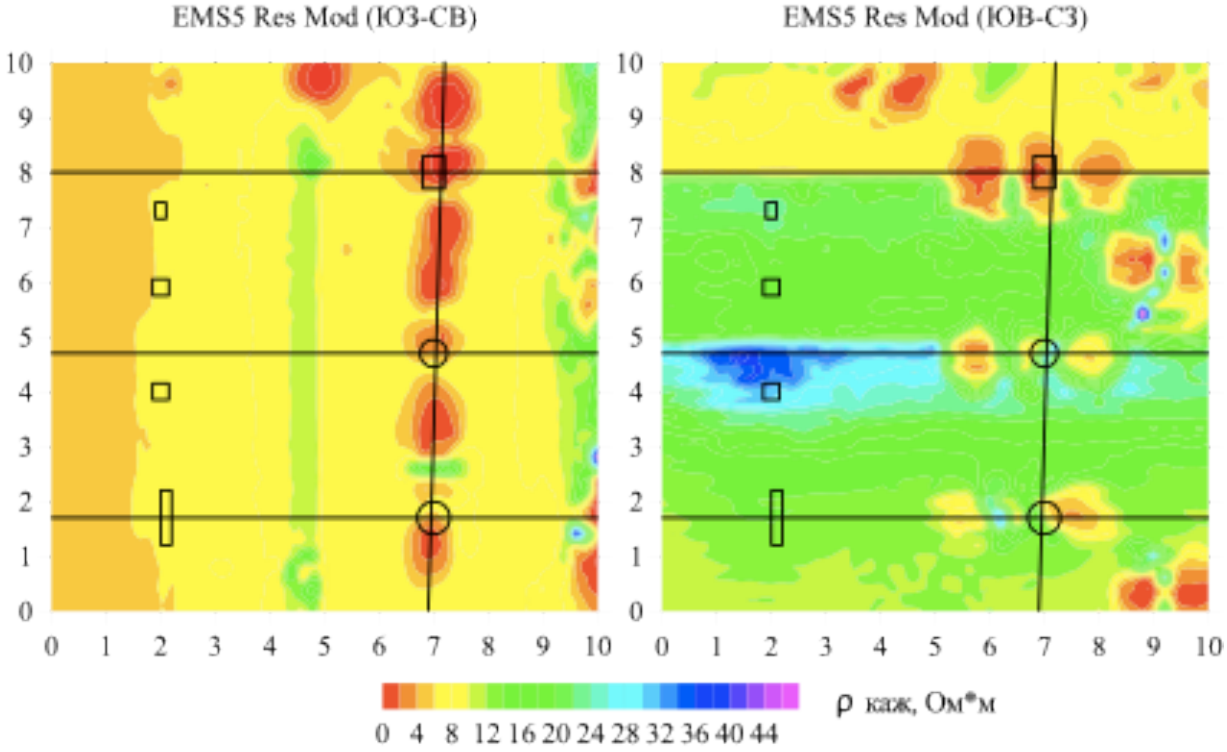

Figure 11 – Results of areal survey for squarea No. 6. Operating frequency on maps is 5.1 kHz.

The data from the left part of square No.6 (Figure 12) were processed additionally for better detection of other targets from the same square. We plotted four types of maps for two frequencies (f#3=3.19 kHz, f#13=111.1 kHz). All targets are visible on the maps plotted from the signal modulus and the real part of signal (for higher frequency). Target No.4 (the shallow one) can be seen on maps that process the data on the phase of differential signal (for both frequencies). These objects cannot be seen in other types of maps.

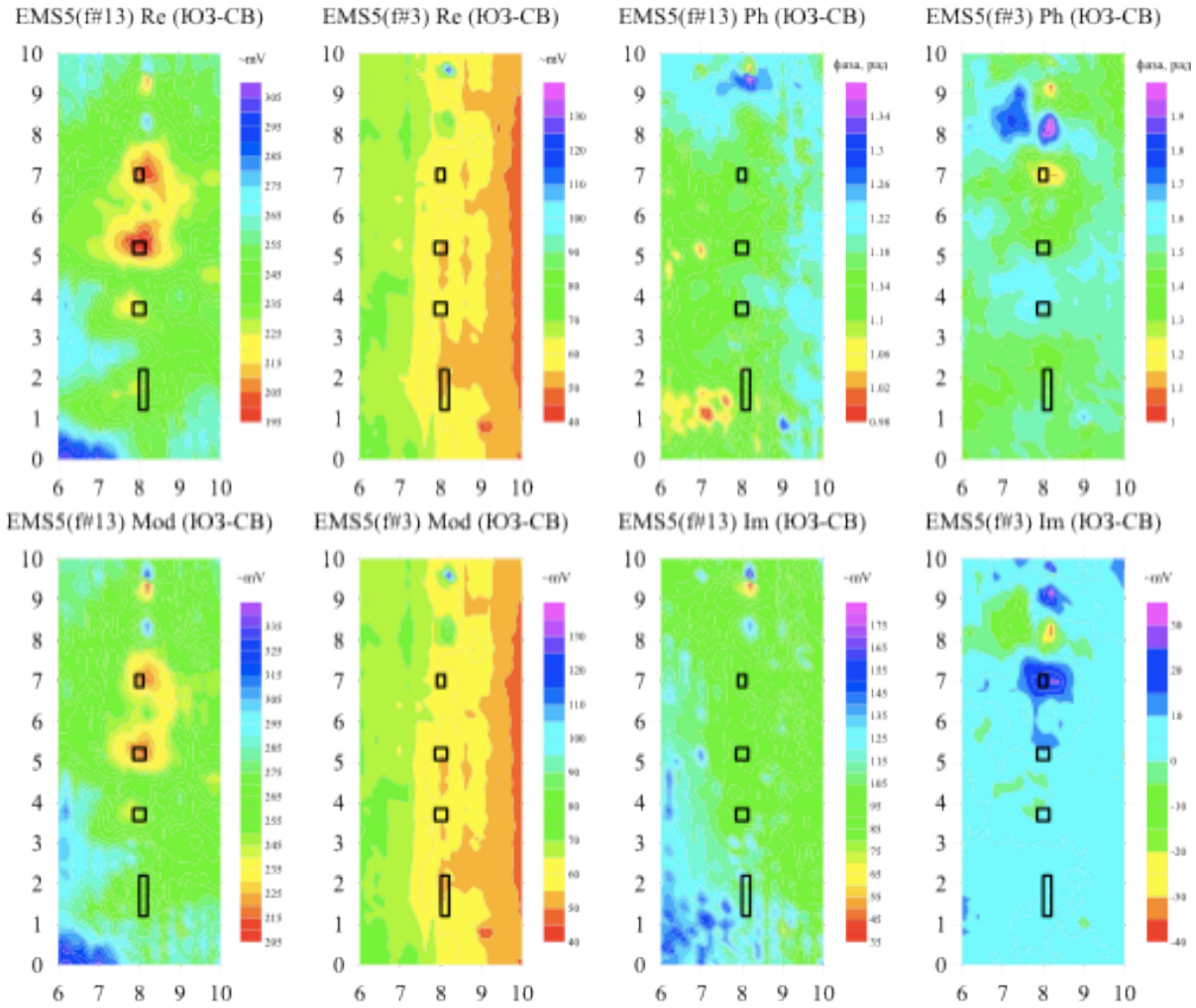

Figure 12– Results of areal data survey for square No. 6 (left part). The operating frequencies for those maps were f#3=3.19 kHz, f#13=111.1 kHz.

The line No.4 goes through squares No.6 and No.8 and on its way it crosses five targets (three targets in the first square and two targets within next one). The targets in square No.8 are deep (No.12 – 1 m deep, and No.13 – 2 m deep), but the targets within square No.6 have been deployed to the depth of 0.5 m. Therefore, the targets in diagrams (Figure 13) are seen as anomalies of different intensity. Targets No.12 and No.13 are quite visible in diagrams plotted for signal modulus or signal's real part (especially for a higher frequency scanning). Targets No. 8, No.9, No.10 are visible in all diagrams. But unlike for two other targets, the best choice is the imaginary part of signal for low-frequency scanning. The same diagram exhibits splitting of the peak for all three shallow-depth targets. The diagram plotted for low frequency and differential signal phase reveal all the targets except for target No.13 (the deepest one). When we plot the diagram for a higher frequency, we can see only the targets as deep as 0.5 m (targets No.8, No.9, and No.10).

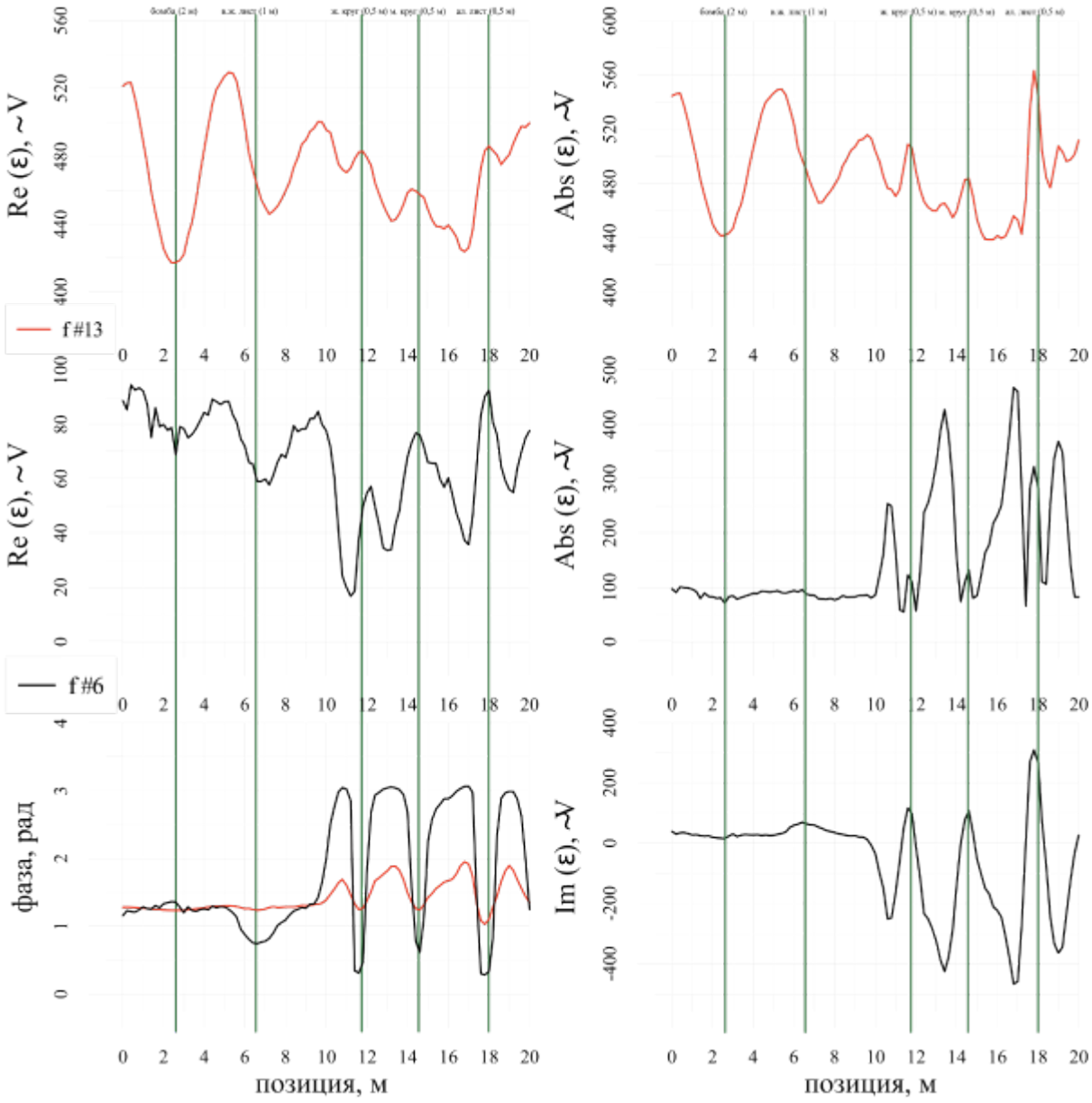

Figure 13 – Diagram for MFS signal No.29 along the line No.4.

The diagram plotted along line No.5 (Figure 14) shows that position of anomalies is not the same as actual position of objects. This may be caused by operator's mistake in identifying of lines current coordinates or by a wrong step in taking the measurements. One can see distinctively only target No.11, which has the highest depth of burial – 2 m. The diagrams plotted from data on signal modulus or imaginary part (for lower frequency) we can see the other anomalies. But we cannot identify them with specific targets because of coordinates mismatch.

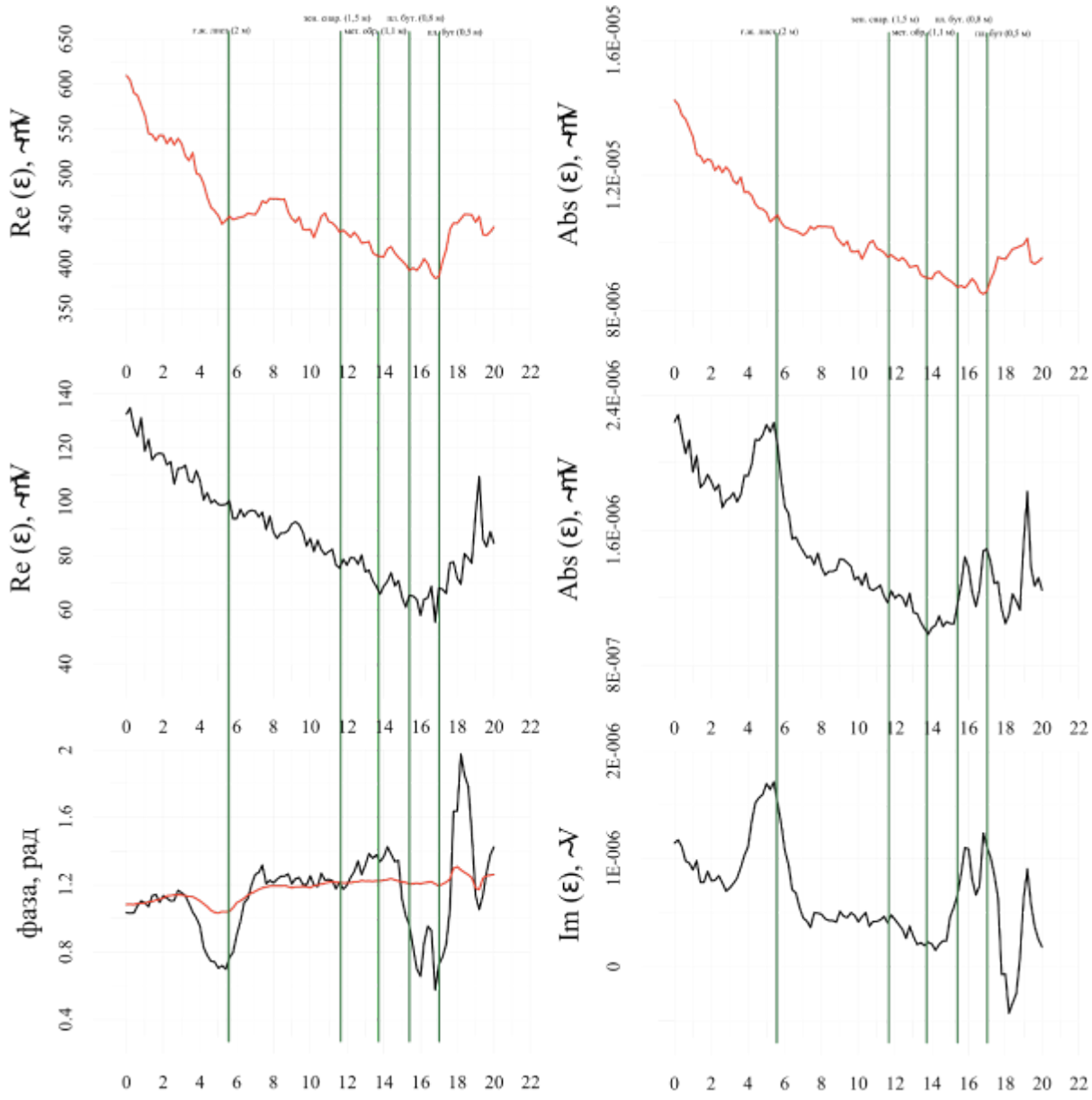

Figure 14 – Diagram for MFS signal No.27 along the line No.5.

The sections along line No.4 (Figure 15) and diagrams also give a rather accurate identification of target coordinates in the line. In all section-processed data, the anomalies are seen for targets No.8, No.9, No.10 (depth 0.5 m). Only for a section reconstructed from the real part of signal, the anomalies are blurred. The other types of sections show all three targets and the target No.12 as well. This target No.12 is visible in the section plotted from the data of differential signal phase (this section shows the images from target No.13).

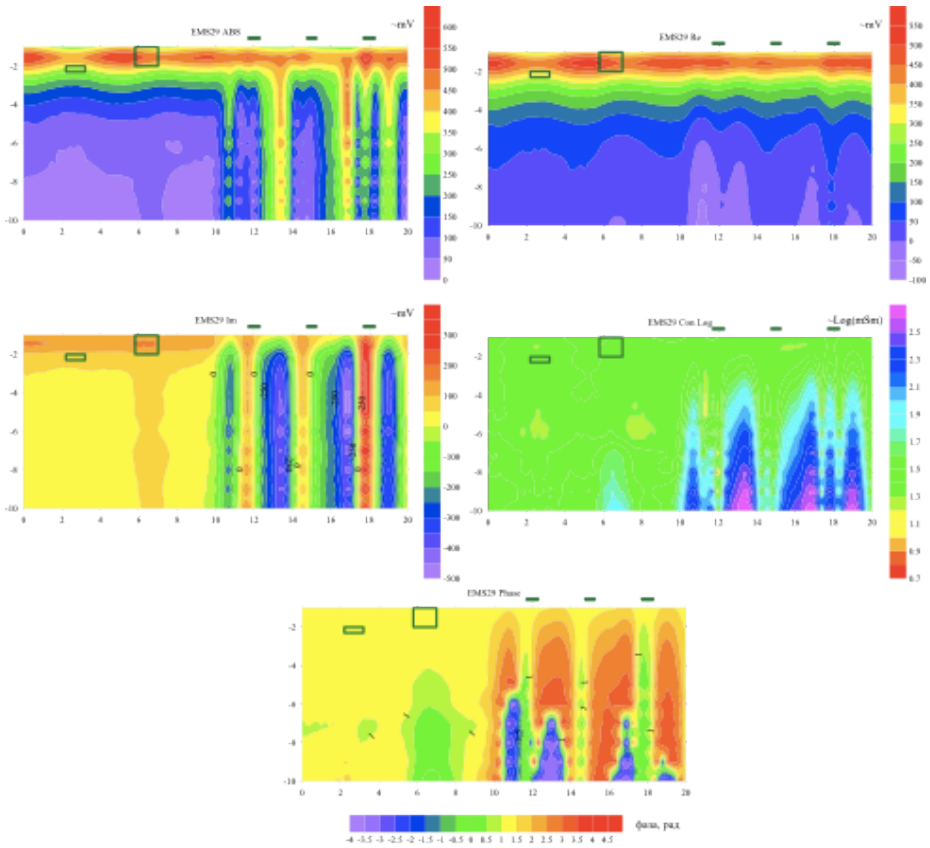

Figure 15 - Sections plotted from MFS data No.29 along the line No.4

Along the line No.5 (Figure 16) we plotted sections and target No.11 is very distinctive in this figure. The section build from real-part signal carries no anomaly that would reflect position of an object along this line. Like for the plotting along previous lines, this type of section is less informative. The section plotted from data on differential signal phase, we see not only anomaly of target No.11, but also the position of target No.7 on this line. Targets No.4 and No.5 are traced down, but anomalies from these objects overlap partially. Here target No.6 is best seen in the section produced from data on conductivity logarithm.

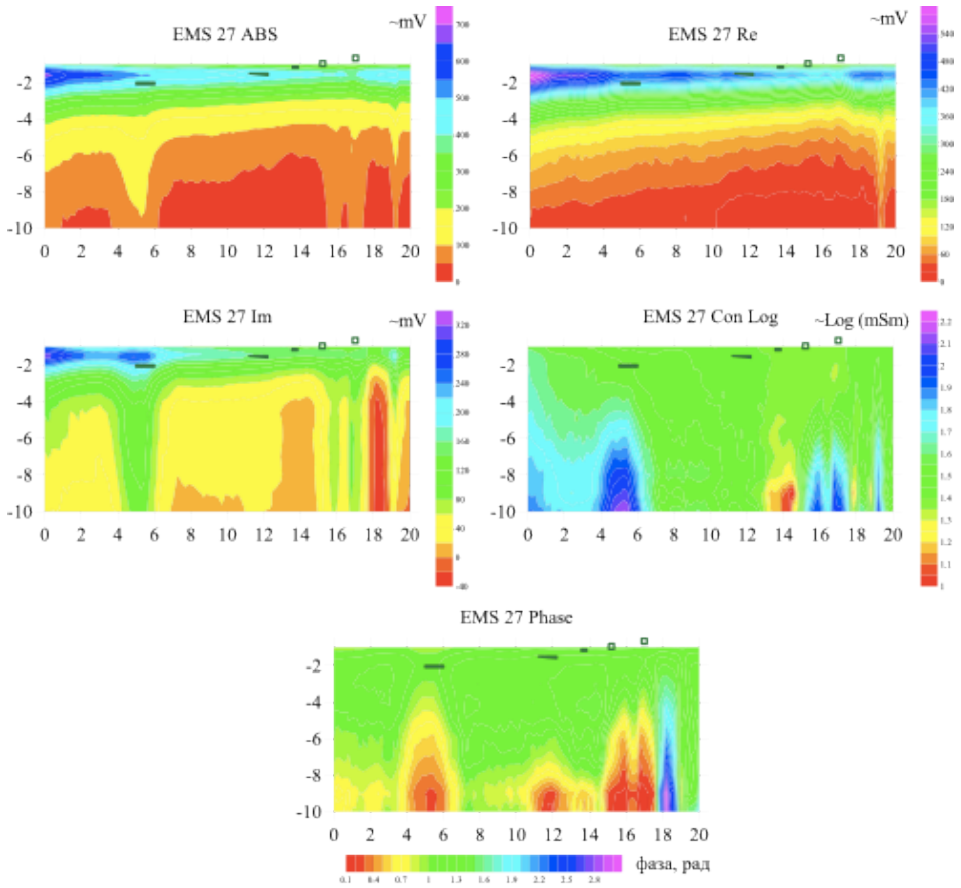

Figure 16 - Sections plotted from MFS No.27 along line No.5

2.4 Results of jobs on electric tomography taken in the modes of resistivity method and induced polarization (data taken along line No.1)

We took measurements along line No. 1 (Figure 3); the scanning method was electric tomography in the mode of resistivity measurement and induced polarization.. We applied different configuration of measurement apparatus (Figure 17, Figure 18): Schlumberger (SCH) array, two-electrodes configuration (PP), direct and reverse trielectrode (PD), dipole (DD), and multigradient (MG). We made inversion of primary data on the limited and extended grid of resistances (see the subscript **ext** in graphs).

The sections obtained by inversion from resistance parameter reflect the geological structure of the medium along the tested line. One can see the difference in scanning depth, resolution of method and inversion artifacts: this agrees with results of simulation and synthetic data described above. Local conducting (metallic) objects are not revealed in geoelectrical sections. Inversion of data from induced polarization method obtained on dipole-based apparatus (Figure 18) give us certainly positions of all deployed targets (two aluminum churns and two metal barrels, see table 1). The deeper targets are seen no so distinctively as shallow ones. One can see also several artifacts of inversion that is the case of actual field jobs

could be falsely interpreted as a metallic object. It seems reasonable to test out different versions of apparatus in the induced polarization mode ort variation of inversion parameters by parameters of induced polarization.

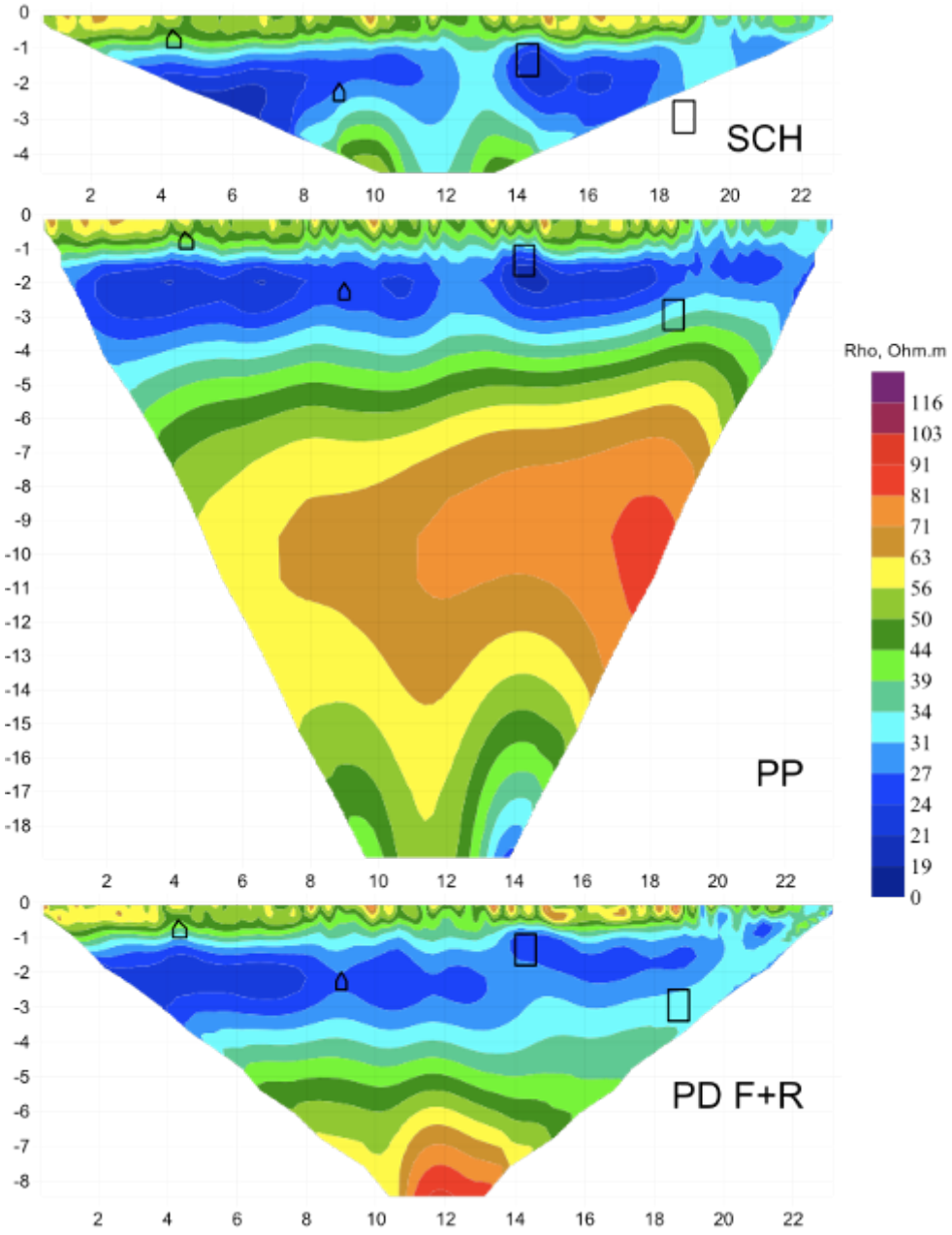

Figure 17 – Result of 2D inversion of data of electric tomography obtained on the test line using arrays Schlumberger, two-electrodes, direct and reverse trielectrode array.

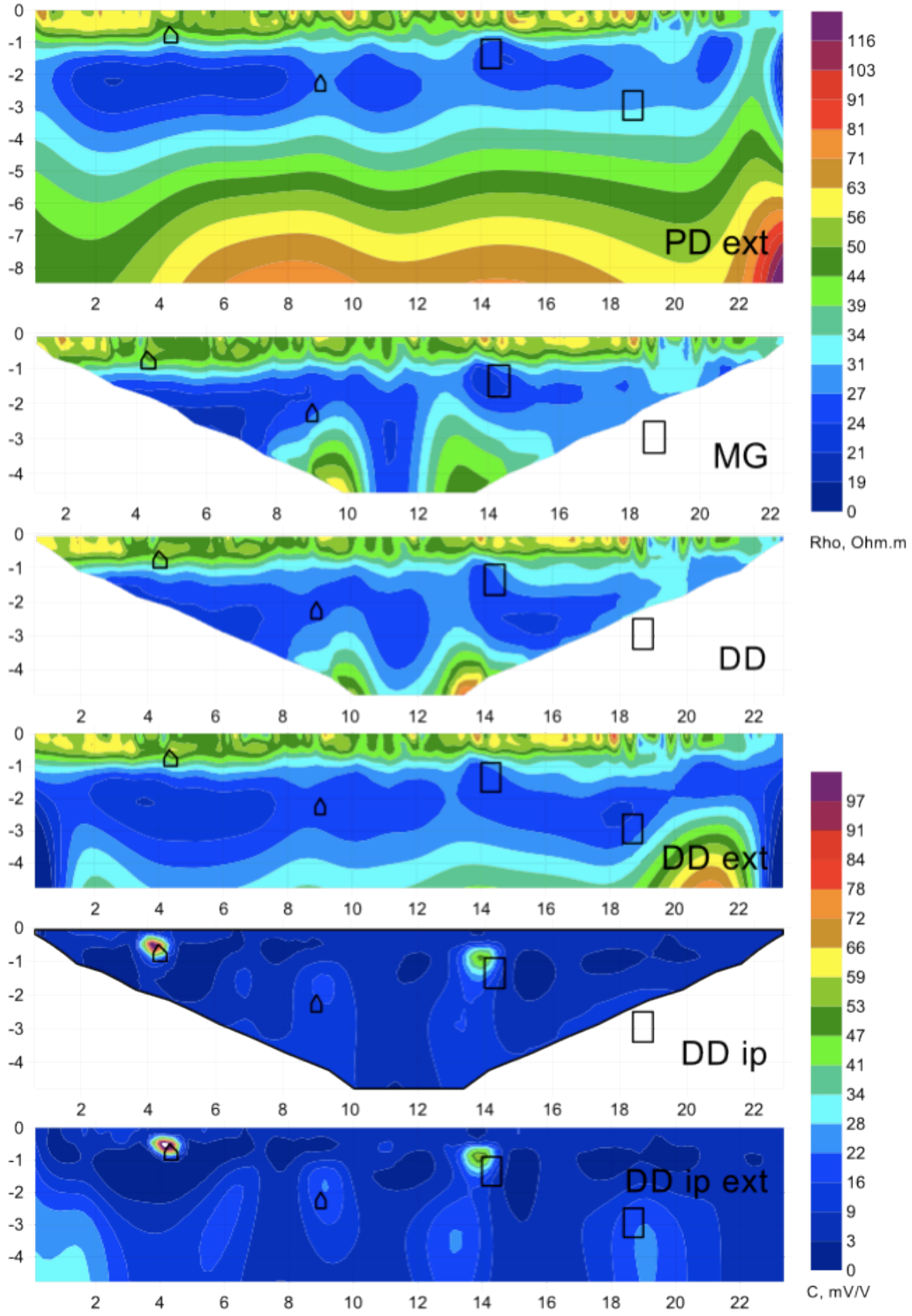

Figure 18 - Result of 2D inversion of data of electric tomography obtained on the test line using trielectrode and dipole arrays.

3 Scanning with discrimination between ferrous and nonferrous metals

In publication [Svetov, 2008] a diagram (Figure 19) is plotted that describes the curves for sounding above non-ferrous and ferrous metals. These graphs have features explained as qualitative difference between behavior of real and imaginary parts of signal.

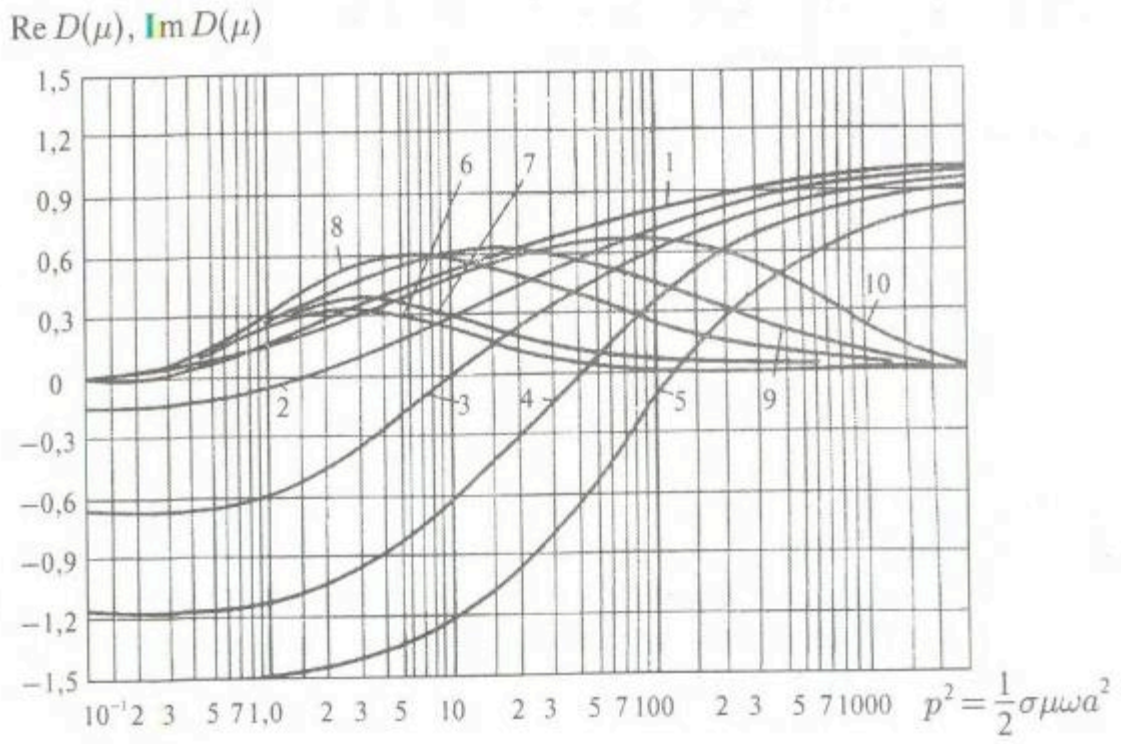

Figure 19 – The plotting of function $D_1(\mu)$. $1-5-\mathrm{Re}\,D_1(\mu), 6-10-\mathrm{Im}\,D_1(\mu)$. **Curves 1 and 6; 2 and 7; 3and 8; 4 and 9; 5 and 10 correspond to parameters**

$\mu_1/\mu = 1{,}0; 1{,}25; 2{,}5; 5{,}0; 10{,}0.$

To study the possibility of differentiating different types of metals with the multifrequency sounding method implemented in MFS apparatuses, we carried out the following experiments. Different types, of metal sheet (copper, aluminum, iron) were deployed underground on one scanning line. The line length was 20 m, and scanning step on this line was 0.5 m. Thus, we obtained three sets of curves as the device was moved along every object. Here we present the graphs of signal variation along the line (Figure 20). We analyzed separately the real and imaginary part of signal for every station. Depending on a station, the curve behavior was different. Even when metallic objects produce a strong working signal, the curves not always have characteristic differences. At the station of 10 m, nearby placement of metal sheets, the behavior of curves produced by an iron sheet is different for that for non-ferrous metals

(Figure 21). These differences in curves are similar to description published by Svetov (Figure 19).

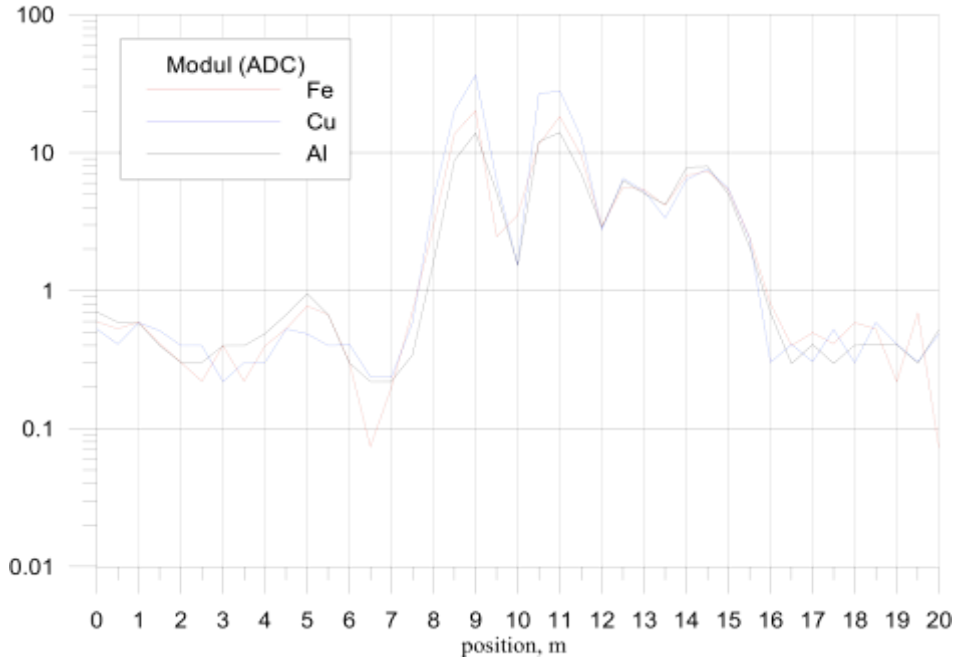

Figure 20 - Variation in signal modulus for every type of metal along the line of scanning.

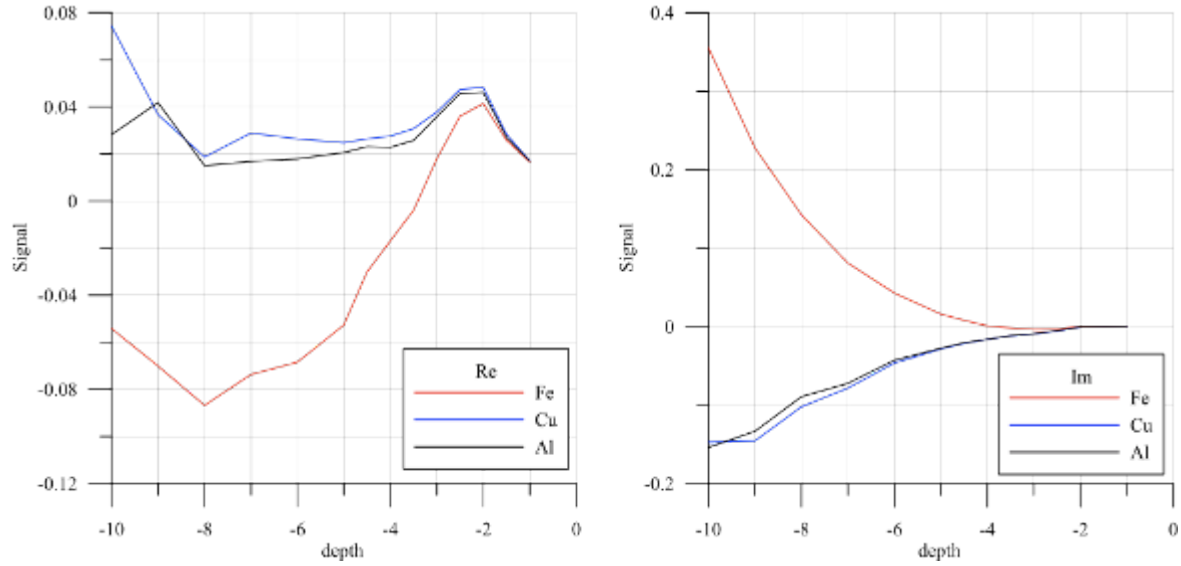

Figure 21 – Curves for Re and Im parts of signal vs. frequency for the 10 m station.

With the goal of studying this effect in field conditions, a series of field jobs was carried out with MFS devices on the Klushi test site. Different metallic objects have been buried within square No. 14 at this test site. The field data were calculated into map of apparent resistivity distribution (Figure 22). The top part of this square hides three copper sheets with different orientation, and the bottom part of this square hides iron sheets buried. We picked up the direction of scanning line South-North, and the distance between scanning lines was 0.2 m.

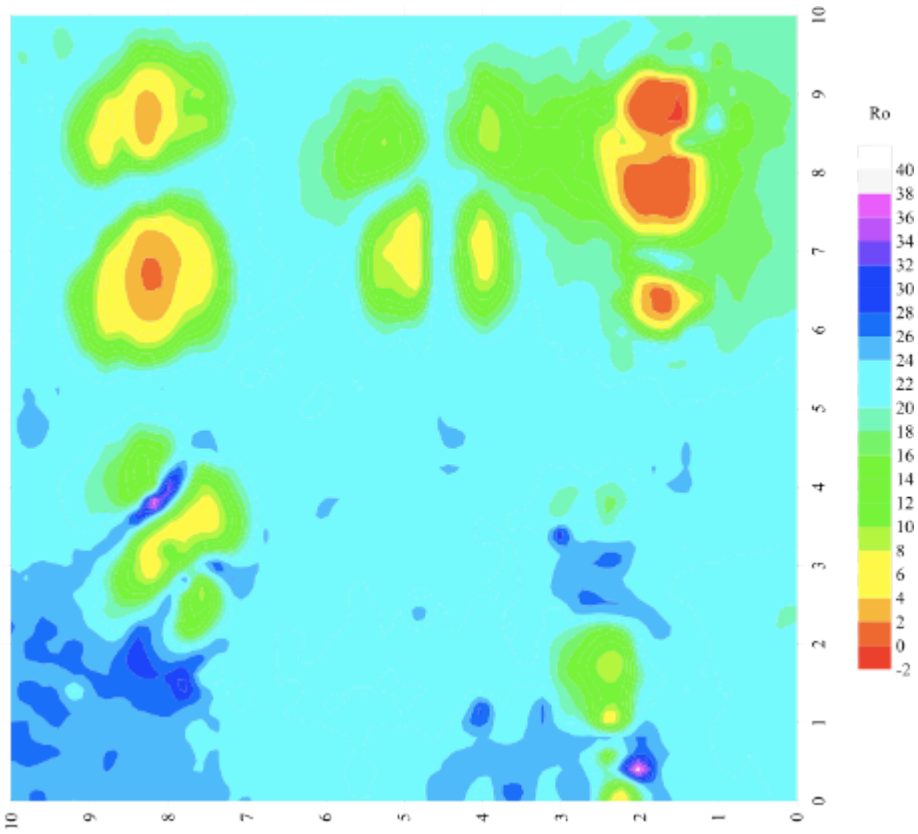

Figure 22 – Resistance map for square No. 14.

Then we plotted the sounding curves for the real and imaginary part of signal. While data processing, we made normalization on the phase, current, zero, and frequency. Every component of signal has two tables. The data from the first table (Graph) was the basis for plotting of curves along lines for any value of frequency. The data from the second table (Tabl) was the input for curves for all frequencies (frequencies are recalculated into depth parameter) for every station on a chosen line.

The curves of MFS sounding were analyzed for the selected lines (also called profiles) passing directly through a metal object and slightly apart of the target. The curves were plotted for frequency 7 kHz, and pictures depict the level of signal which is enough for founding the object underground.

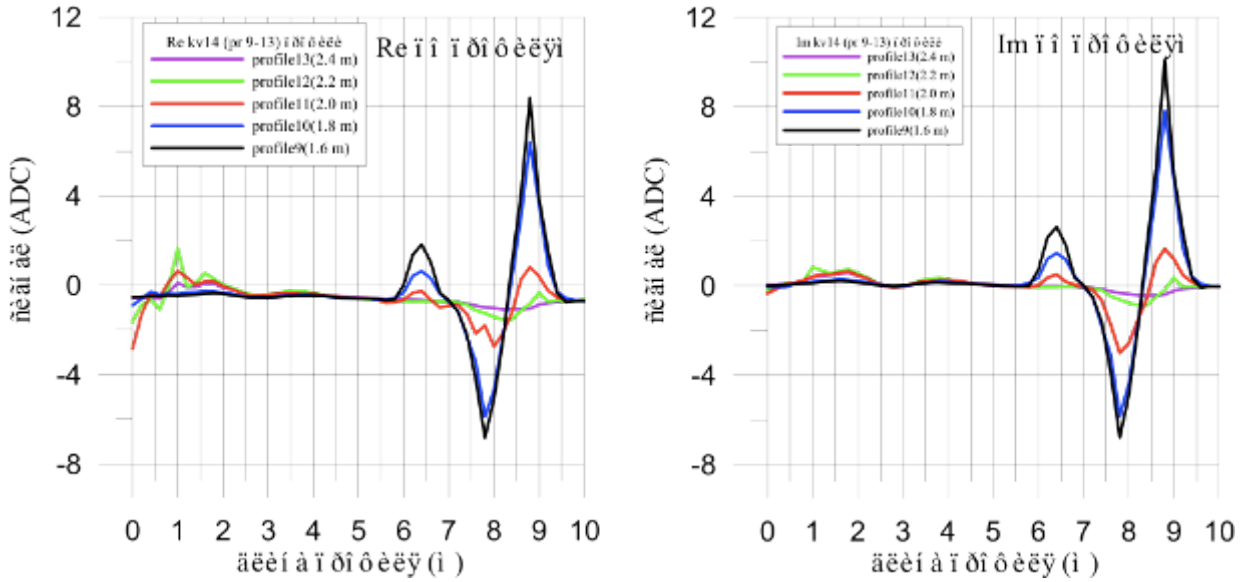

Figure 23 – Plotting of signal for all profiles at frequency # 5.

All plotted diagrams show that the behavior of curve is different for scanning results for non-ferrous and ferrous metals. We also plotted two types of diagrams: with normal signal (from field experiment) and a signal with the reference-medium signal subtracted (Figure 24, Figure 25).

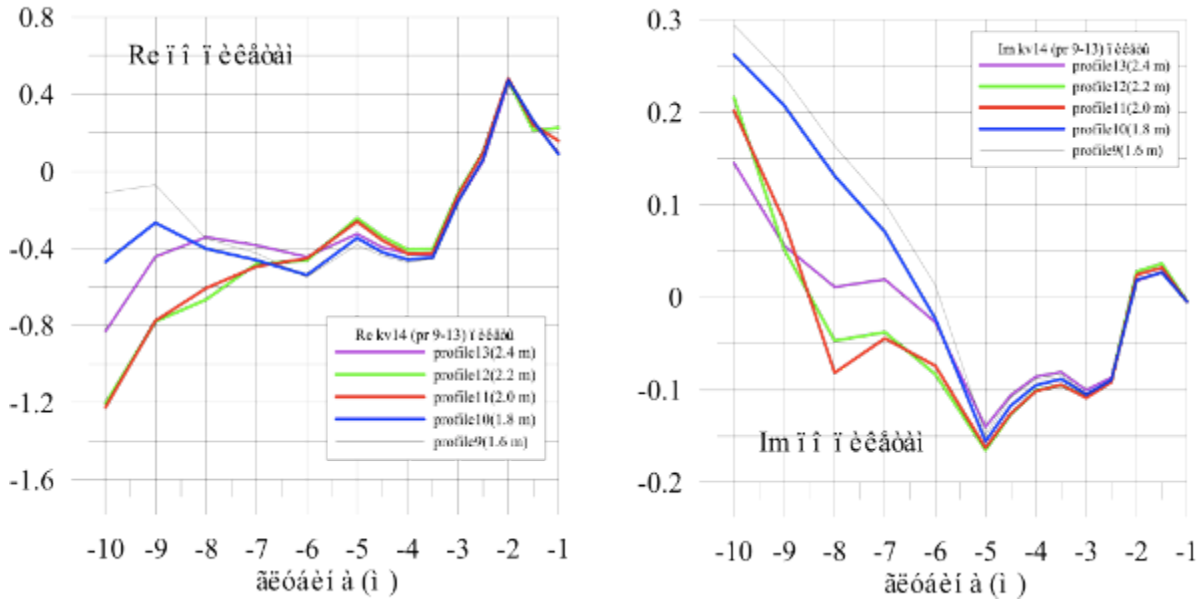

Figure 24 – Curves of object sounding, Re and Im components (normal signal) for a 2.8 station taken for different lines of scannng. The station is close to an object composing ferrous metal.

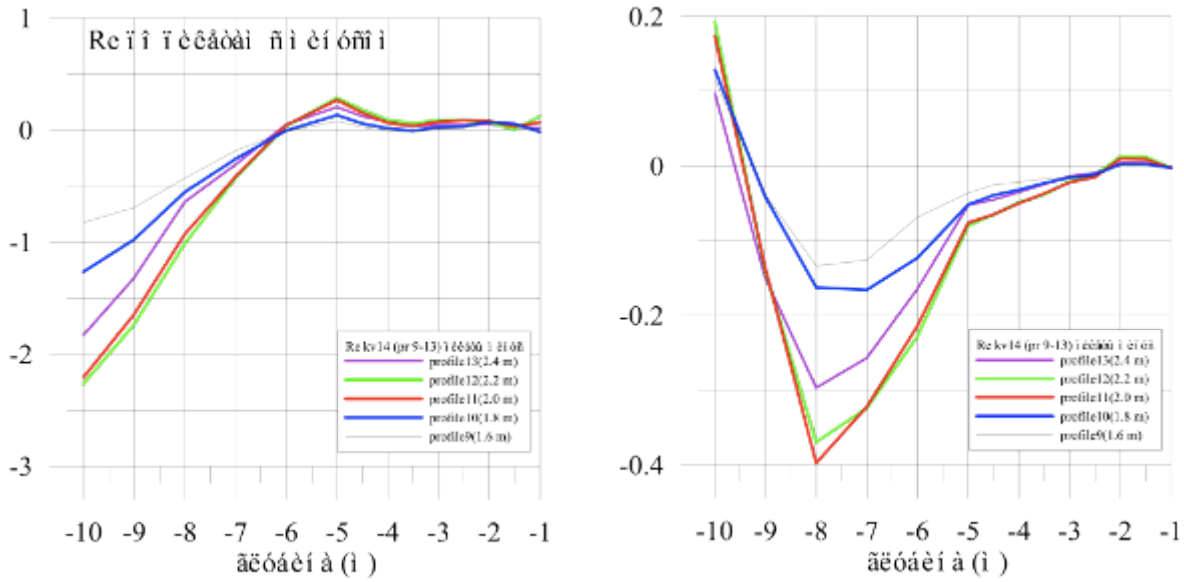

Figure 25 – Curves of sounding, Re and Im components (signal with subtraction of signal from reference medium) for the 2.8 station taken for different lines. The station is close to an object comprising ferrous metal.

These curves (Figure 24, Figure 25) demonstrate the following behavior. The real component of signal begins from negative values, and then it crosses the zero level and then deviate from zero towards positive and negative halves. As for the imaginary component of signal, it starts from positive values and later it crosses the zero level. This behavior is typical for curves of scanning above a ferrous metal object.

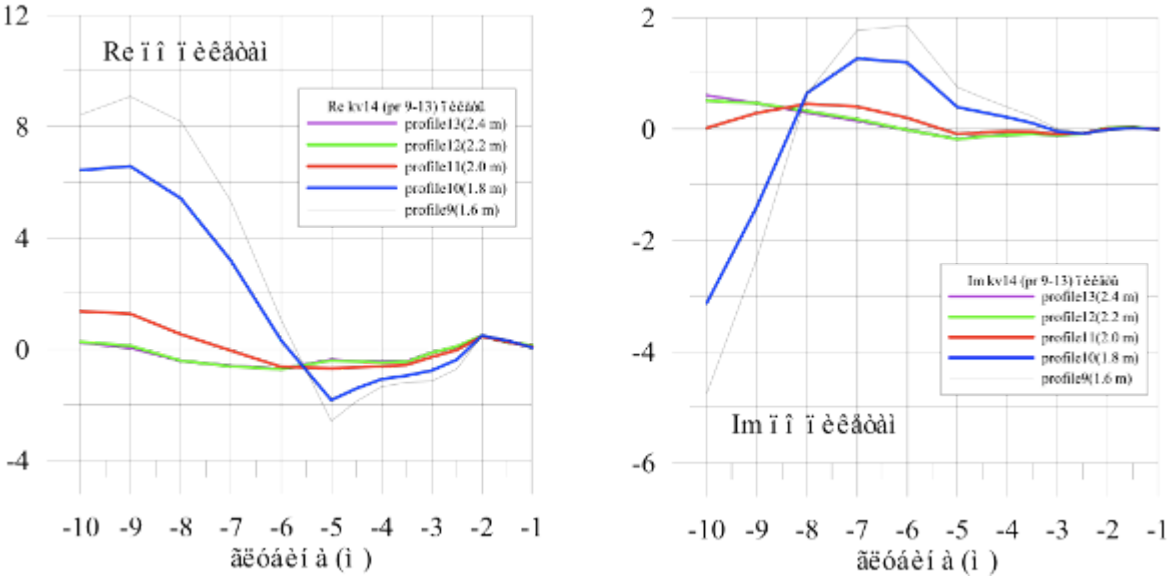

Figure 26 - Curves of sounding, Re and Im components, (normal signal) for the 6.6 station at different lines. The station is close to an object made of non-ferrous metal.

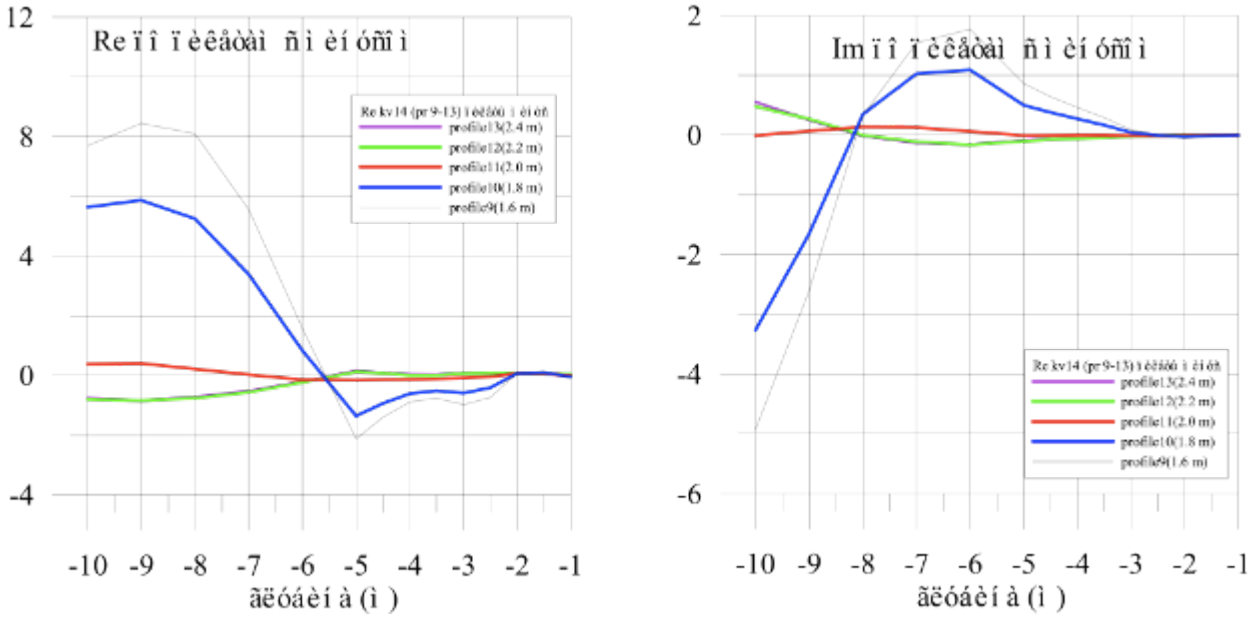

Figure 27 - Curves of sounding, Re and Im components, (signal with background subtraction) for the 6.6 station taken for different lines. The station is close to an object made of non-ferrous metal

The curves taken for 6.6 station (Figure 26, Figure 27), the following behavior is typical. Curves for the real part of signal start off from positive values, cross the zero level and deviate slightly to positive or negative side. For the imaginary part of signal, quite opposite, the value starts in negative half and then crosses the zero. This is typical behavior of objects mad of non-ferrous metal.

Behavior of signal at a station that corresponds to the reference medium (background signal) is similar for behavior of signal from non-ferrous metal, but the level of signal is much lower (Figure 28).

In summary, we should admit that interpretation of data collected at the test site is difficult because of irregularity of sounding curves. Even the attempt to make correction for a reference system did not solve this problem. The possible reason is low quality of calibration (adjustment) of the versions of MFS devices used in these test field jobs.

However, the collected data allow us to claim for curtain that MFS technique can be applied for discrimination of metals underground. The key approach to this discrimination is analysis of behavior of sounding curves obtained above anomalies: separately for real and imaginary parts of signal. The correction of this technique and receiving the results compatible to theoretical calculations needs additional testing on the test site with properly calibrated devices.

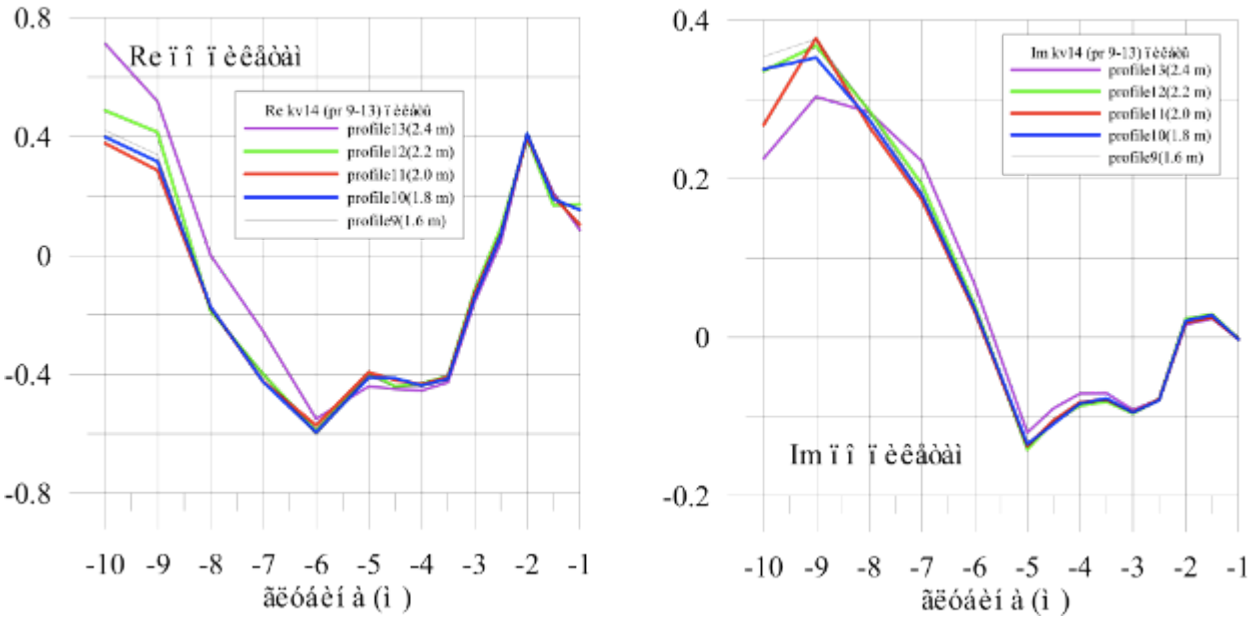

Figure 28 - Curves of sounding, Re and Im components, (normal signal) for 5.0 station along different lines. The station is above the reference medium.

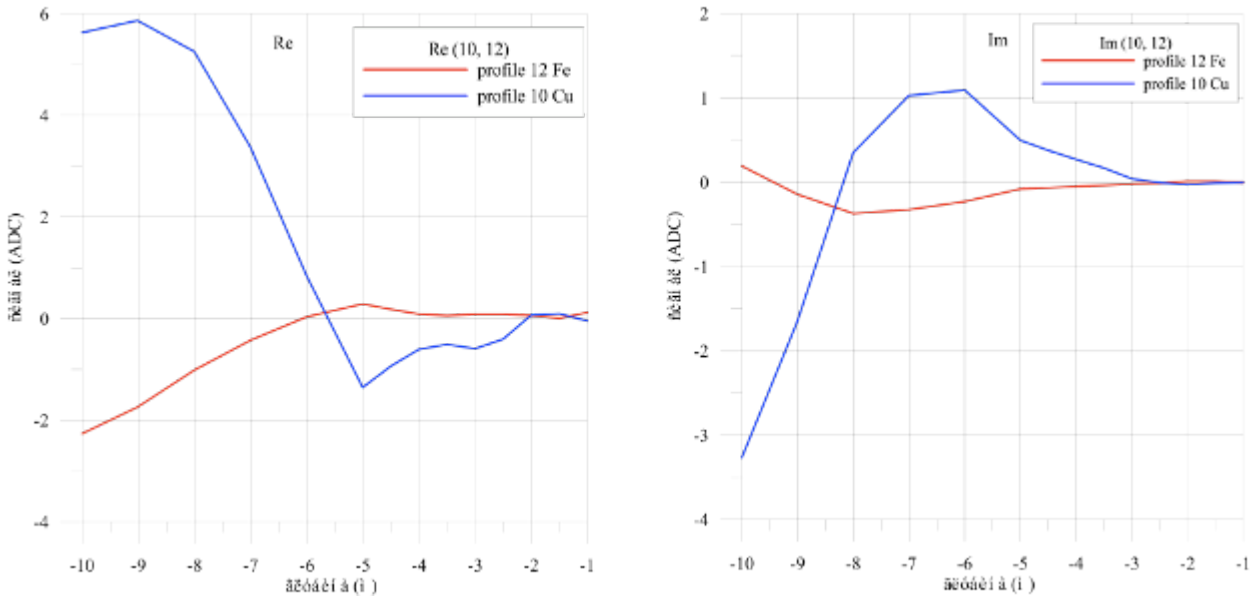

Figure 29 – Curves of Re and Im components of signal above iron and copper objects

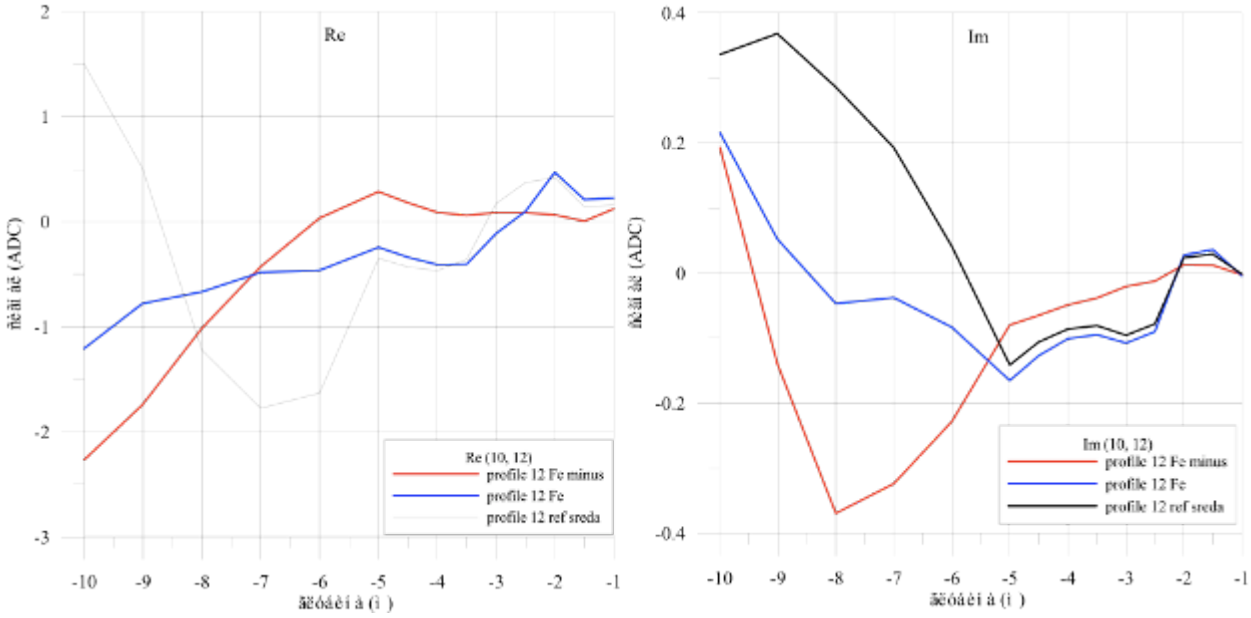

Figure 30 – Curves for Re and Im components of signal above iron object (normal signal) and a signal with subtraction of contribution from reference medium (and a curve for reference medium)

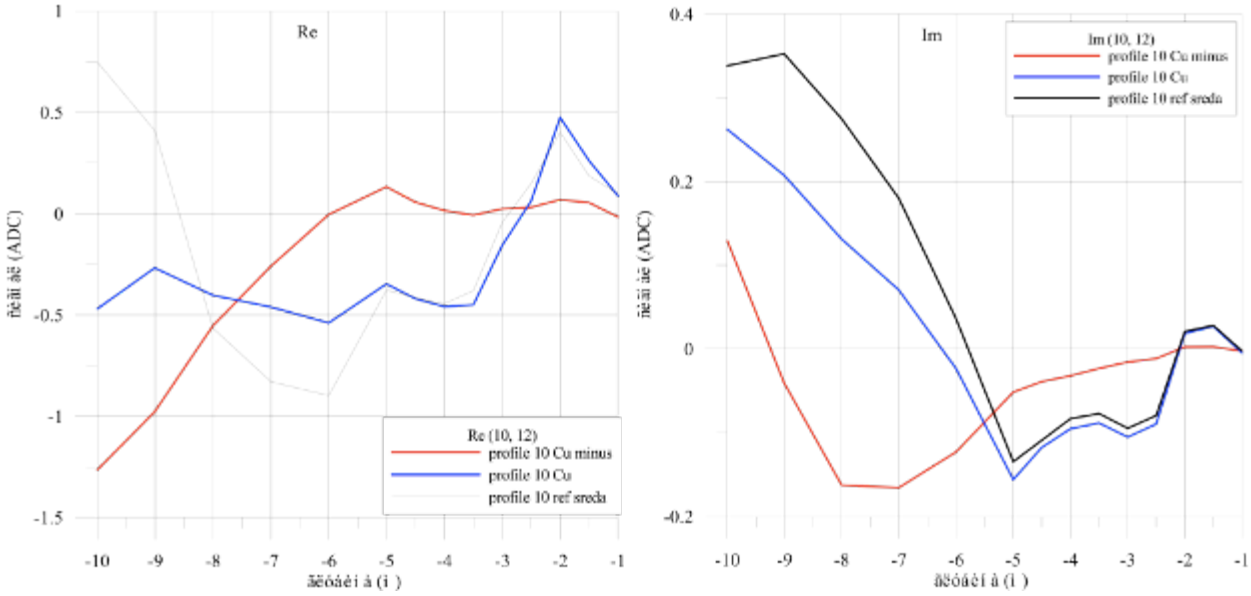

Figure 31 – Curves for Re and Im components of signal above the copper object (normal signal), the signal without reference medium contribution, and signal from reference medium

CONCLUSION

In the framework of development a low-depths test site at the territory of Institute's stationary facility, we made some preliminary testing using MFS device: this was need to clear positions of any possible pipelines or cables (utilities) already available at this territory and to

identify the area suitable for deployment of test targets. We picked up 10 squares with area of 100 sq.m. each, where we deployed 33 test targets that imitate different real objects.

We have conducted areal survey of 5 squares with MFS methods, performed linear sounding along 7 standard lines using different versions of MFS devices. Electric tomography method was applied to one square, and one reference line was chosen for ET method in the modes of resistance and induced polarization.

All acquired experimental data gave us information about the scanning depth limit and resolution of applied tools; this put foundations for further improvement of methodology of MFS and ET methods.

To the present moment, only a smaller part of planned field jobs have been completed. And the amount of totally processed and interpreted field data (from the entire bulk of data) is about 65%.

Table 2 – Aggregated analysis of multifrequency sounding along lines No. 1 ,2, 4, 5

			Score				Re			Im				
	No.	Object	Re	Im	Abs	Ph	EMS 26	EMS 27	EMS 29	EMS 26	EMS 27	EMS 29	EMS 26	EM
	21	Churn 0.5 m	0	2	2	2	0	0	0	-	-	-	+	
	22	Churn 2 m	1	0	1	2	+	+	+	0	0	0	+	
	23	Barrel 0.9 m	2	2	2	2	-	-	-	-	-	-	+	
Line1	24	Barrel 2.5 m	0	0	0	0	0	0	0	0	0	0	0	
	27	Sheet 0.8 m	1	1	1	1	+	+	+	+-	+-	+-	+-	
	28	v. sheet 0.45	1	1	1	1	-	+	-	+-	+-	+-	+-	
	29	Sheet 0.2 m	1	1	1	1	+	+	+	+-	+-	+-	+-	
	25	Barrel 1.3 m	1	1	0	2	-	-	-	-	-	-	-	
Line2	26	Barrel 1.8 m	0	1	0	1	0	0	0	-	-	-	0	
	13	Bomb 2m	2	0	2	1	-	-	-	0	0	0	-	
	12	V. met.sheet 1m	1	1	1	2	-	-	-	+	+	+	+-	
	10	Fe sheet 0.5 m	2	2	1	1.5	0	+-	+-	+-	+-	+-	0	
	9	Co sheet 0.5 m	1	2	1	1.5	0	+-	+-	+-	+-	+-	0	
Line4	8	Al sheet 0.5 m	1	2	1	1.5	0	+-	+-	+-	+-	+-	0	
	11	Fe sheet 2. m	0	2	1	2		-			+			
	7	Projectiles 1.5 m	1	0	0	1		-			+			
	6	\Landmines 1.1m	1	0	1	1		-			-			
	4	Treasure 15 l 0.8 m	1	1	1	1		-			+			
Line5	3	Treasure 5l 0.5 m	1	1	1	1		-			+			
		Total score	18	20	18	25.5								

with three sets of MFS devices: No. 26, 27, 29

The aggregated table (Table 2) presents the evaluation of data analysis obtained for electromagnetic scanning along line (profiles) No.1,2,4,5 using three sets of MFS devices (No. 26,27,29). Table 4-7 present (in scorers) the evaluation of target founding using different components of the signal: “0” stands for absence of anomaly above the target, , “1” stands for moderate level of anomaly, “1.5” * good level, “2” – perfect. Using this type of scoring, we estimated productivity of all components of signal taken for 14 underground objects laid along the selected lines (Figure 32). Even at this semi-qualitative approach for evaluation, we can see that if we take for analysis the real component (18), imaginary component (20), and signal modulus (18), their capacity is almost equal. However, using of phase of signal as input data (score 25.5) creates better opportunities. This is because the revealing of a target through the differential signal phase usually not worse (or slightly worse) than for the “best” of signal components. We should say that this is also not true about the signal modulus. WE should emphasize that the real and imaginary parts of signal are complimentary in information obtained – they work differently for different types of targets.

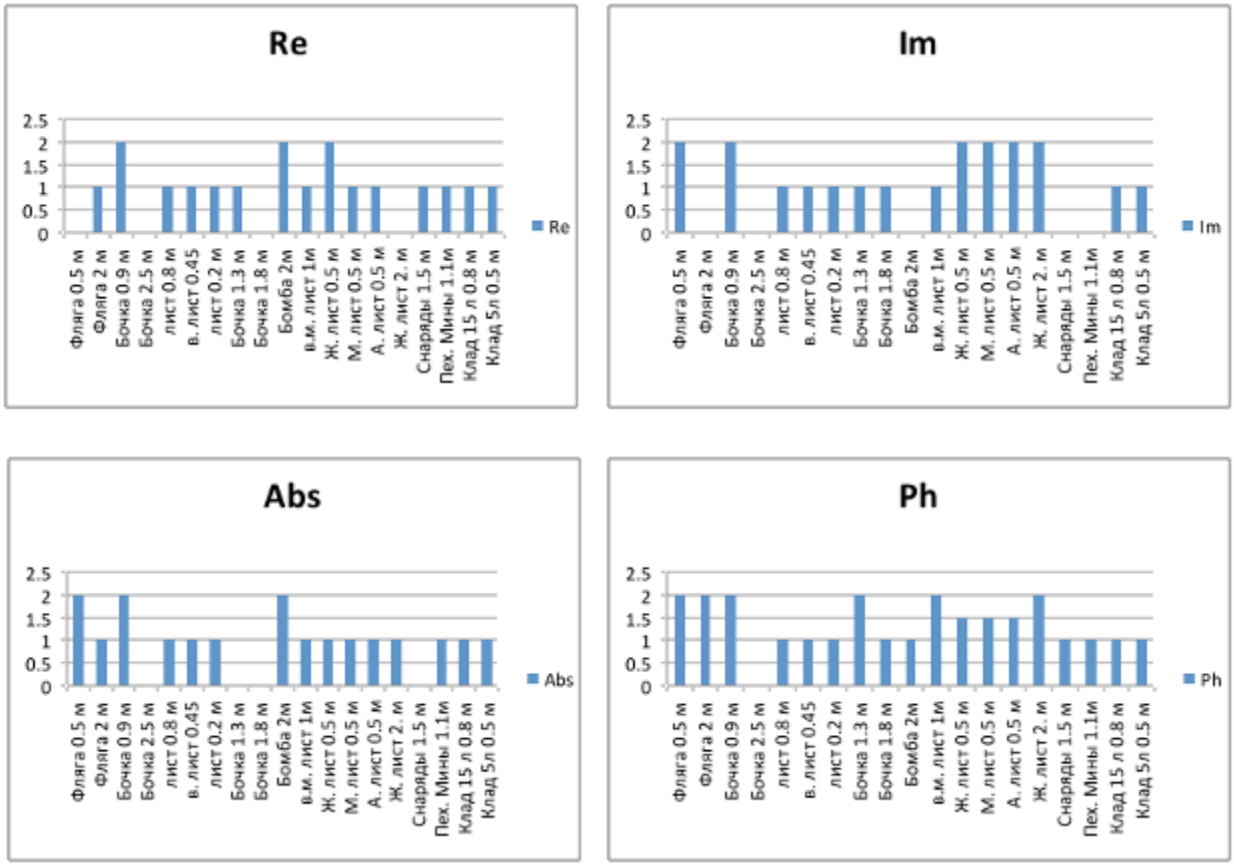

Figure 32 – The score evaluation for working with different components of a signal

The analysis of field data also demonstrated the fact that scanning results can be different for using of different species of similar devices. The reason for this is some subjective small

factors as tracking the scanning line (done just before the job), orientation and elevation of teh device above the ground. Not for a single line from three selected line, it was possible to get identical data, even in qualitative sense – (see Table 3). The data for MFS No.27 in two cases were shifted. Data fro MFS No.26a and MFS No.29 were different form the rest of data for two case. This tells us about necessity to bring some corrections into methodology of works.

No.	MFS26	MFS27	MFSC29
Line1	+	+ Shift	+
Line2	+	+	-
LIne4	-	+ Shift	+

Table 3 – Comparison of results obtained with different devices

In this project the diagrams and sections along the selected lines were plotted in the ADC units which a proportional to registered e.m.f. (V) and to electrical conductivity. These units were chosen to make the mean square of device's noise to bell than 1 unit of ADC. The visual (qualitative) analysis of data along selected lines demonstrated that often the noise in diagrams is by factor of 2-3 higher than these values. However, it a half of jobs this negative effect can be reduced by choosing a higher frequency. For the rest of data the level of noise remains almost the same on all frequencies. We present the evaluation of this effect (see Table 4): "=" means that noise remains steady, and "-" means that the noise declines with frequency growth. Actually, any regularity for this phenomenon was not discovered al all. Any unique device (during one field job) does not show stability in the noise level. Maybe, this is related to imperfection in electric screen-out (protection) of apparatuses.

	MFS26		MFS27		MFS29	
No.	Re	Im	Re	Im	Re	Im
Line1	=	-	=	-	-	-
Line2	-	-	-	-	=	-
Line4	=	=	=	-	-	-

Table 4 – Evaluation of change in the noise level with a higher frequency

The interim conclusions of this stage of project are the following and we can emphasize several effects about electromagnetic sounding:

1. Different types of targets are identified using either real or imaginary component of the signal. The target position is better characterized by the imaginary component.

2. More often, the deep metallic objects are identified only through data about real component of e.m.f., and this is seen as reduction of electric conductivity in comparison with environment.
3. The differential signal phase is a good tool for presenting of sounding results: it reflects peculiarities of both components of signal. Moreover, some targets are better identified through phase of signal. Although we can show the cases than the imaginary component is more informative in interpretation of profiles.
4. Although the signal modulus also carries information about both components, the diagrams, sections, and maps based on this class of values are less informative than alternatives.
5. We observed regular jumps in phase value (+\- π radian) for scanning with low frequencies.
6. We recorded different levels in apparatus noise: sometimes it reduces with frequency growth, but it also varies from a device to device and from a line to another line.
7. There was no compete consistency in survey results: they can vary depending of version of device, operator, procedure of putting a line, etc.
8. There are some problems in matching of map pieces after interruption in a job (caused by schedule, weather conditions, battery recharge).
9. We observe “stripes” on maps caused by pure mating of adjacent profiles.
10. The targets of different shape, buried at different depths and with different orientation might give several images (from one to five) with this type of devices. This creates problems with interpretation of this input data if the methodology support is insufficient.
11. On the current stage of project, differentiation between objects of ferrous and nonferrous metals is complicated problem: this is explained by inconsistency of results obtained from different targets. In some situation this differentiation between types of metal is possible when linked to theoretical knowledge. But this does not work for all objects.
12. The target object “dig-out" (arranged in square No.10) underwent collapse and this target has no initial geometry parameters.

If the research in this direction is continued, the following tasks are ranked as most important:

1. To give classification for targets and write the technology description that describe the types and number of anomalies (images) from different classes of objects. The instruction shall give recommendation for choosing the most productive component of signal and the form of presentation.
2. To deal with jumps of signal phase.

3. To accomplish a permanent marking of reference lines. To define the uniform orientation of MFS device for further research.
4. To develop a technique of operation with MFS devices using a support (chose of material, height of support) which would help to eliminate inconsistency in scanning along the same line (or one job for several lines).
5. To study and eliminate the cause of pure matching of map sections after device on/off.
6. To study and find solution for better electrostatic protection of devices.
7. To learn more about problem of differentiation between ferrous and non-ferrous metals.
8. Continue field tests with objects deployed but not scanned yet.
9. To evaluate necessity of modification of available targets and deploying the new targets at the test site.

APPENDIX 1

Here is a photo report about the test site development, parameters and stricture of geophysical underground targets.

Fig. 1. Plastic tube with length 1.8 m, D= 110 mm. Deployment depth is 0.5 m.

Fig. 2. Plastic tube with length 3.7 м, D= 60 mm. Deployment depth is 0.5 m.

Fig. 3. Trench refilled back without any target. Trench depth is 0.5m.

Fig. 4. Plastic bottle 1 item. (5 leters) with metallic shavings. Deployment depth is 0.5 m.

Fig. 5. Plastic bottle 1 item. (5 leters) with metallic shavings. Deployment depth is 0.8 m.

Fig. 6. Pieces of metal pipes (D 100 мм). The size of target 30*30 см. Deployment depth is 1.1 m.

Fig. 7. «Antiaircraft projectiles». Pieces of round metallic bars with length 1.1 and 0.7 m, D= 7 cm. Piled side by side. Deployment depth is 1.5 m.

Fig. 8. Aluminum sheet 60*40 cm. Deployment depth is 0.5 m.

Fig. 9. Copper disk, D = 0.5 m. Deployment depth is 0.5 m.

Fig. 10. Iron disk, D= 0.6 m. Deployment depth is 0.5 m.

Fig. 11. Horizontal iron sheet 1*1.25 m. Deployment depth is 2 m.

Fig. 12. Vertical iron sheet 1*1.25 m. The top edge reaches the depth of 1 m.

Fig. 13. «Aviation bomb». An iron item made of a tube with length 0.85 м, D= 0.3 m and a welded basement 0.55-0.65 m. H of basement is 0.1 м. Deployment depth is 2 m.

Fig. 14. Steel pipe with length of 4 m, D= 100 mm. Deployment depth is 1 m.

Fig. 15. Steel pipe with length of 5 м, Дом 100 mm. Deployment depth is 2 m.

Fig. 16. Dig-out (room 2*2 m and corridor 1*3м), the roof is at the depth 1 m, the dig-out depth is 1.5 m.

Fig. 17. Plastic can (1 item). Size 35*25*20 см. Deployment depth is 0.5 m.

Fig. 18. Plastic can (3 items). Size 35*25*20cm. Deployment depth is 1 m.

Fig. 19. Plastic cans (4 items). Size 35*25*20 cm. Deployment depth is 1.5 m.

Fig. 20. Brick wall. Wall thickness is 0.5 m, H= 1 m. The П-shaped masonry. The bar length is 3 m, left leg is 3.5m, right leg is 2.3 m. The top face is at the depth 0.5 m.

Fig. 21. Aluminum churn. D of bottom part is 0.35 m, H = 0.5 m. Depth down to the lid is 0.5 m.

Fig. 22. Aluminum churn. D of the bottom part is 0.35 m, H= 0.5 m. Depth down to the lid is 2 m.

Fig. 23. Iron barrel. D= 0.56 m, H= 0.9 m. Depth down to the upper face is 0.9 m.

Fig. 24. Iron barrel. D = 0.56 m, H= 0.9 m. Depth down to the upper face is 2.5 m.

Fig. 25. Iron barrel. D= 0.56 m, H= 0.9 m. Depth down to the upper face is 1.3 m.

Fig. 26. Iron barrel. D 0.56 m, H 0.9 m. The upper face is at the depth 1.8 m.

Fig. 27. Horizontal copper sheet 1*0.6 m tilted to axis. Deployment depth is 0.8 m.

Fig. 28. Vertical copper sheet 1*0.6 m. Depth down to the upper face is 0.45 m (Put on the 1m side).

Fig. 29. Horizontal copper sheet 0.5*0.6 m.. Deployment depth is 0.2 m.

Fig. 30. Vertical iron disk D= 0.6 m. Depth down to the upper face is 0.5 m.

Fig. 31. Horizontal iron disk D= 0.6 m. Deployment depth is 1 m

Fig. 32. Steel pipe with length of 3 m, D 42 mm. Deployment depth is 0.65 m.

Fig. 33. Iron bar with length of 7.5 m. Cross-section 20*30 mm. Deployment depth is 0.7 m.

APPENDIX 2

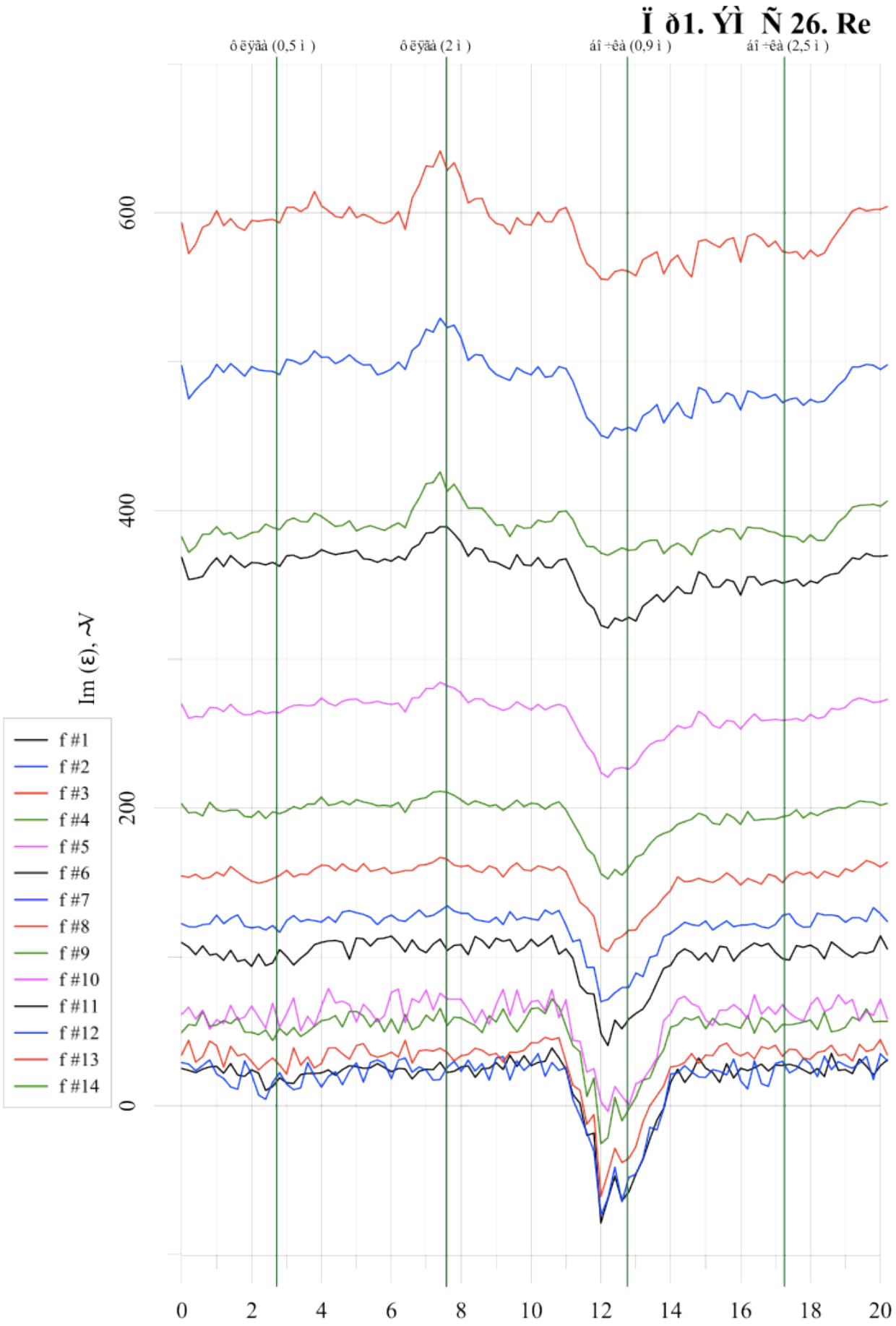

Figure 1. Line No.1. MFS 26. Real part e.m.f.

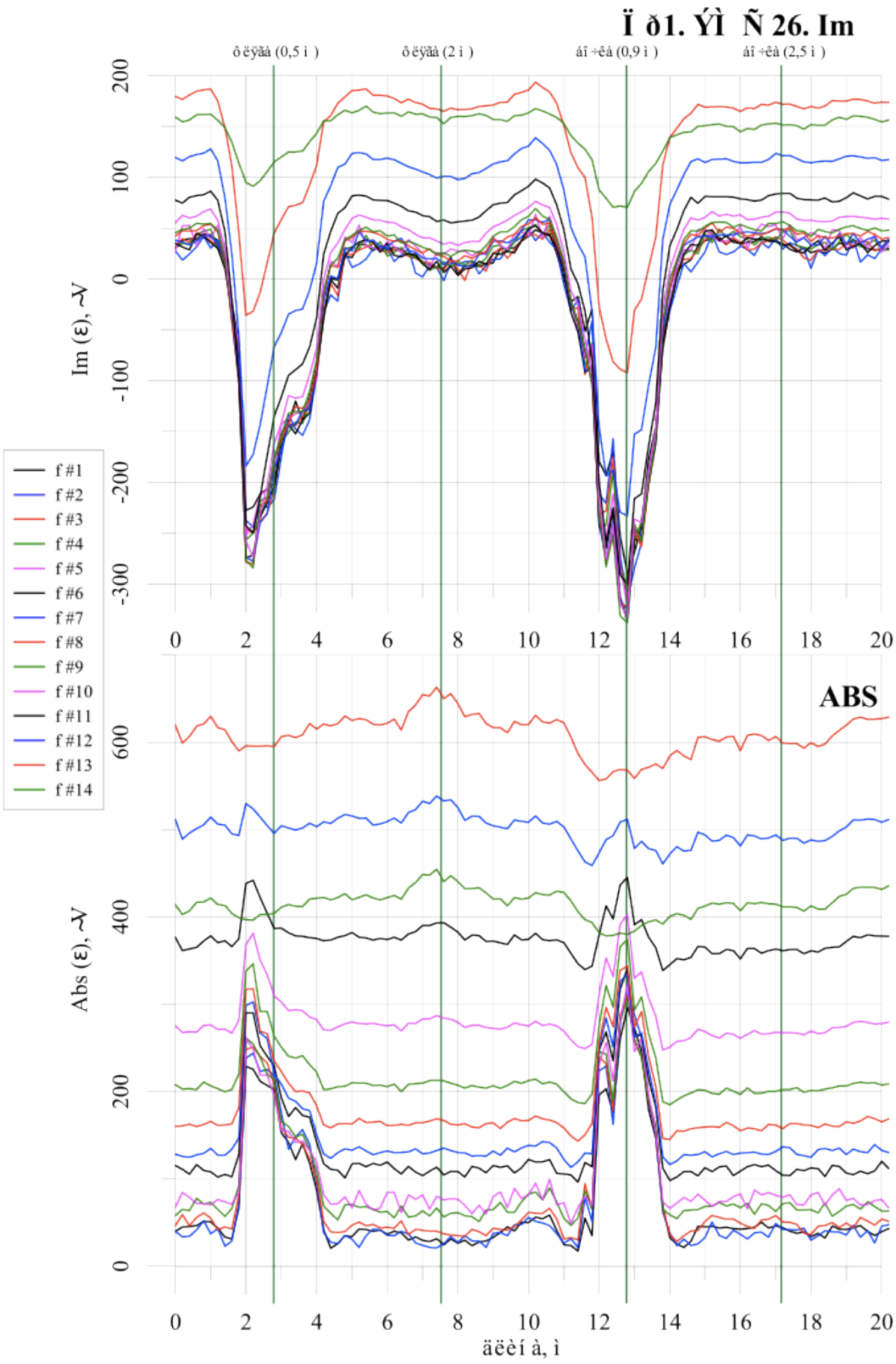

Figure 2. Line No.1. MFS 26. Imaginaryl part e.m.f. and module of e.m.f.

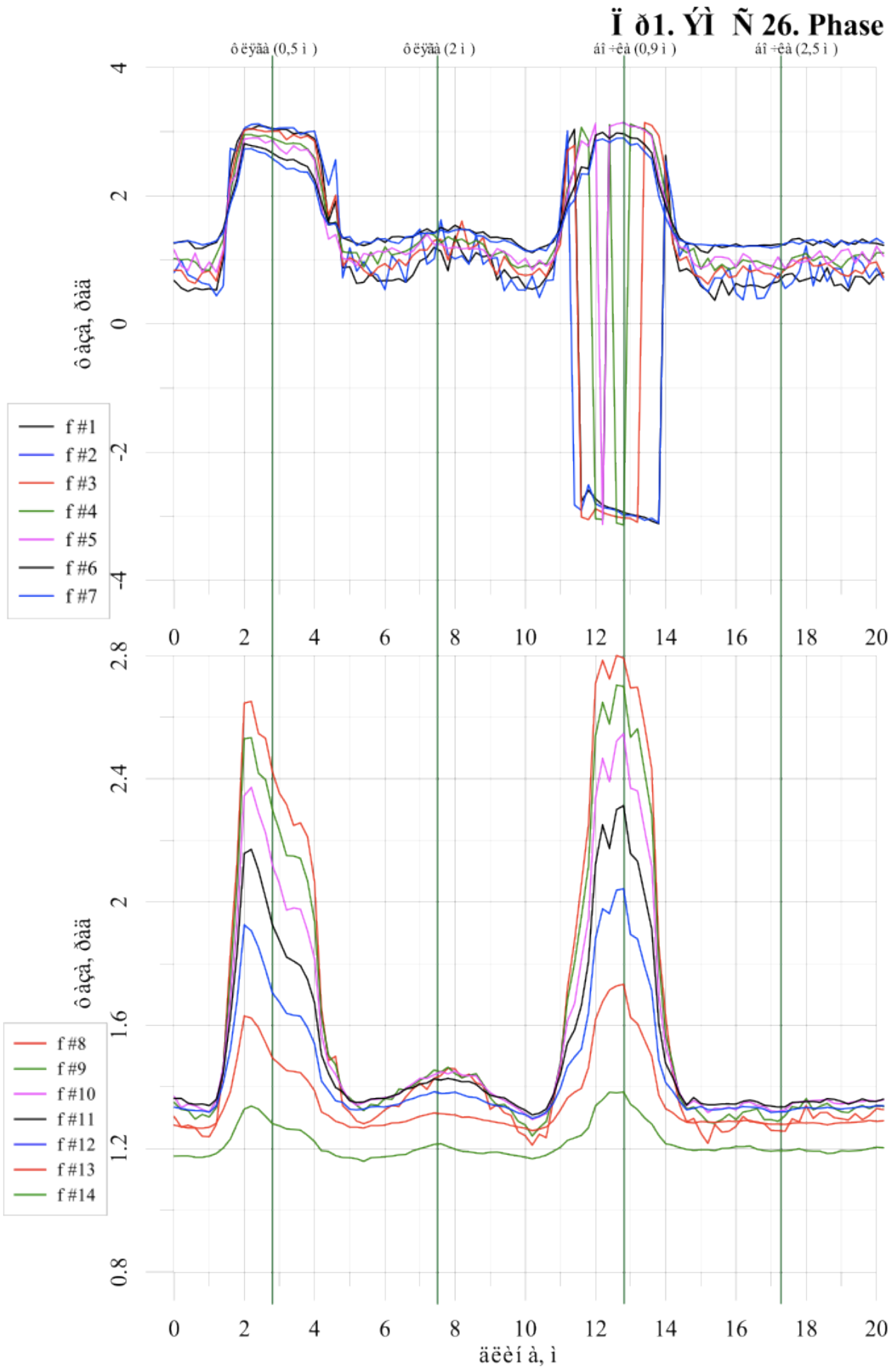

Figure 3. Line No.1. MFS 26. Phase of e.m.f.

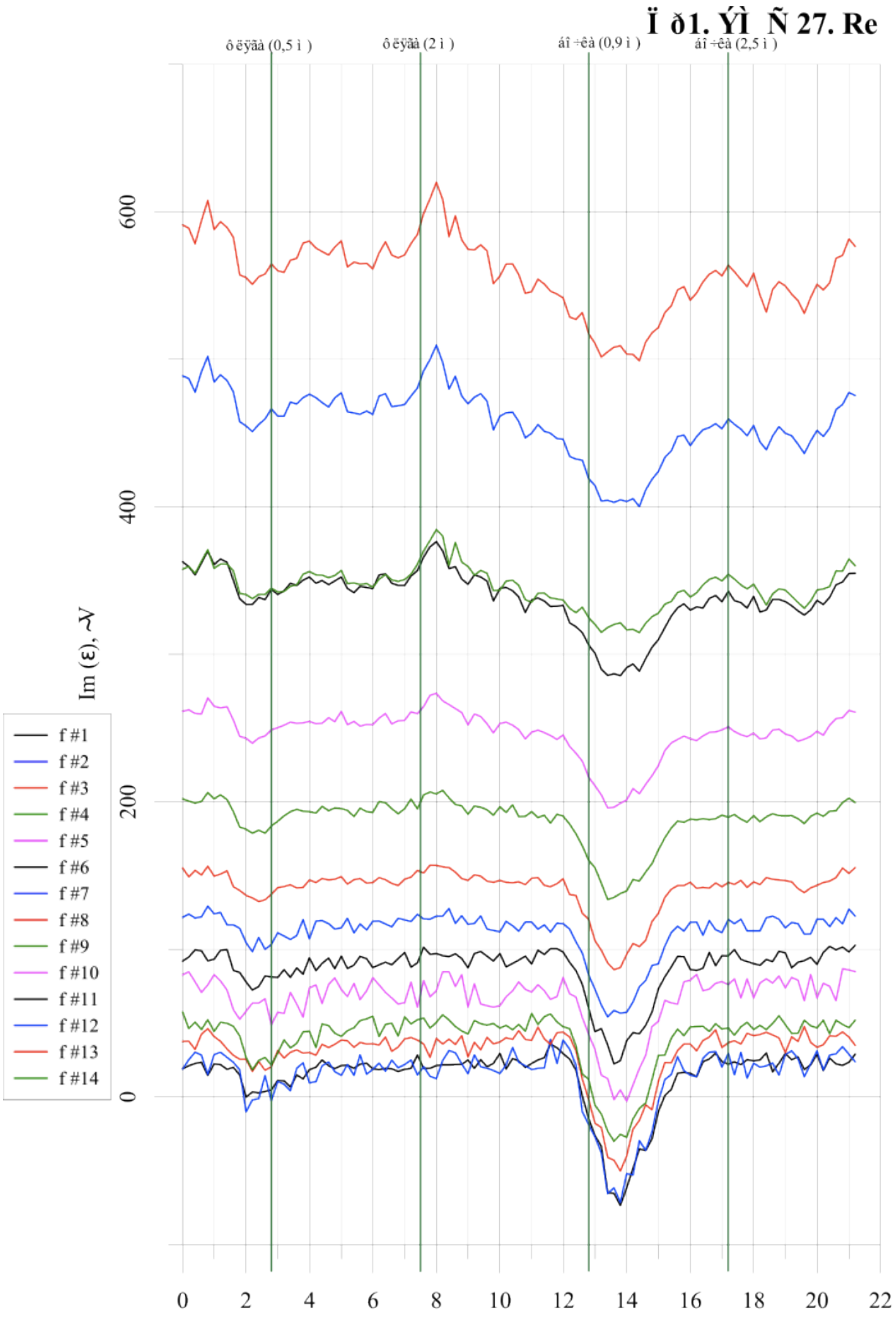

Figure 4. Line No.1. MFS 27. Real part e.m.f.

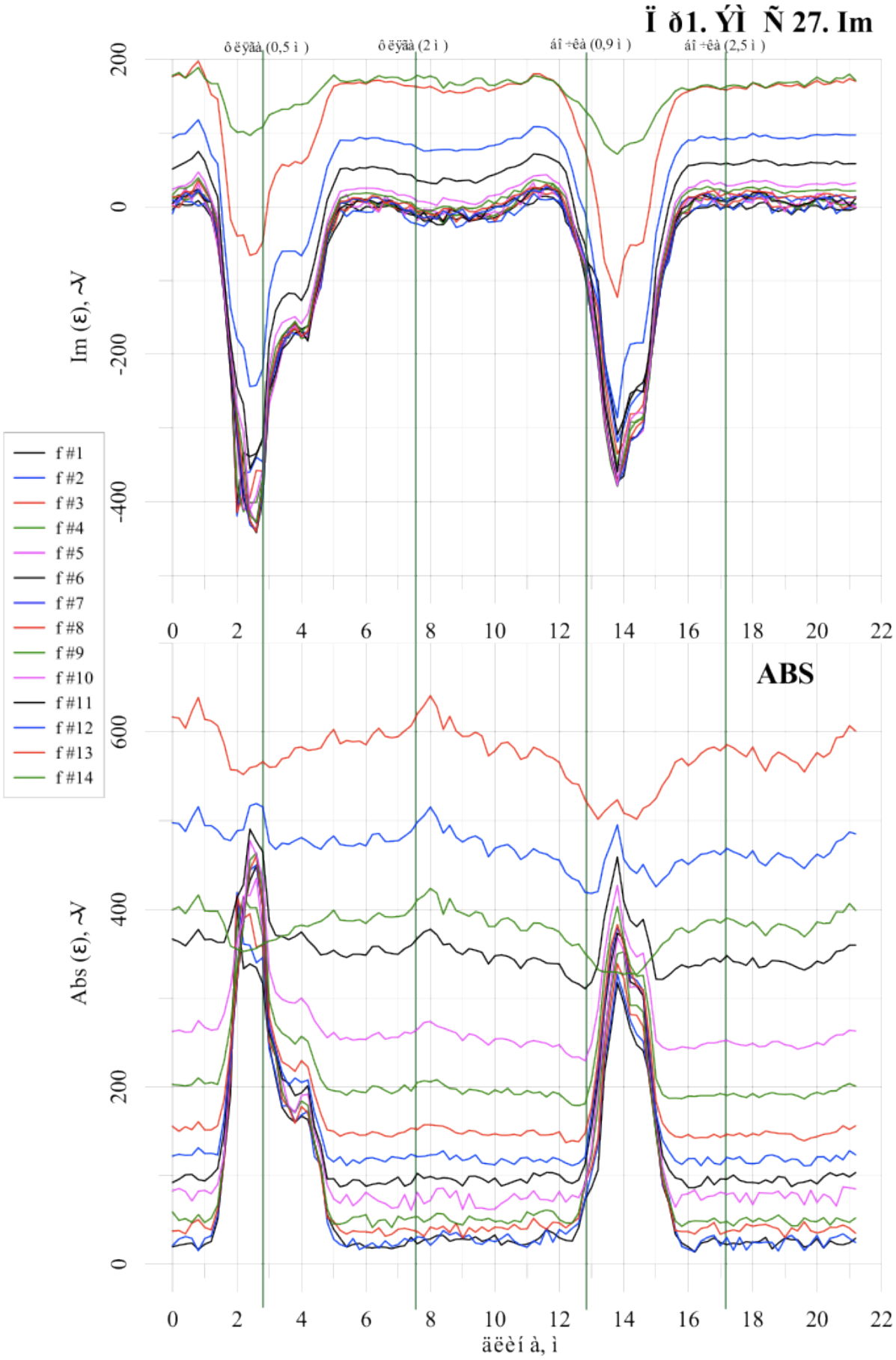

Figure 5. Line No.1. MFS 27. Imaginaryl part e.m.f. and module of e.m.f.

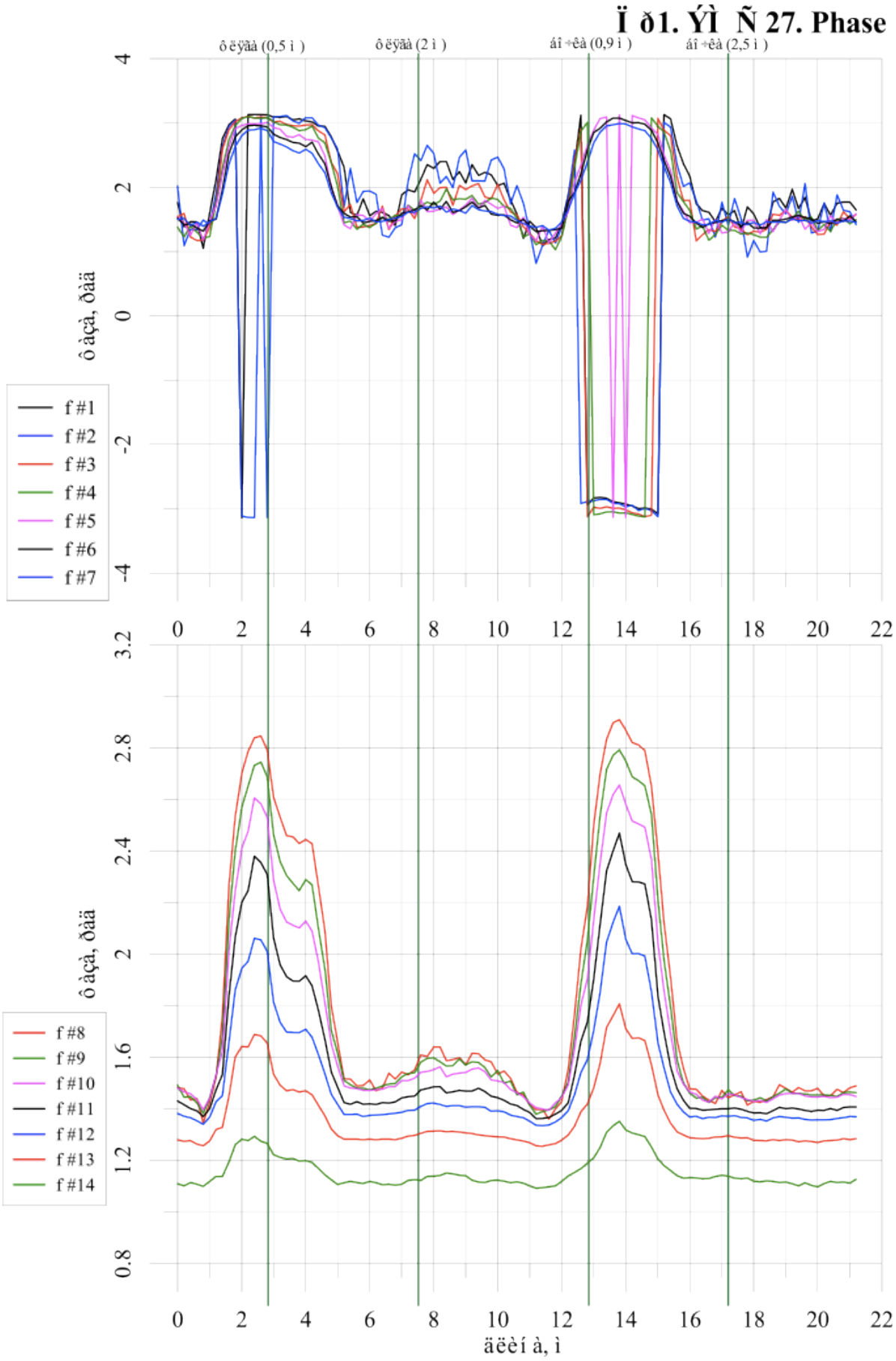

Figure 6. Line No.1. MFS 27. Phase of e.m.f.

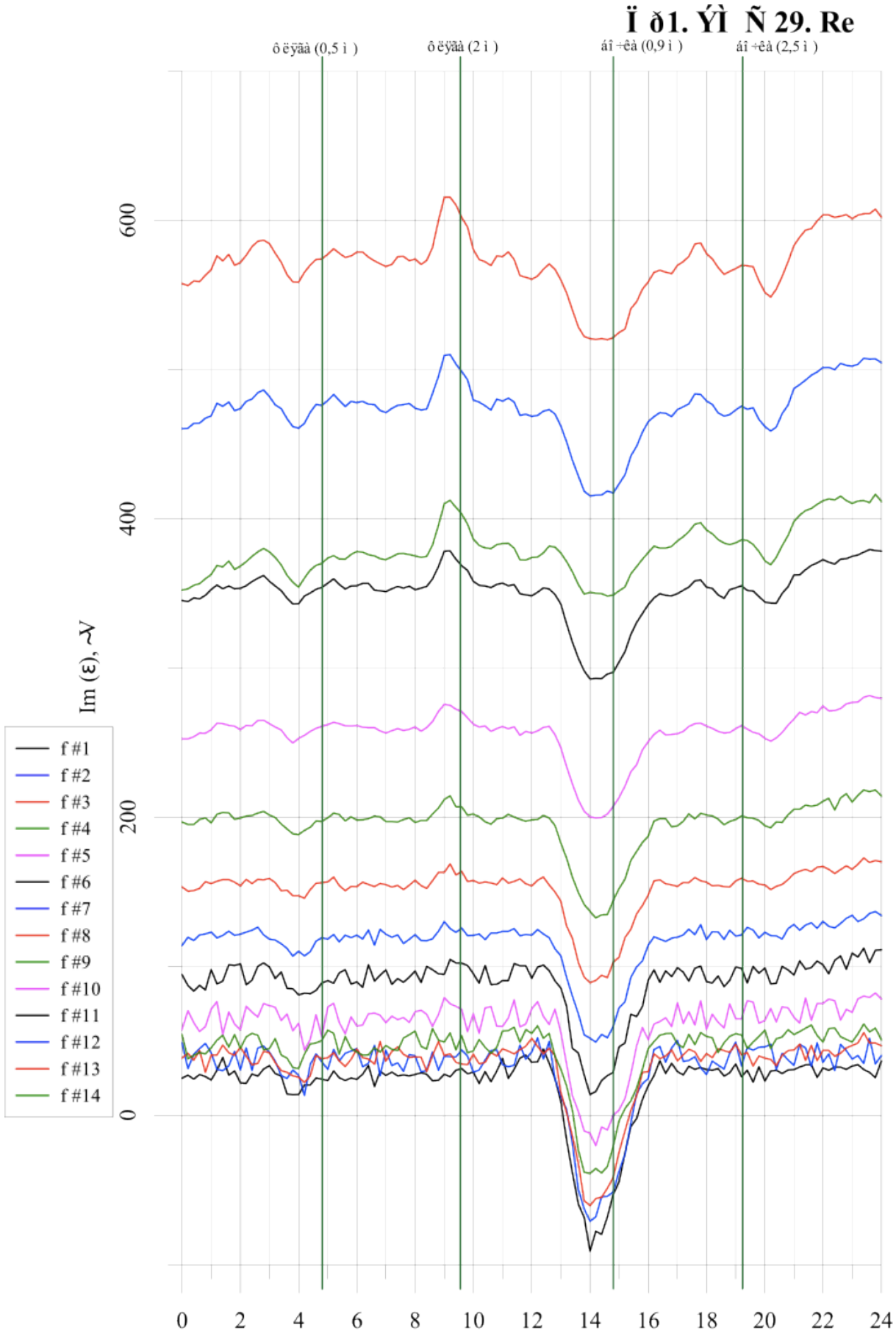

Figure 7. Line No.1. MFS 29. Real part e.m.f.

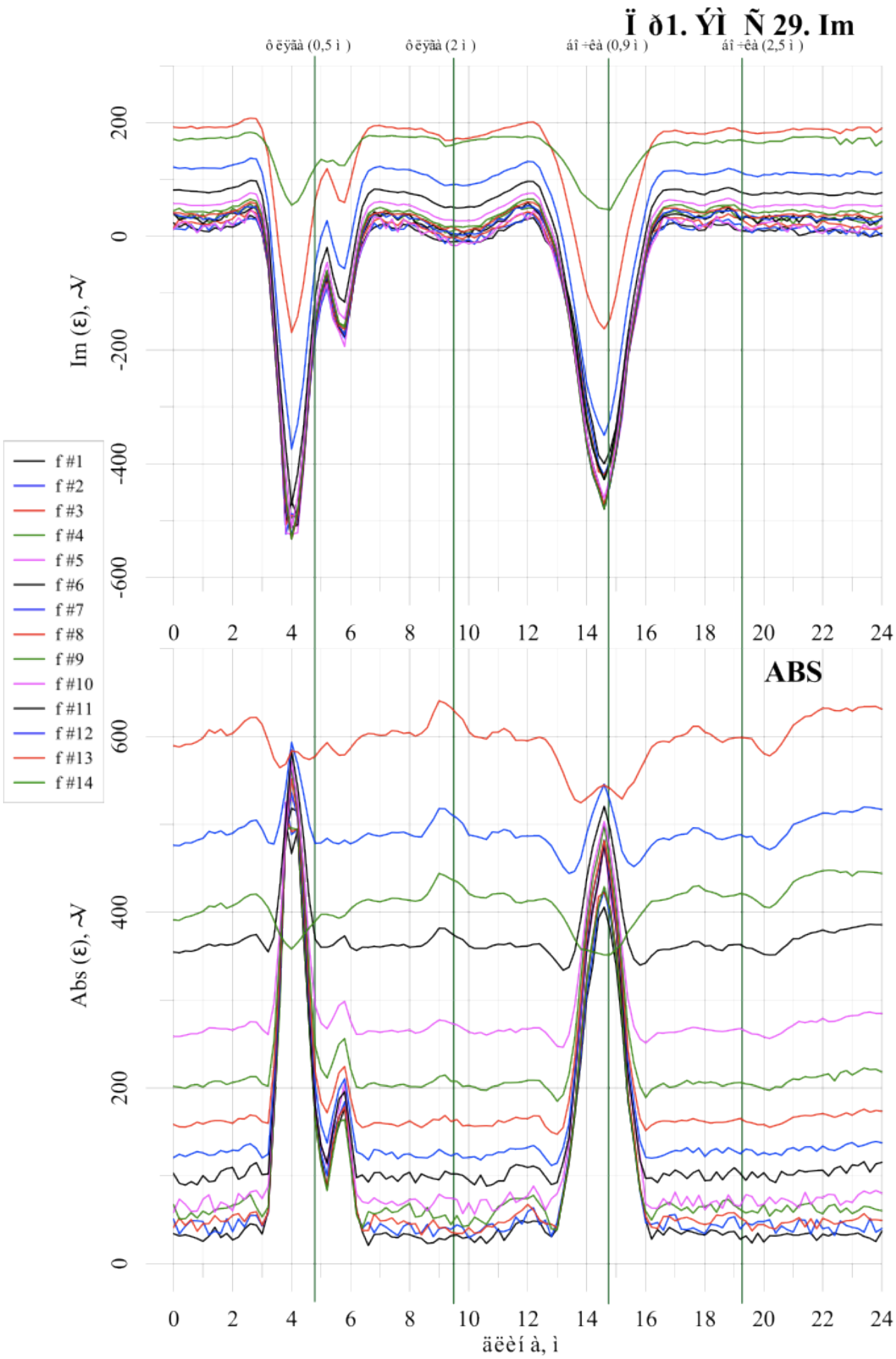

Figure 8. Line No.1. MFS 29. Imaginaryl part e.m.f. and module of e.m.f.

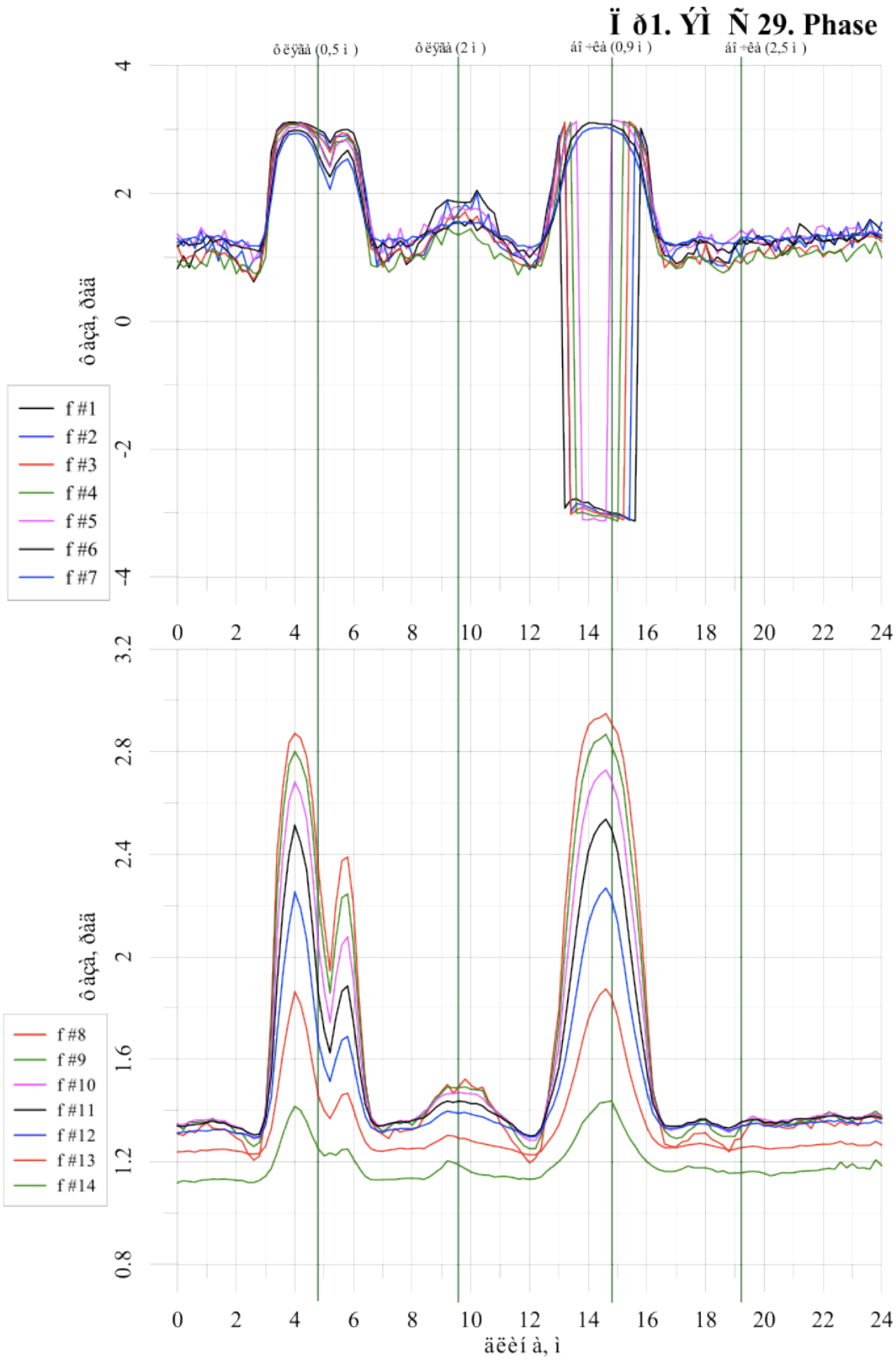

Figure 9. Line No.1. MFS 29. Phase of e.m.f.

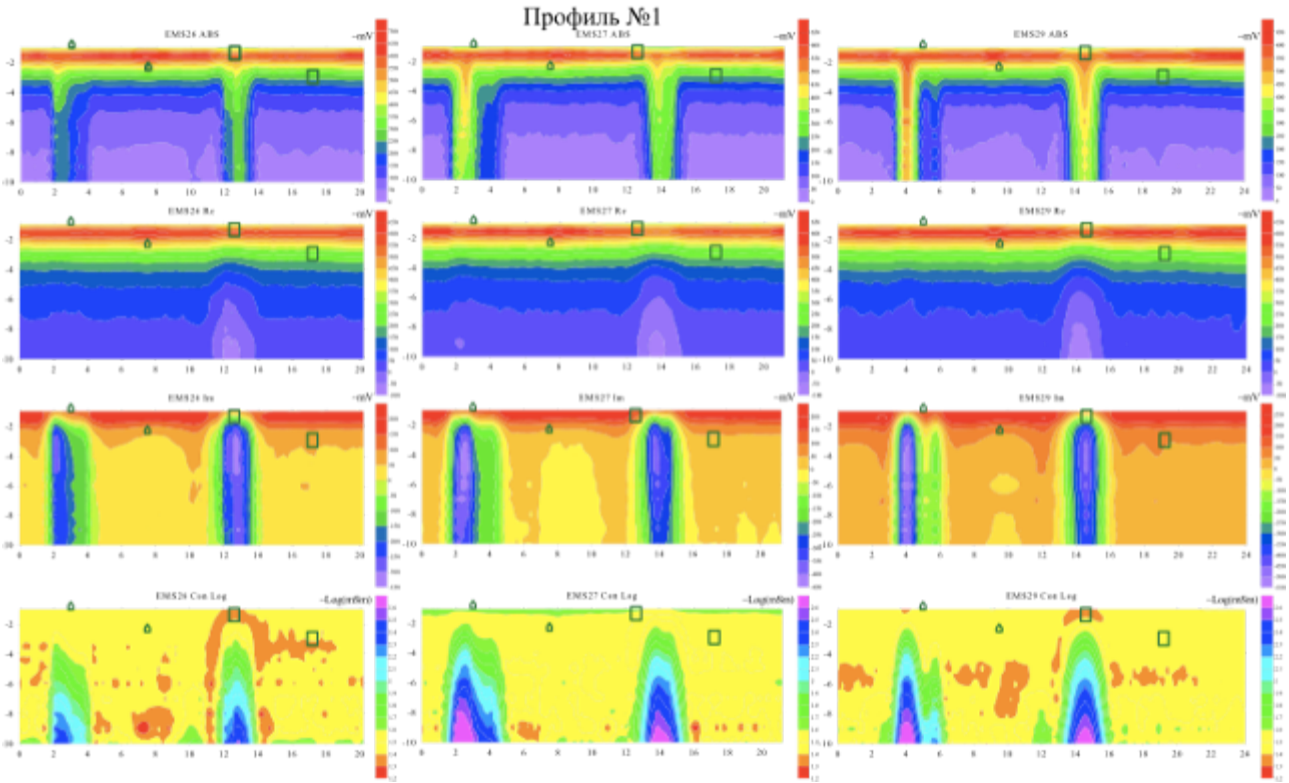

Figure 10. Cross-sections for line No.1.

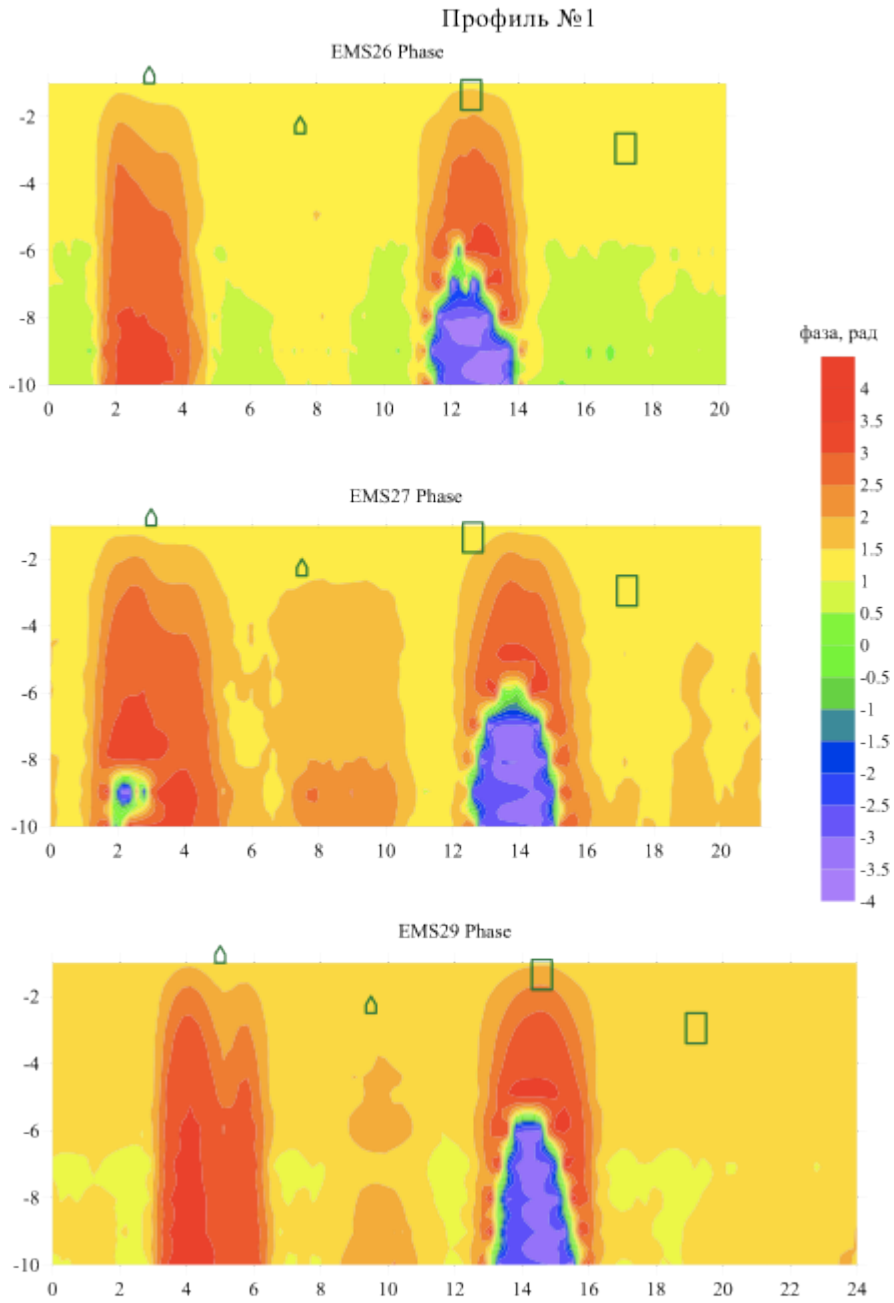

Figure 11. Section for line No.1. Phase of signal.

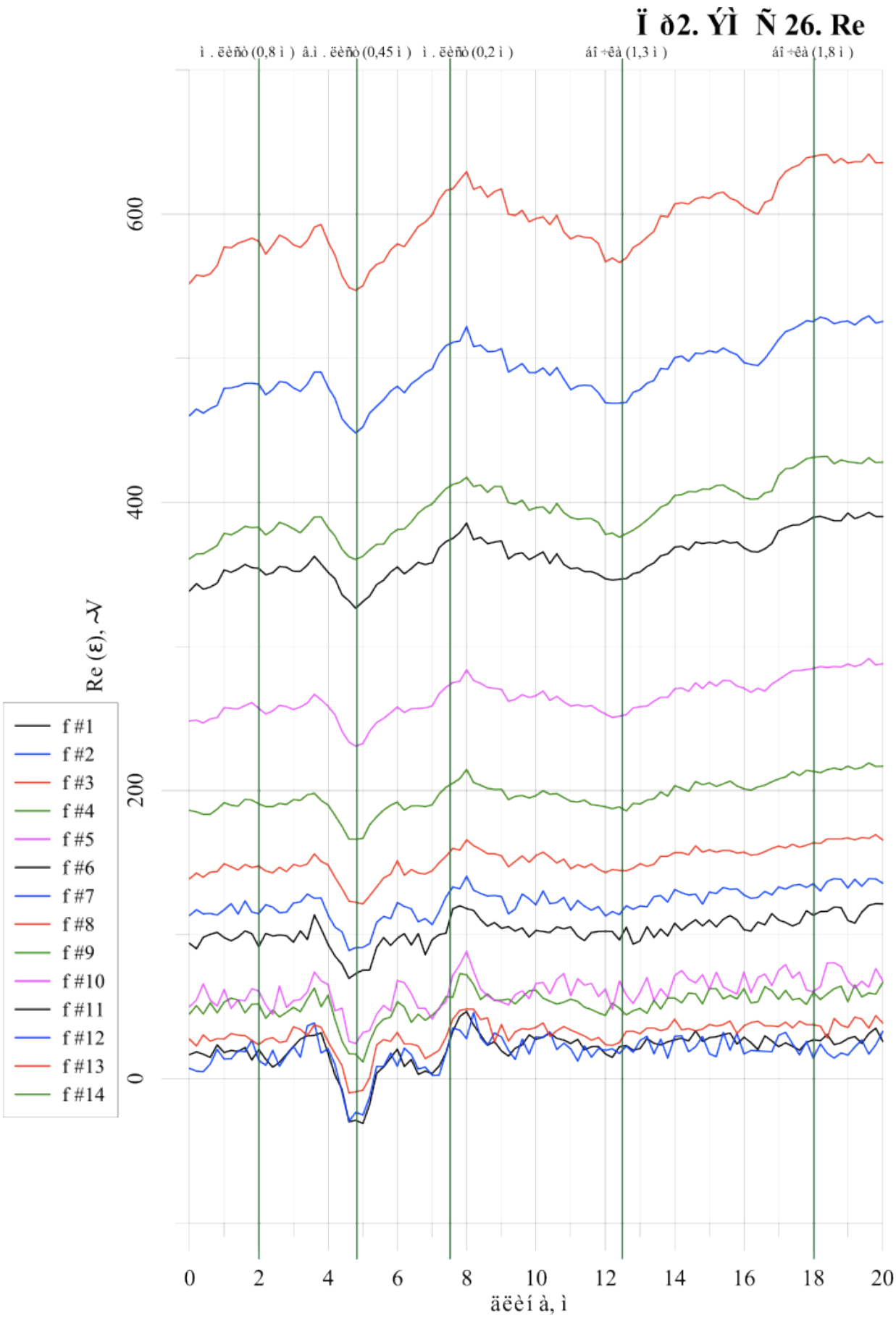

Figure 12. Line No.2. MFS 26. Real part e.m.f.

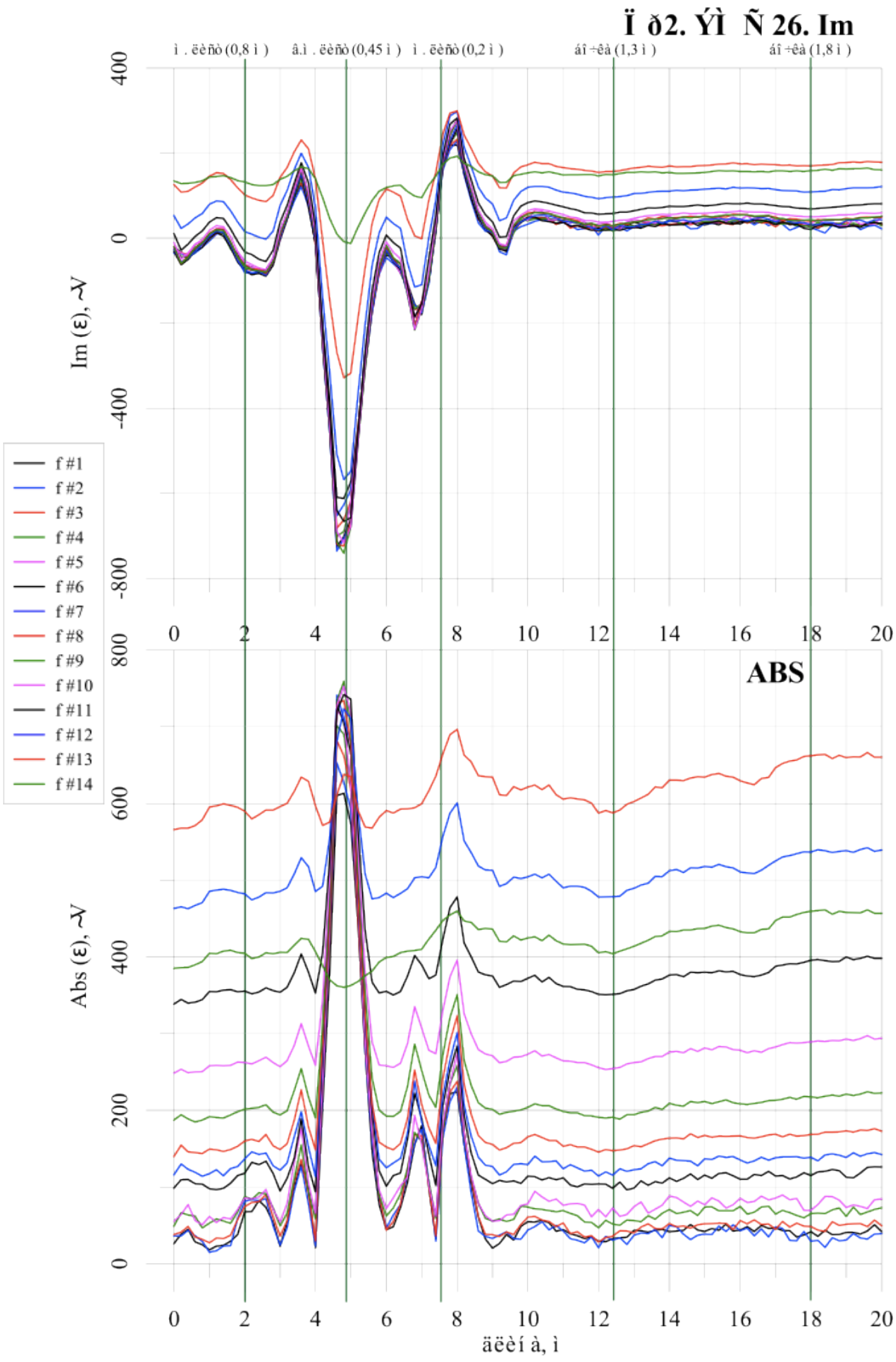

Figure 13. Line No.2. MFS 26. Imaginaryl part e.m.f. and module of e.m.f.

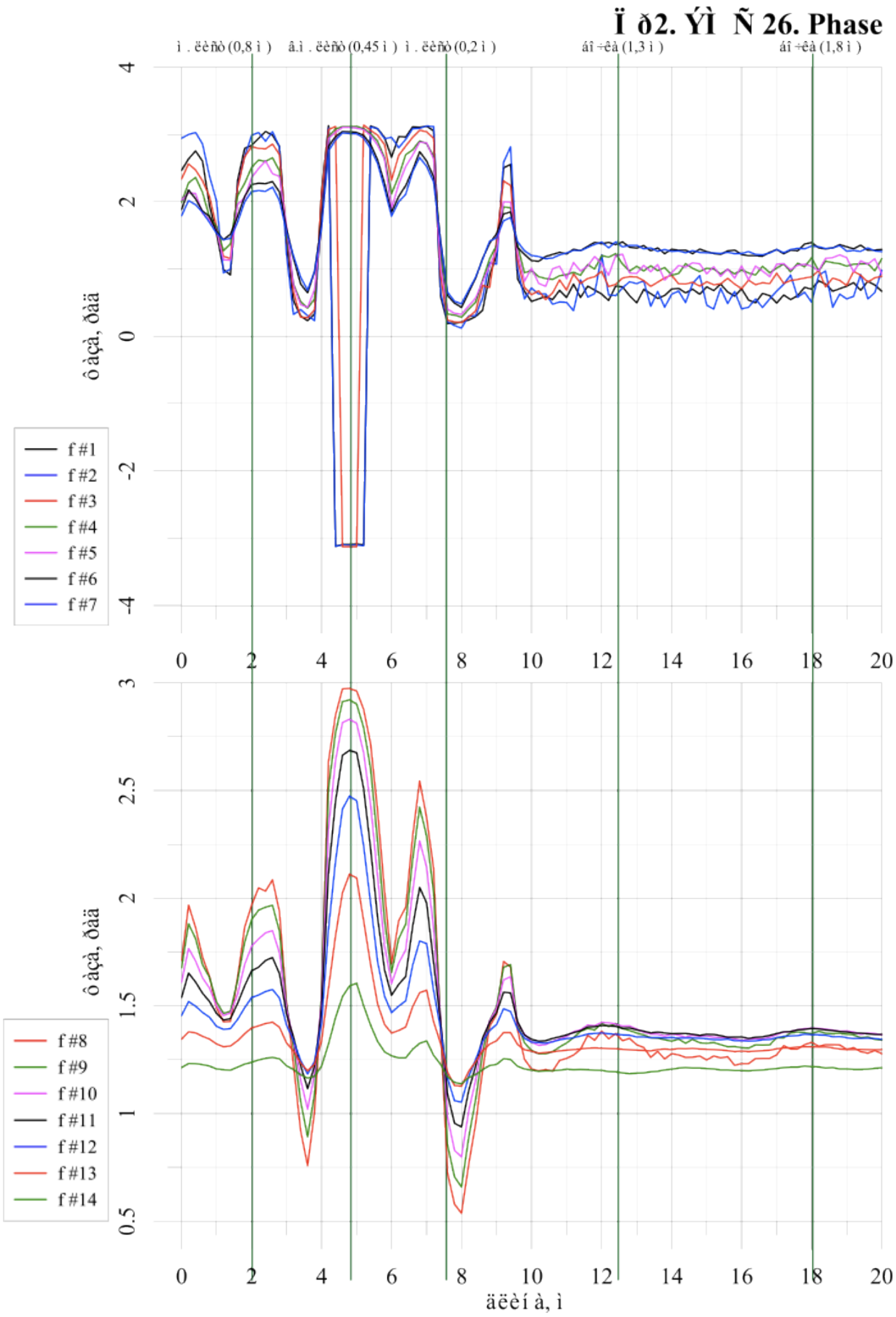

Figure 14. Line No.2. MFS 26. Phase of e.m.f.

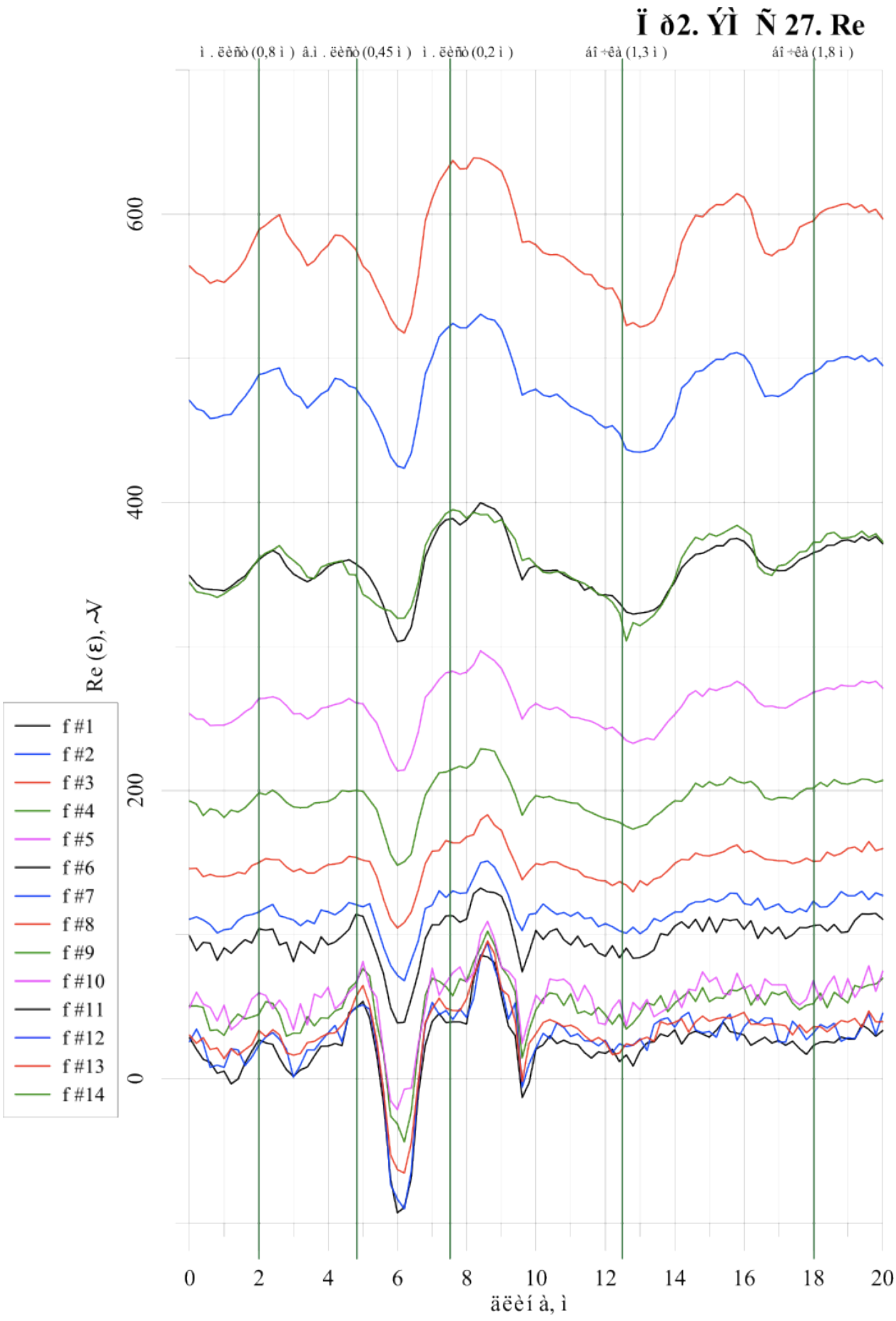

Figure 15. Line No.2. MFS 27. Real part e.m.f.

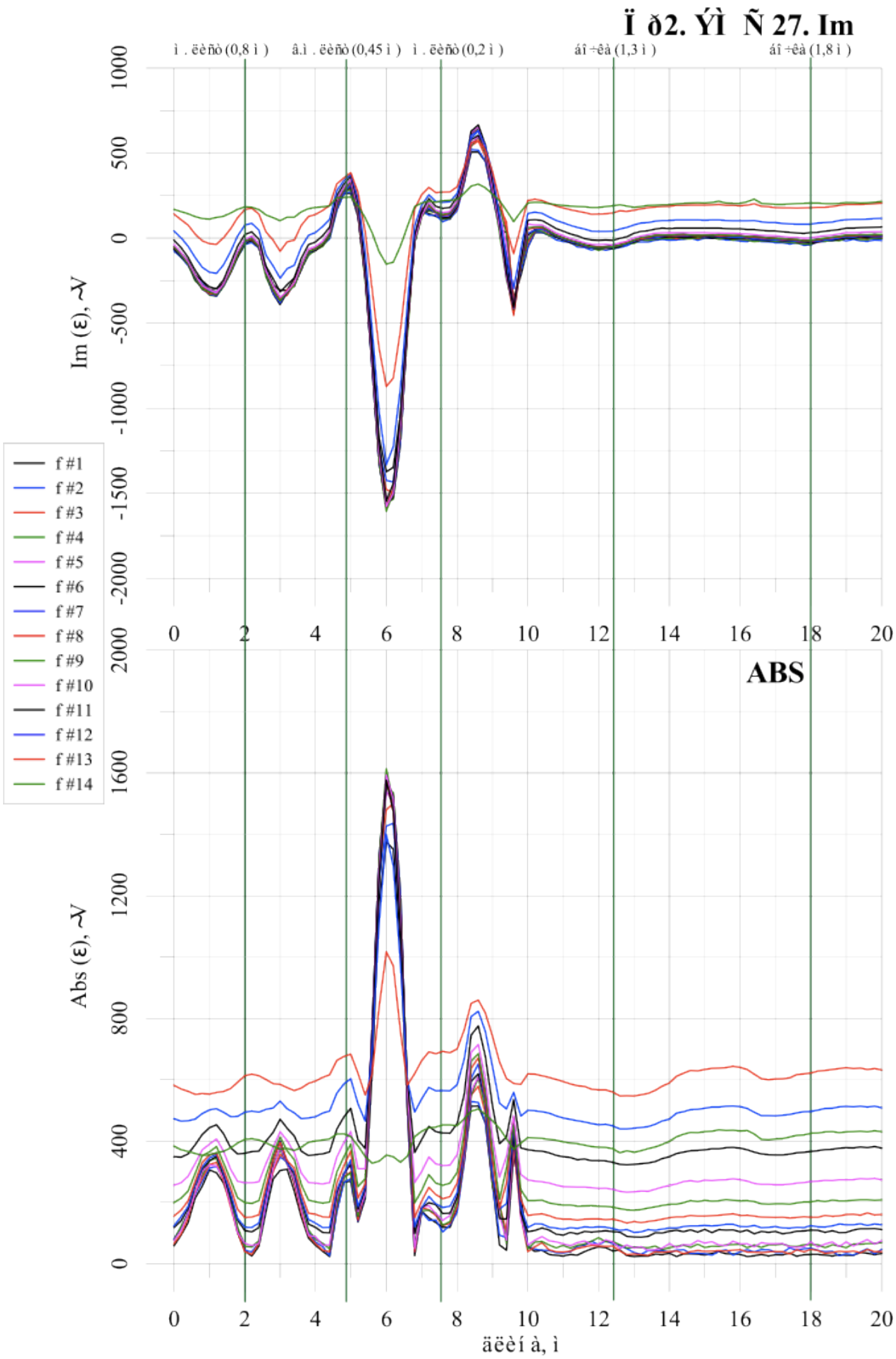

Figure 16. Line No.2. MFS 27. Imaginaryl part e.m.f. and module of e.m.f.

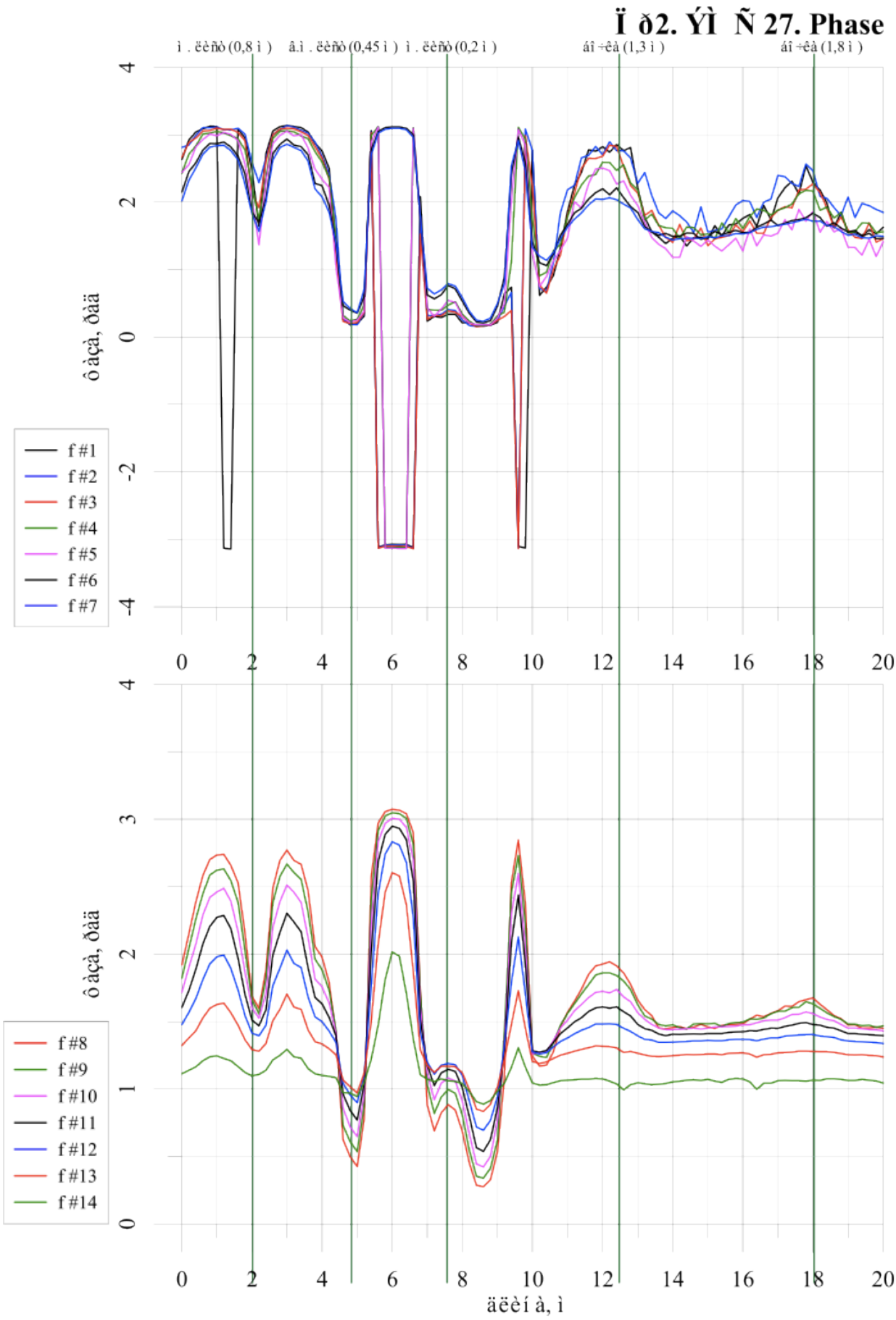

Figure 17. Line No.2. MFS 27. Phase of e.m.f.

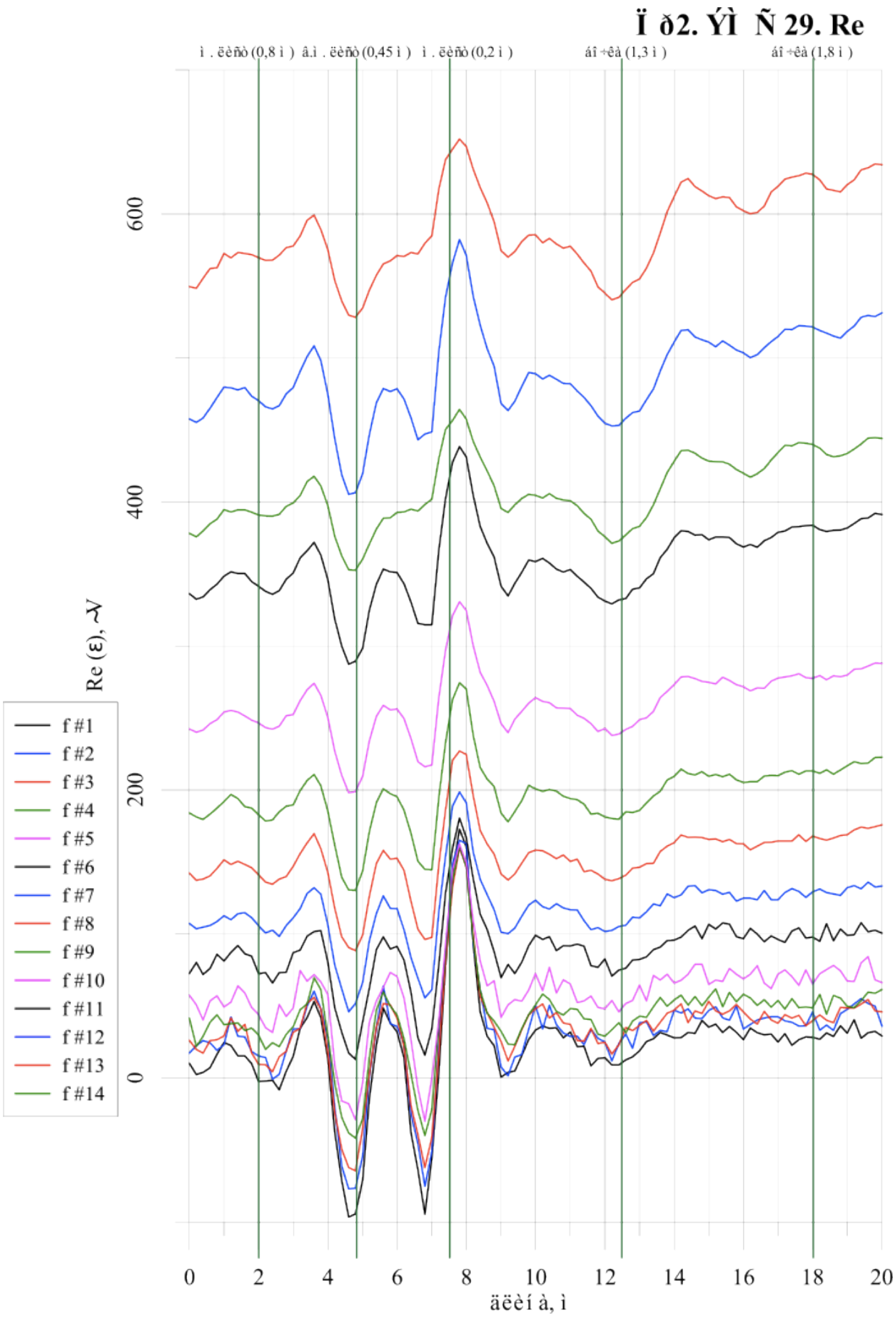

Figure 18. Line No.2. MFS 29. Real part e.m.f.

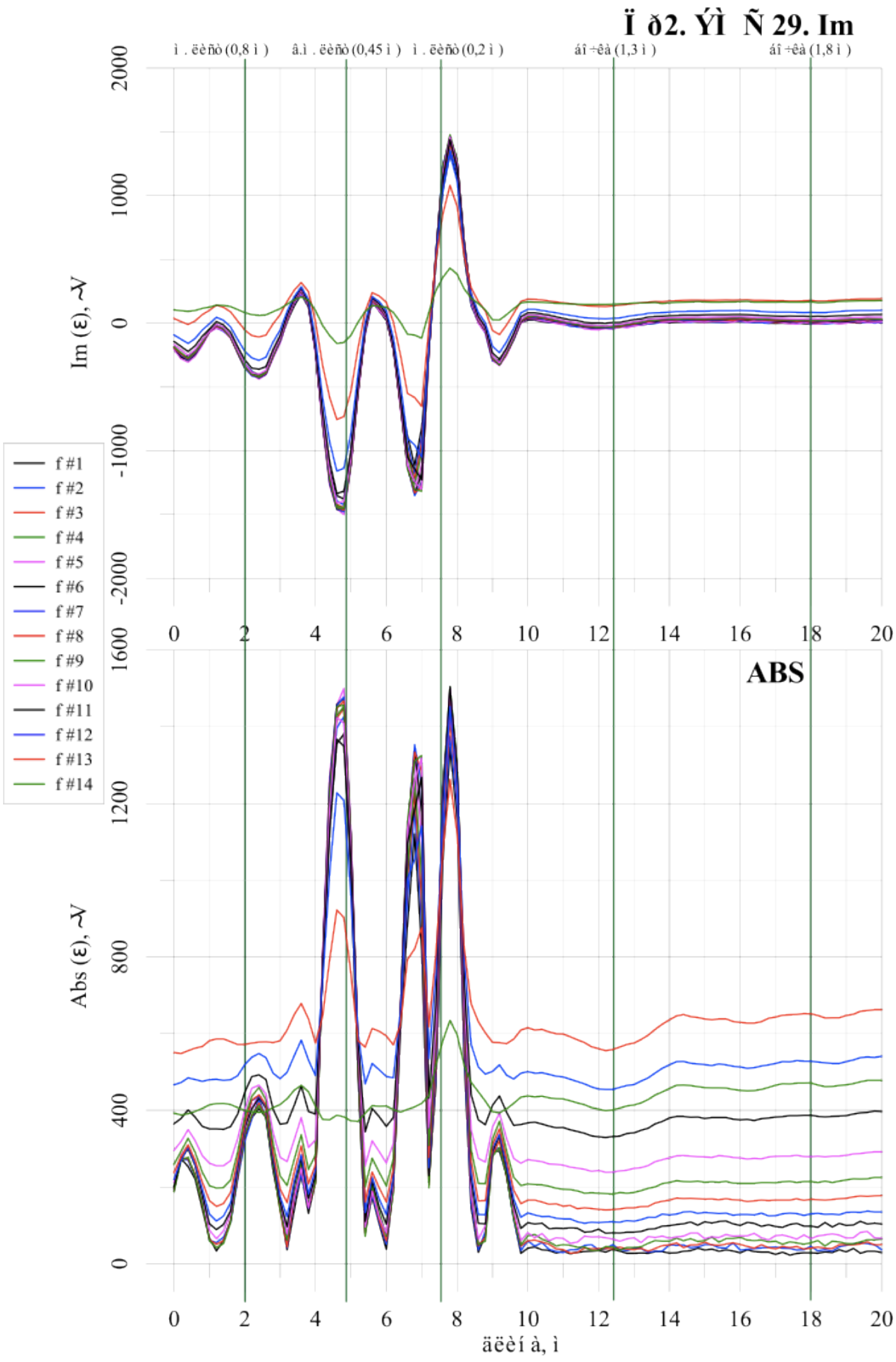

Figure 19. Line No.2. MFS 29. Imaginaryl part e.m.f. and module of e.m.f.

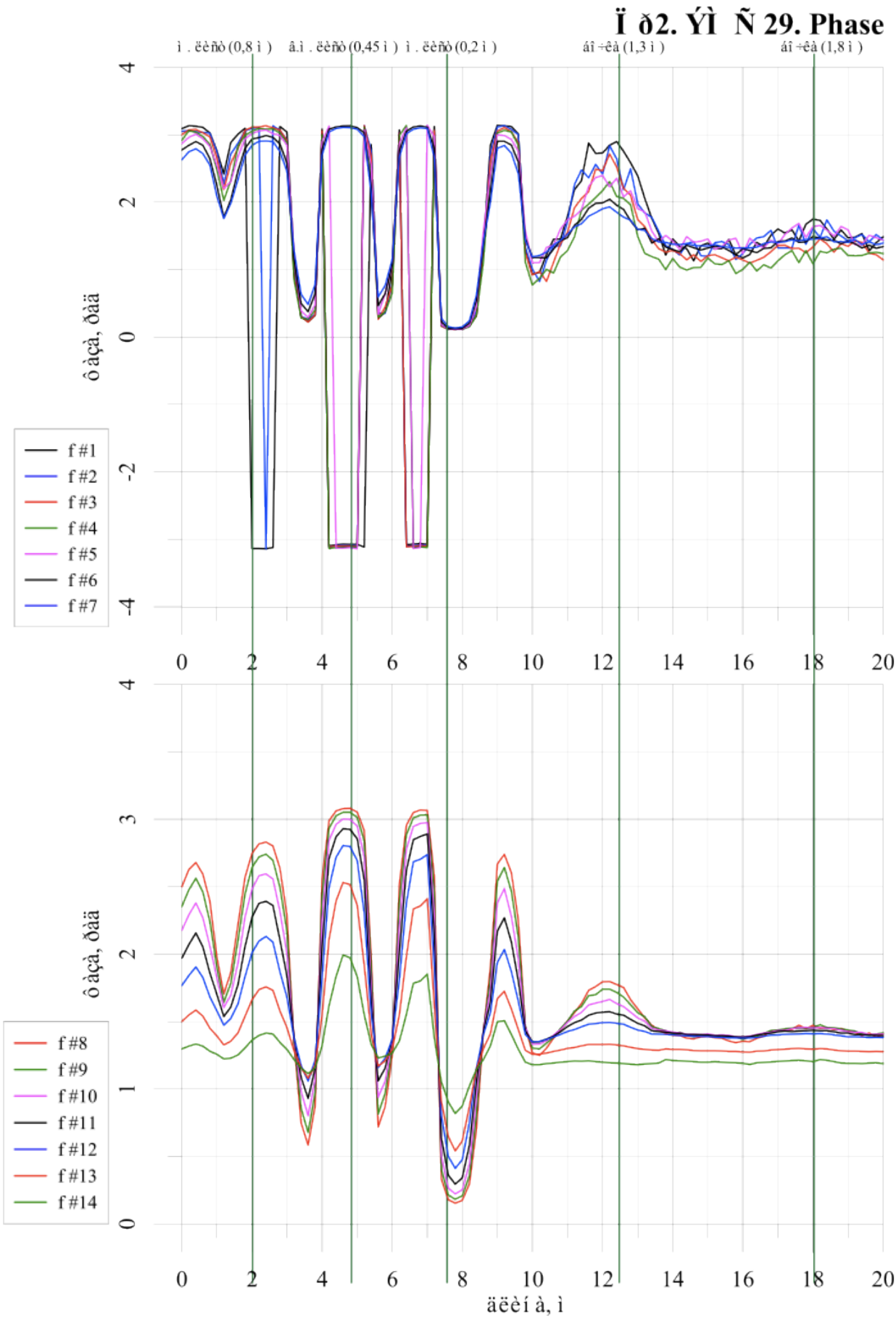

Figure 20. Line No.2. MFS 29. Phase of e.m.f.

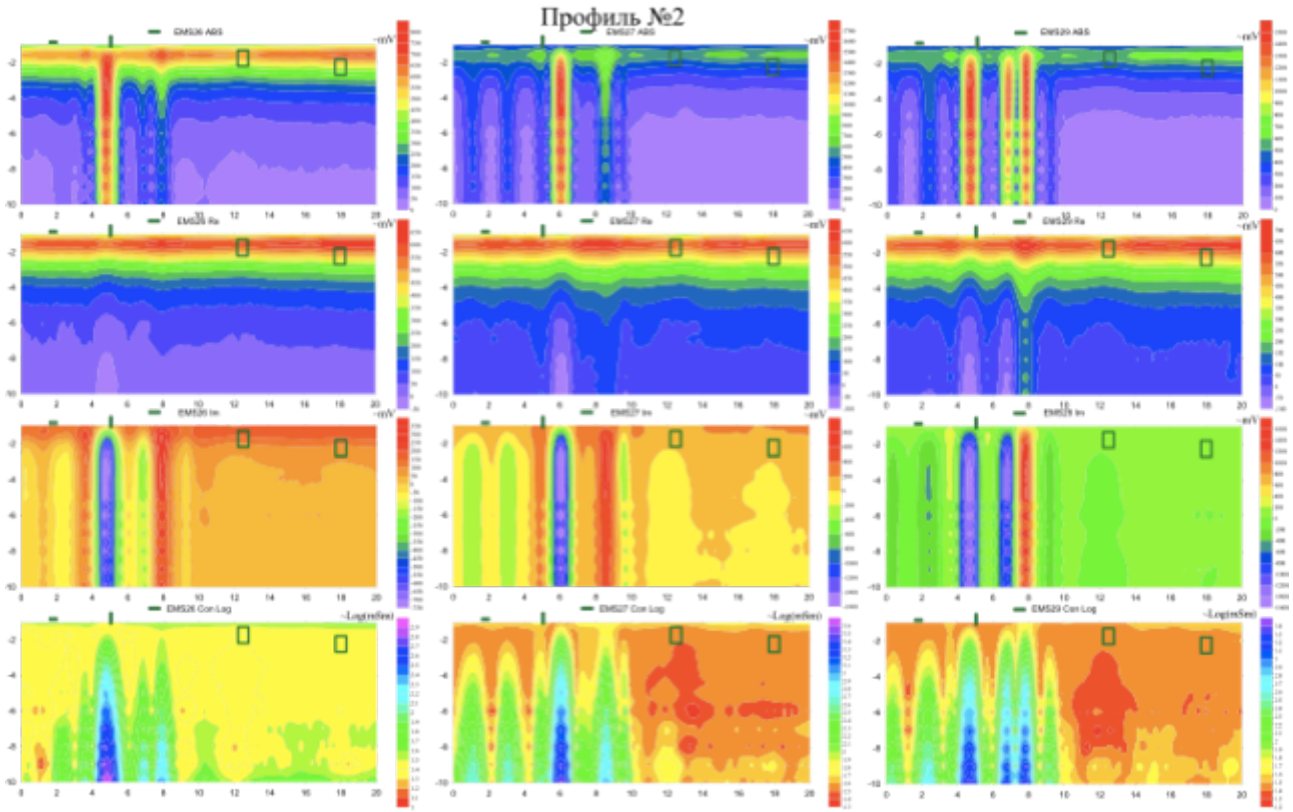

Figure 21. Section for line No.2

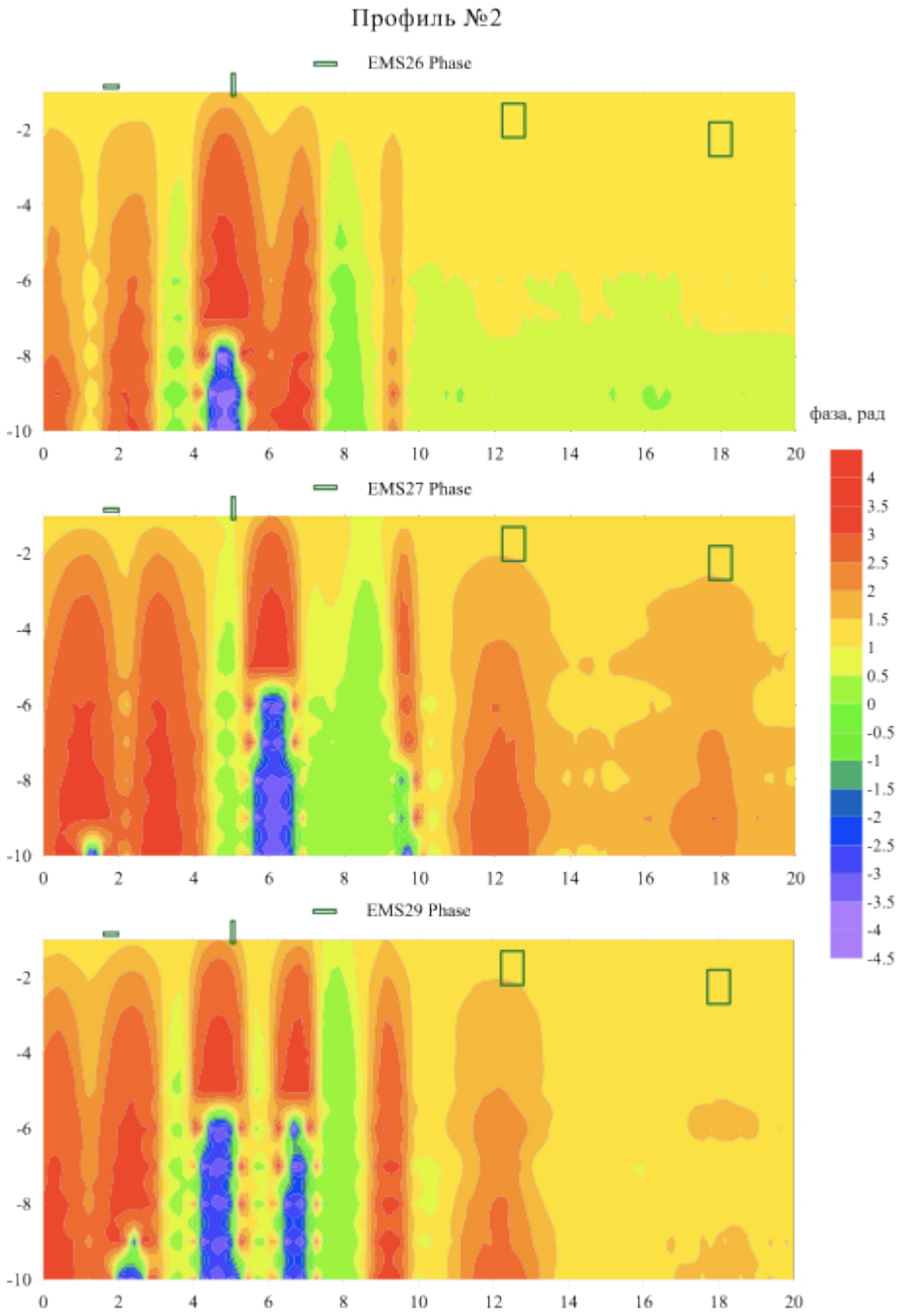

Figure 22. Section for line No.2. Phase of signal.

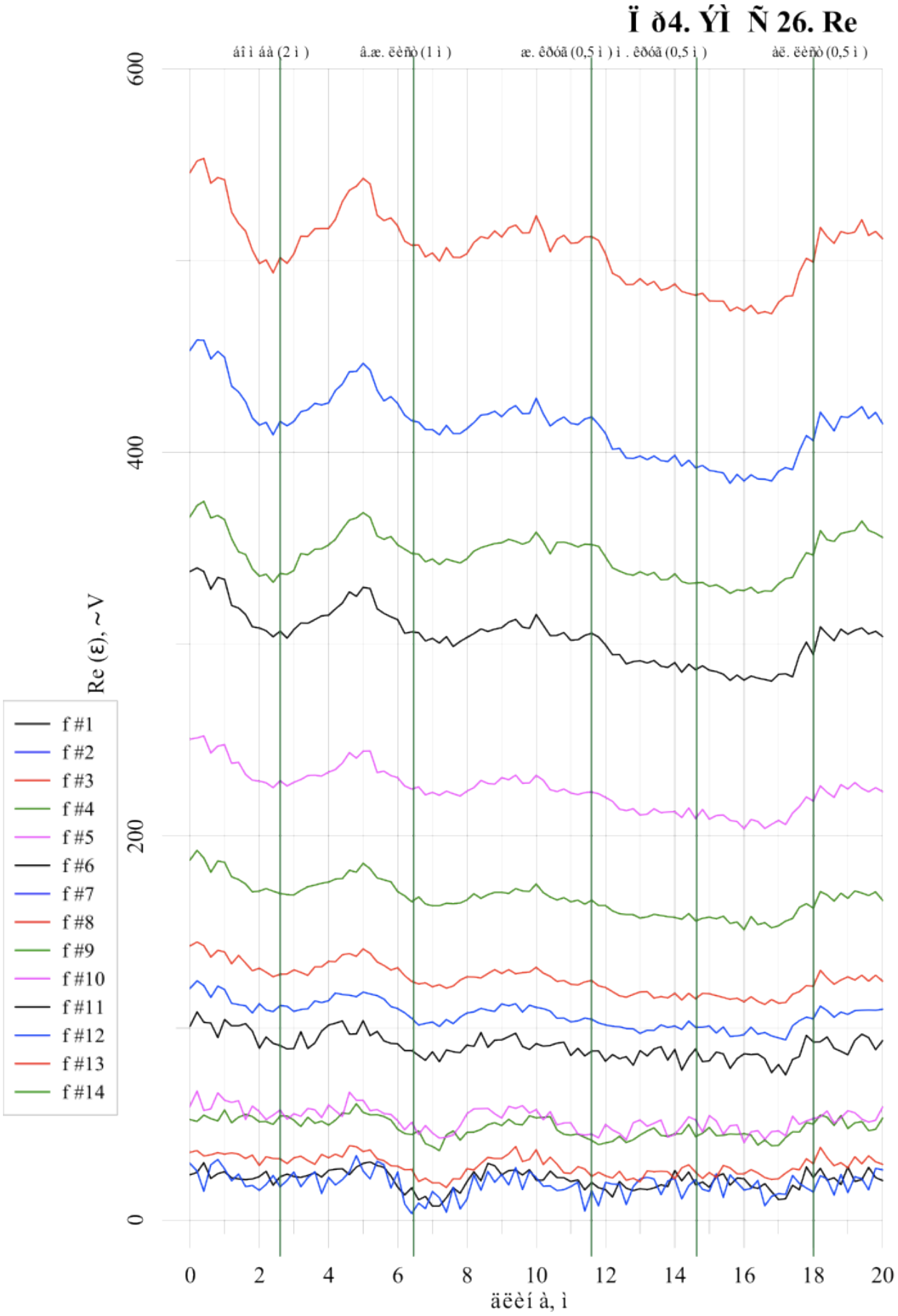

Figure 23. Line No.4. MFS 26. Real part e.m.f.

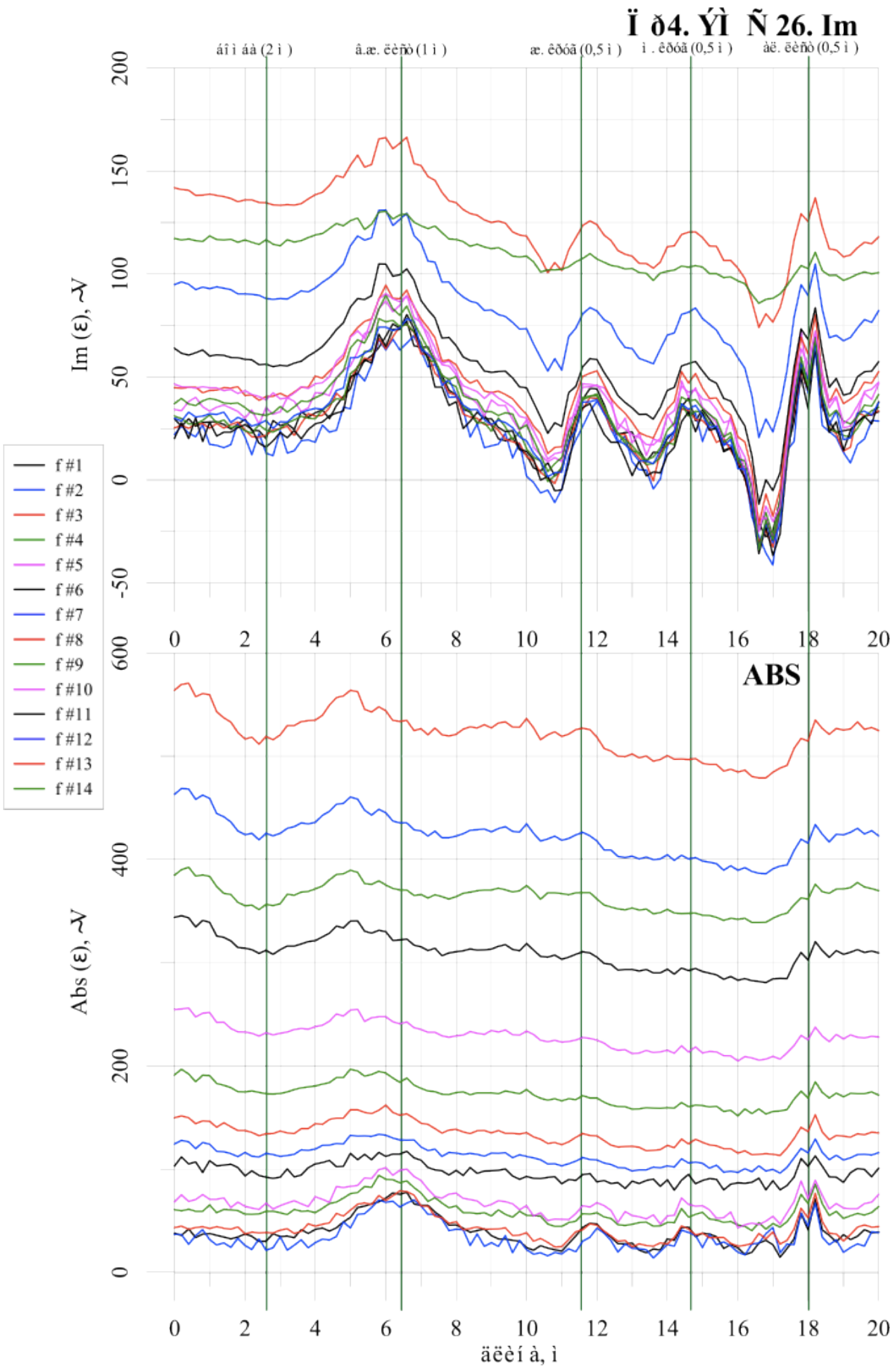

Figure 24. Line No.4. MFS 26. Imaginaryl part e.m.f. and module of e.m.f.

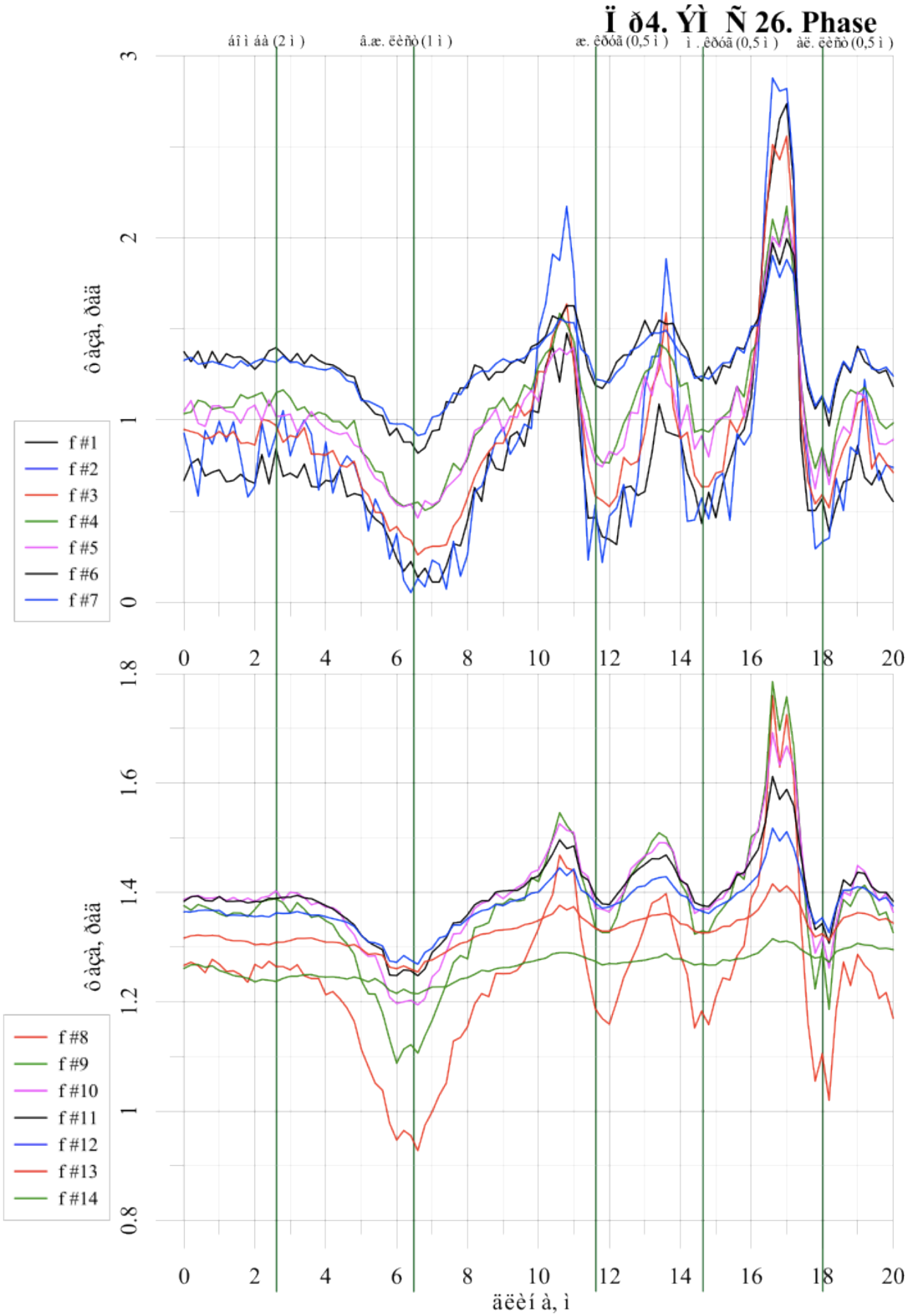

Figure 25. Line No.4. MFS 26. Phase of e.m.f.

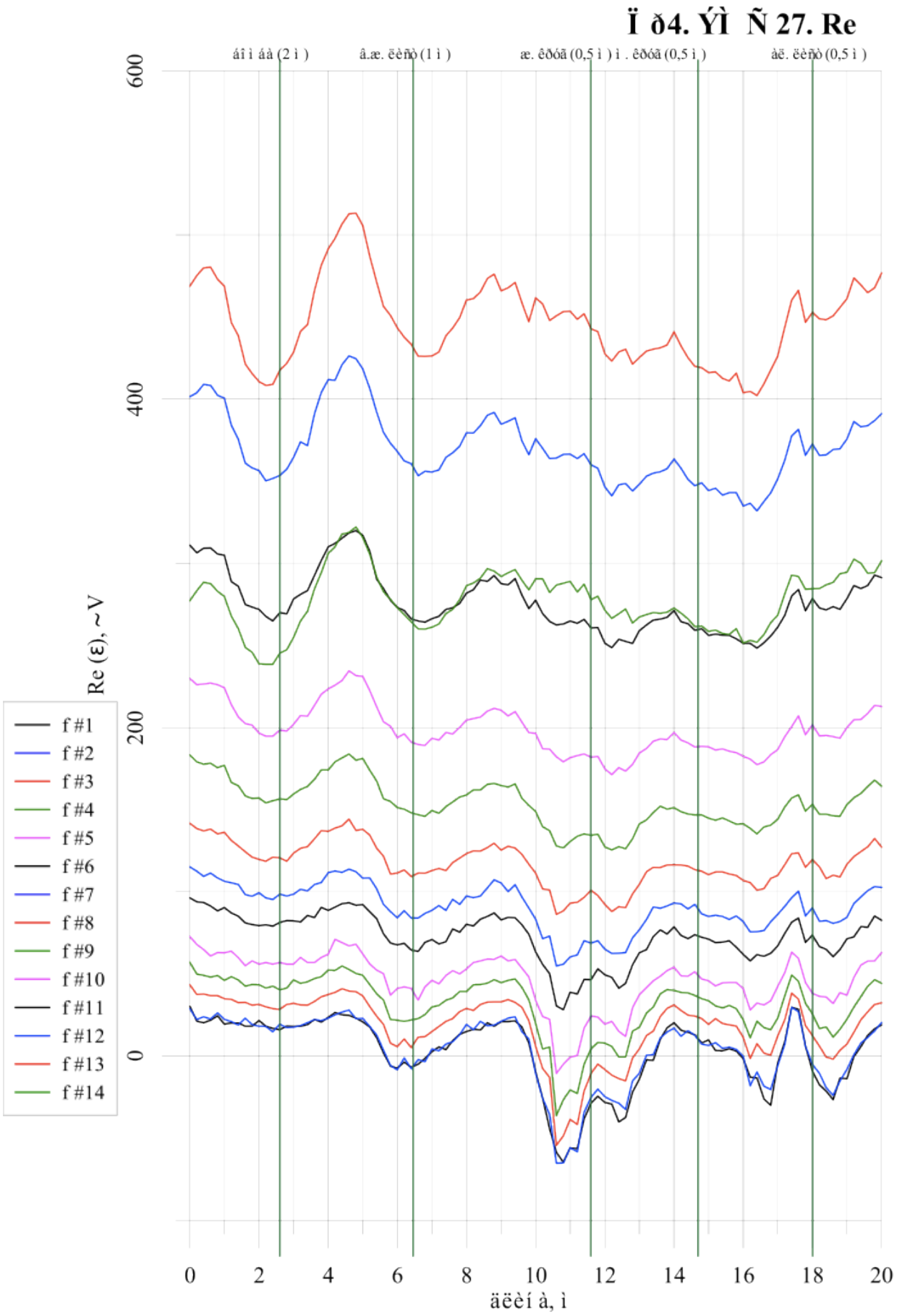

Figure 26. Line No.4. MFS 27. Real part e.m.f.

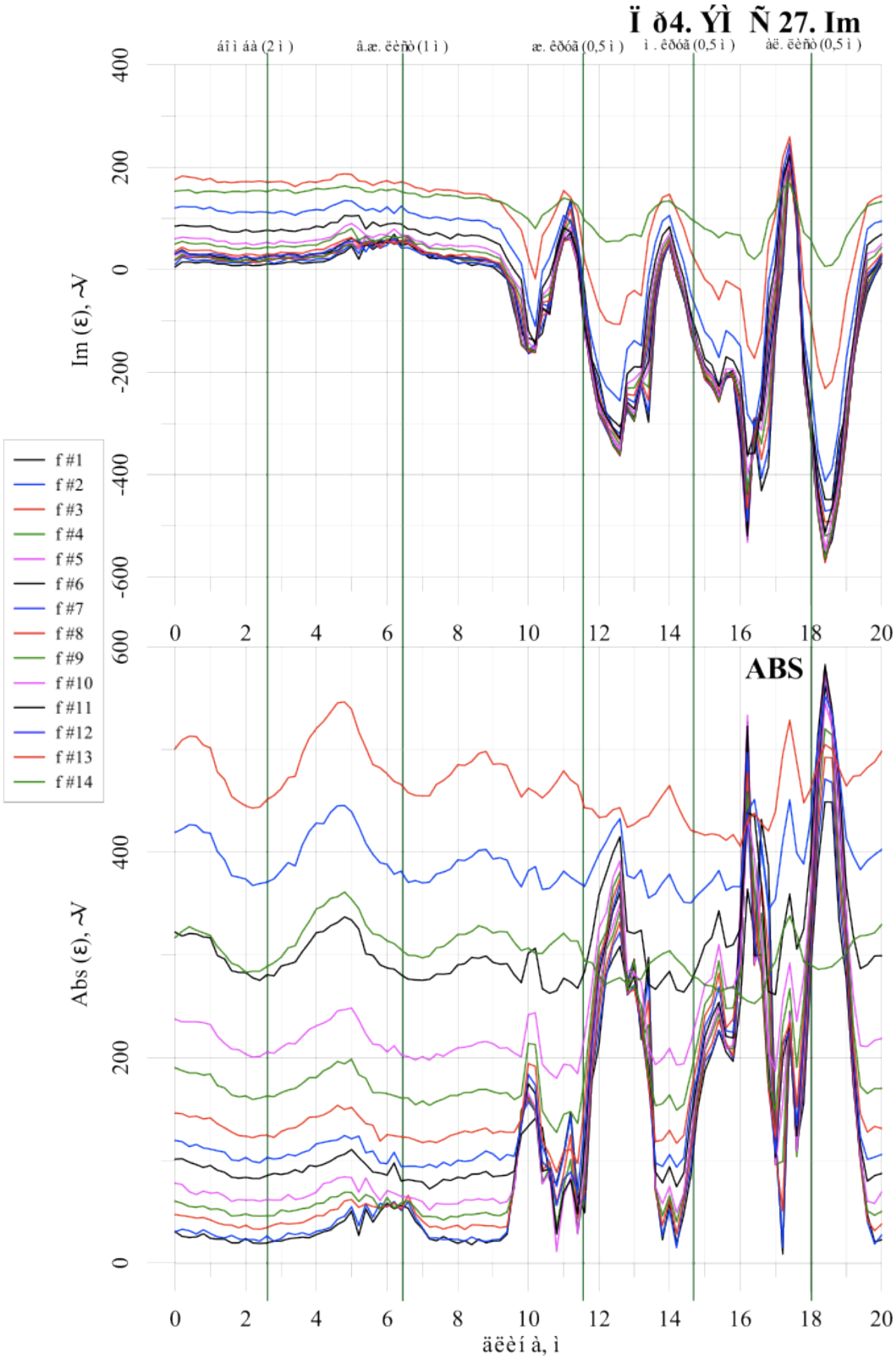

Figure 27. Line No.4. MFS 27. Imaginaryl part e.m.f. and module of e.m.f.

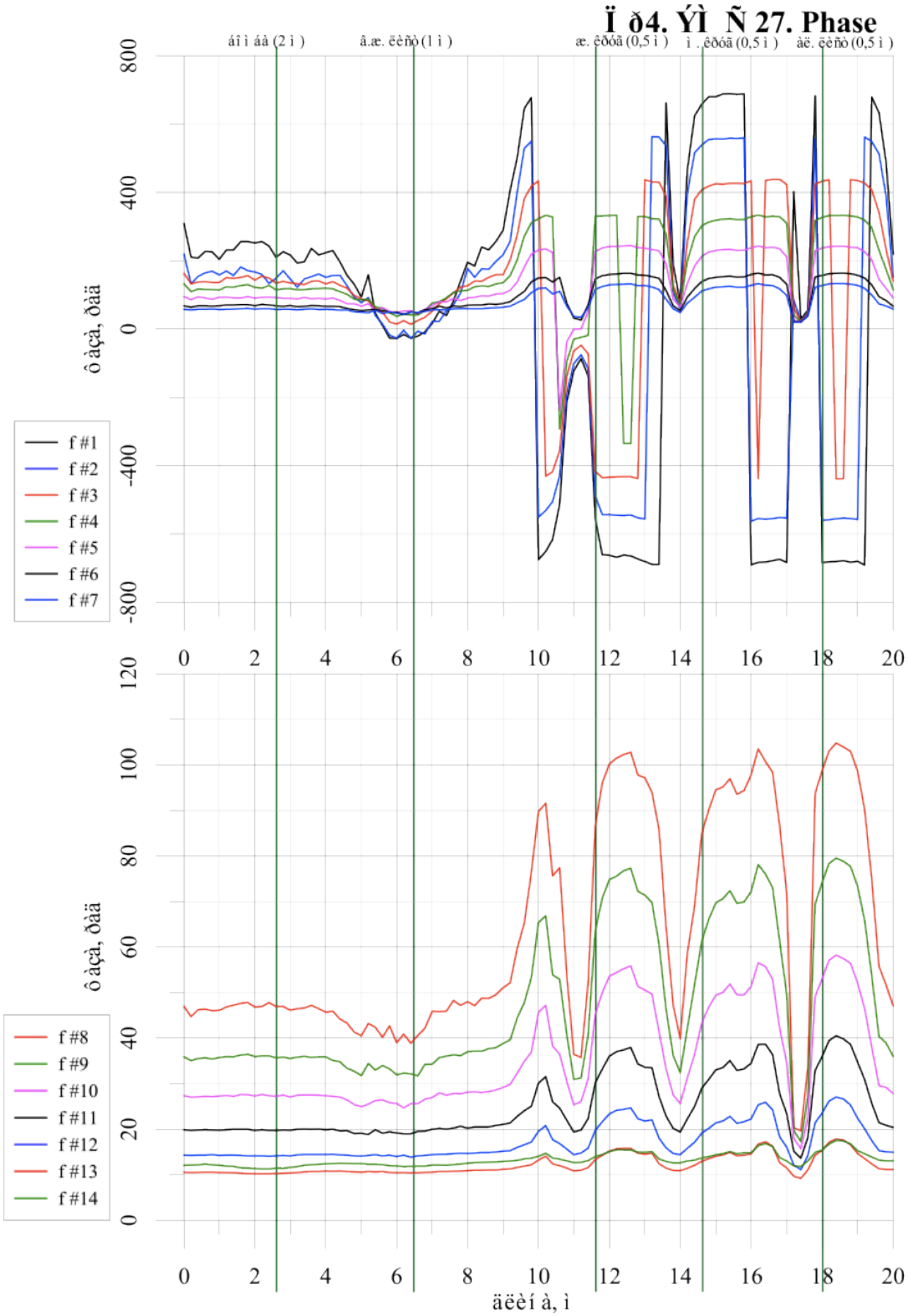

Figure 28. Line No.4. MFS 27. Phase of e.m.f.

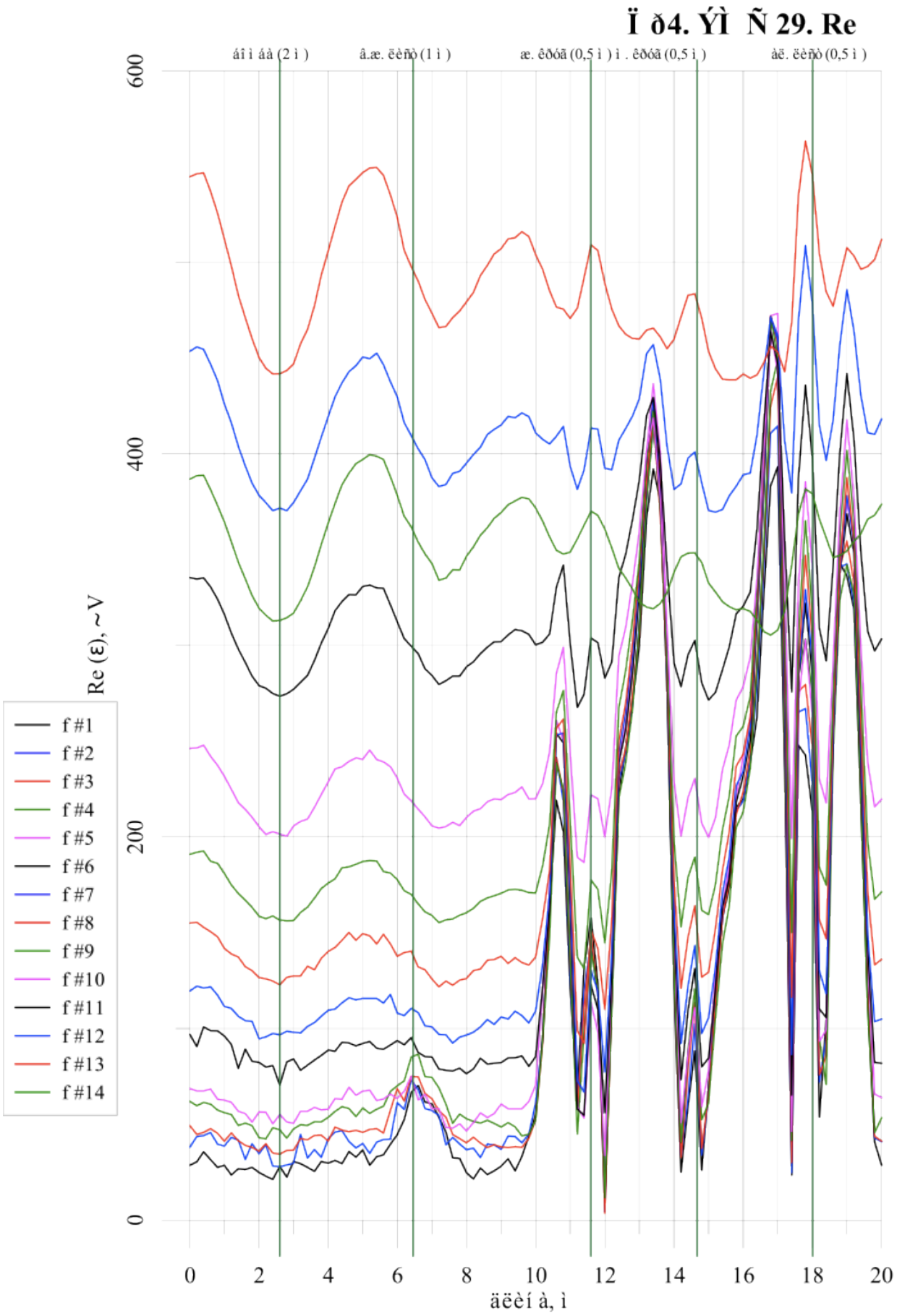

Figure 29. Line No.4. MFS 29. Real part e.m.f.

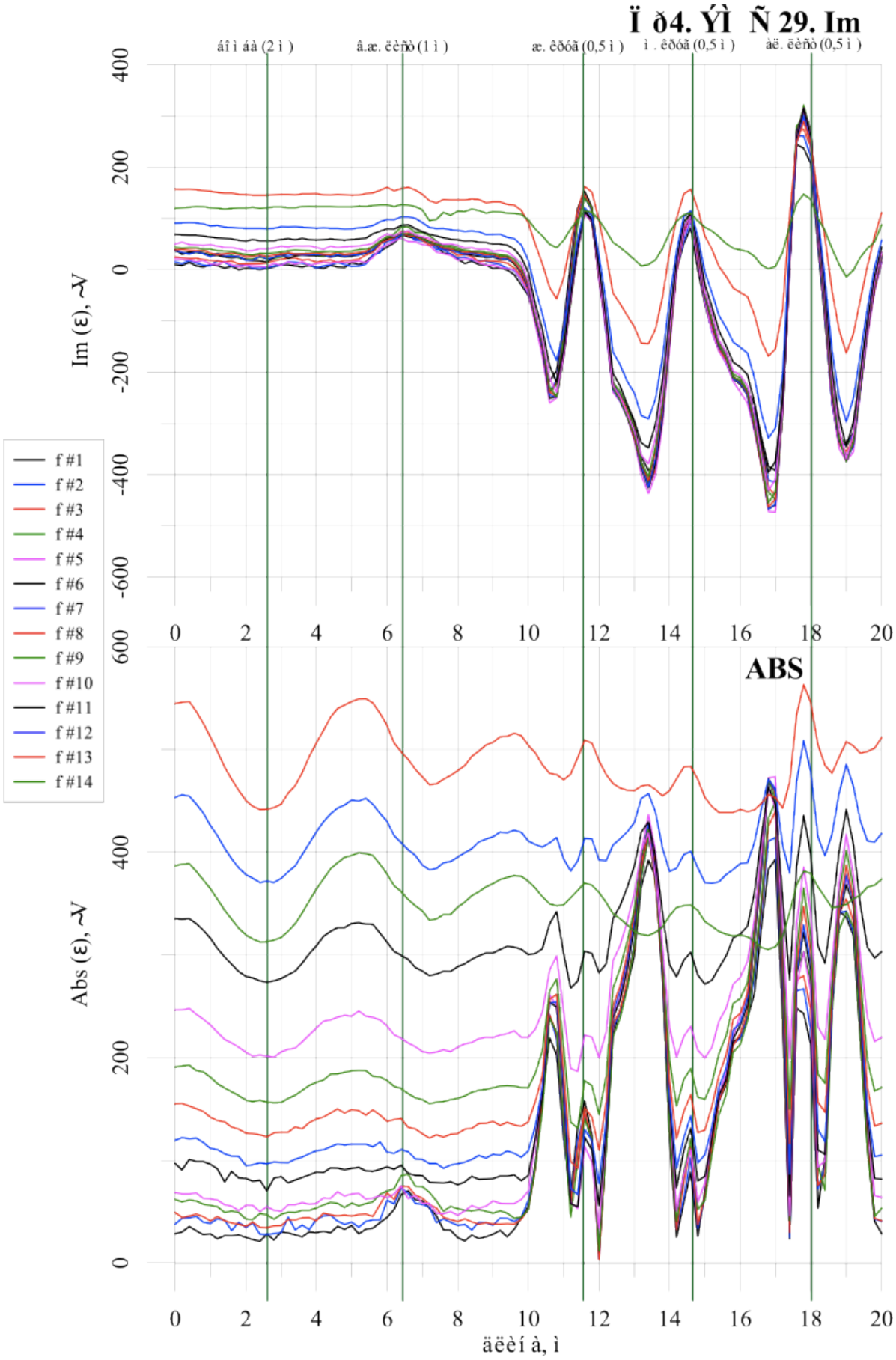

Figure 30. Line No.4. MFS 29. Imaginaryl part e.m.f. and module of e.m.f.

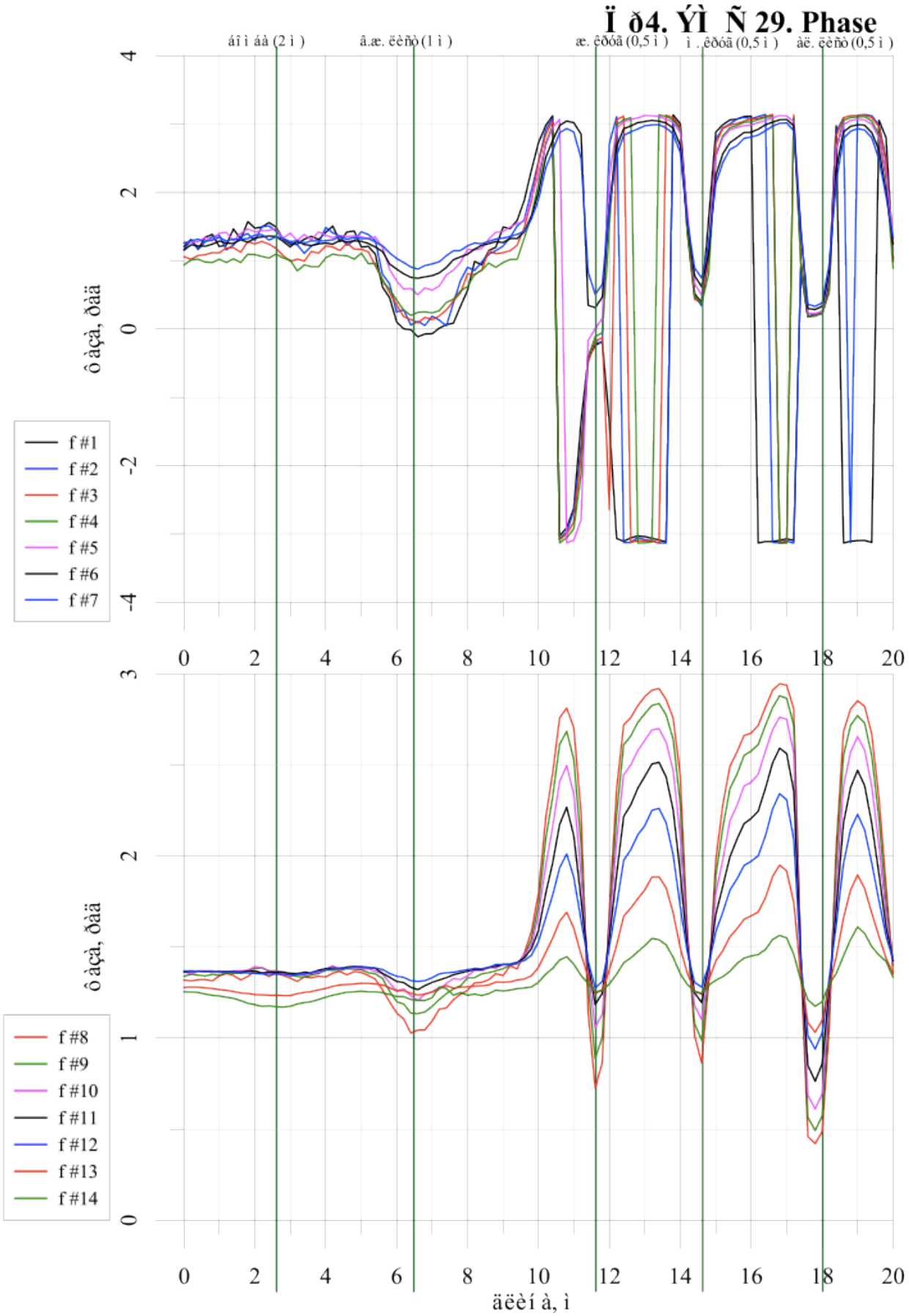

Figure 31. Line No.4. MFS 29. Phase of e.m.f.

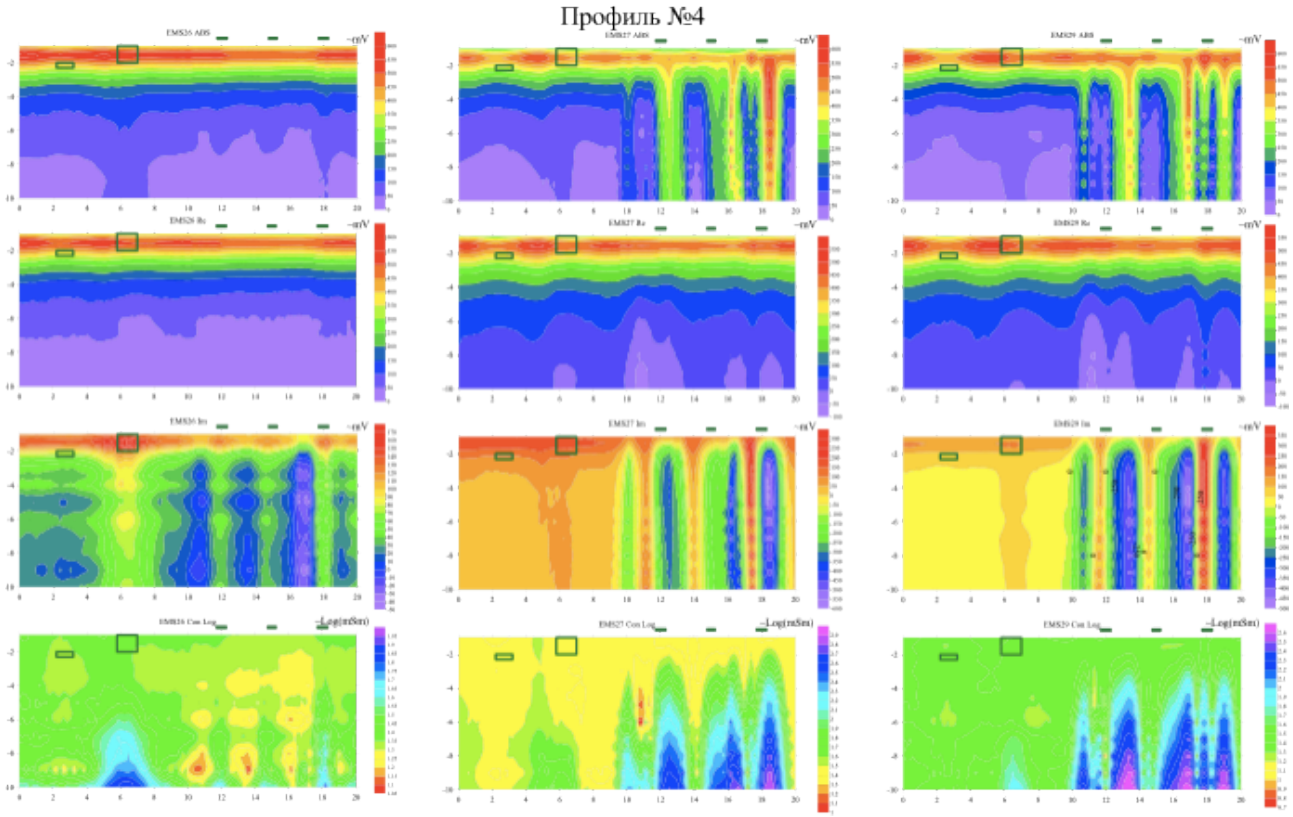

Figure 32. Section for line No.4

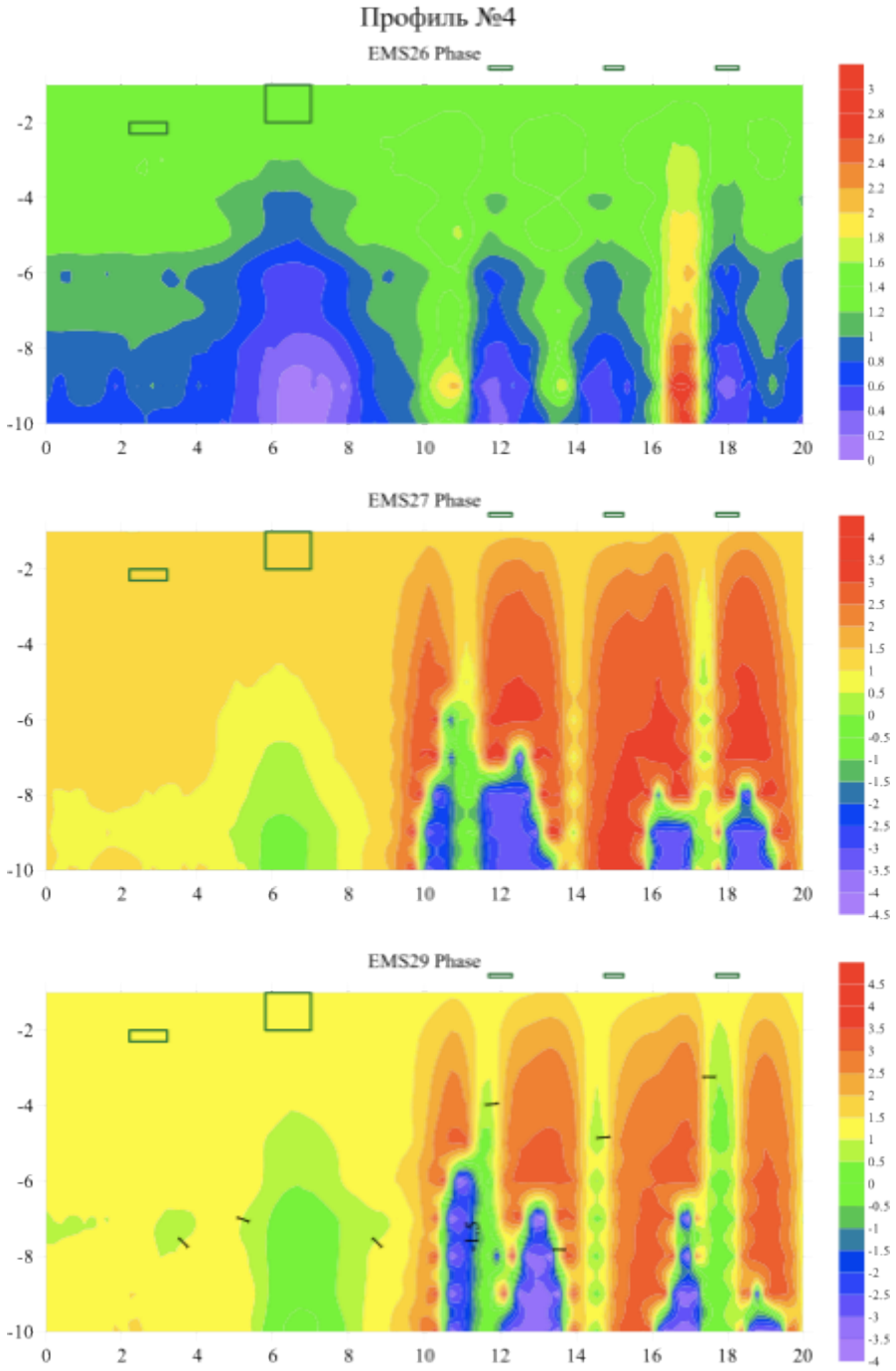

Figure 33. Section for line No.4. Phase of signal.